Theses and Dissertations

2002

A fundamental investigation of process efficiencies in the Laser Engineered Net Shaping (LENS) solid freeform fabrication process

Raymond R. (Robert) Unocic
Lehigh University

Follow this and additional works at: http://preserve.lehigh.edu/etd

Unocic, Raymond R.

A Fundamental Investigation of Process Efficiencies in the Laser Engineered Net Shaping…

January 2003

A Fundamental Investigation of Process Efficiencies in the

Laser Engineered Net Shaping (LENS™)
Solid Freeform Fabrication Process

by

Raymond R. Unocic

A Thesis

Presented to the Graduate and Research Committee

of Lehigh University

in Candidacy for the Degree of

Master of Science

in

Materials Science and Engineering

Lehigh University

July 25, 2002

CERTIFICATE OF APPROVAL

This thesis is accepted and approved in partial fulfillment of the requirements for the degree of Master of Science.

_7-25-02_

Date

Dr. John N. DuPont
(Thesis Advisor)

Dr. G. Slade Cargill III
(Chairman of Department)

ii

ACKNOWLEDGEMENTS

for me. You have always stressed the importance of an education, sometimes even more than I wanted to hear. At this point in my life, I truly understand the meaning and significance of it and for that I am so very grateful for all the sacrifices you have made over these years in giving me the opportunity to expand my horizons and to further my quest for knowledge. This is by far the greatest gift you have ever given to me. To my brother Frank thanks for all the laughter, good times, and advice you have given me throughout my life. You have been and always will be a great person to look up to. To my sister Jennifer thanks for taking care of me in our undergraduate years when you would always have a hot meal ready for me when I came home late from the library. I want my family to know that I appreciate everything they have ever done for me over these years and that if it wasn't for their love and support I wouldn't be where I am today.

Lastly, I would like to express my deep love and affection for Kinga Janiszewska. Kinga has brought forth sunshine to my life ever since the first day I met and fell in love with her. Her positive attitude, encouragement, and endless smile has given me the inspiration to succeed. She has been there to keep me grounded and to remind me that life is beautiful and that I should enjoy every moment of it. Kinga, you bring meaning to my life...I love you...and I can't wait to spend the rest of my life with you.

TABLE OF CONTENTS

LIST OF SYMBOLS

Cross Sectional Area of Deposit and Melted Substrate	A
Cross Sectional Area of Deposit	A_d
Cross Sectional Area of Melted Substrate	A_s
Dimensionless Parameter (Christensen)	Ch
Specific Heat	C_p
Concentration of Element i in the Deposit	C^i_{dep}
Concentration of Element i in the Substrate	C^i_{sub}
Concentration of Element i in the Powder	C^i_{pow}
Plate Thickness	d
Dilution	D
Heat Content Evolved from Sample	E_{cal}
Temperature Gradient	G
Net heat Input	H_{Net}
Current	I
Thermal Conductivity	k
Modified Bessel Function	K_o
Powder Mass Flow Rate	M_{fl}
Power	P
Cooling Rate	R
Dimensionless Parameter (Rykalin)	Ry
Travel Speed	S

Laser "on time"   t

Temperature   T

Initial Temperature T_o

Voltage   V

Total Volume of Deposited Filler Metal V_d

Total Volume of Melted Filler Metal V_f

Total Volume of Melted Substrate V_s

Volumetric Powder Metal Feed Rate $\dot{V}_{fm}$

Volumetric Melting Rate of Substrate $\dot{V}_s$

Thermal Diffusivity α

Latent Heat of Fusion ΔH_f

Melting Enthalpy ΔH_m

Melting Enthalpy of Filler Metal $\Delta H_{m,f}$

Melting Enthalpy of Substrate $\Delta H_{m,s}$

Energy Transfer Efficiency η_a

Melting Efficiency η_m

Deposition Efficiency η_d

Kinematic Viscosity ν

LIST OF TABLES

LIST OF FIGURES

Chapter 2

Chapter 3

Chapter 4

EXECUTIVE SUMMARY

Laser engineered net shaping (LENS™) is a solid freeform fabrication process that has the capability of fabricating intricately shaped, 3-D structures from a CAD model. A study of the effects of LENS™ processing parameters (laser power, travel speed, and powder mass flow rate) on process efficiencies was conducted. The materials used in this study were H-13 tool steel and copper powder deposited on H-13 tool steel substrates. Laser energy transfer efficiency (η_a) was measured using a Seebeck envelope calorimeter and it was found that η_a varied from 30-50% under the range of processing parameters tested. (Laser output power: 125-500W, travel speed: 5-15mm/s) Powder material feed rate and the type of powder delivered to the molten pool showed no effect on laser beam absorption. Melting efficiency (η_m) was found to increase with increasing laser input power, travel speed, and powder mass flow rate. A dimensionless parameter model that has been used to predict melting efficiency for laser beam welding processing was investigated for the LENS™ process. Good agreement was obtained between experimentally measured η_m data and η_m calculated from the model. From these results, a semi-empirical model was developed specifically for the LENS™ processing window. Deposition efficiency (η_d) was also investigated and results show that under optimum processing conditions, the maximum attainable deposition efficiency was approximately 14%. A semi-empirical model was developed to predict η_d as a function of process efficiencies and LENS™ processing parameters. A dilution model, that incorporates process efficiencies to estimate the degree of mixing between the substrate and deposit material, was investigated. The arc welding dilution model was found to be applicable for the LENS™ process and good correlation existed between experimentally measured and calculated dilution values. A new method of predicting dilution based on Rosenthal's heat flow solution was developed. The method showed good correlation between measured and calculated results. Knowledge of LENS™ process efficiencies measured in this study are crucial since these results are needed to develop accurate heat flow and solidification models for the LENS™ process.

1.0 INTRODUCTION

Laser engineered net shaping (LENS™) is a solid freeform fabrication process that has the capability of producing dense, near net-shaped parts through the use of a computer aided drawing (CAD). The LENS™ process has gained interest throughout academia and industry where the goal is to move this proof of stage concept into full-scale manufacturing, prototyping, and/or repair implementation. In order for this to occur, it is essential to conduct research on the effects of processing parameters on heat flow and solidification behavior during LENS™ processing.

Heat flow models can be developed to control and predict residual stress and distortion that occur during deposition. The results of these models can provide an insight to how processing parameters can be manipulated to produce a metallurgically sound structure while maintaining dimensional tolerance. Tailoring of microstructure and resultant mechanical properties can be predicted and controlled by developing solidification models that incorporate heat flow and thermal cycling behavior during LENS™ processing. The development of these process optimization models is a crucial step before the full capabilities of this rapid prototyping process can be exploited.

The objectives of this research are to measure LENS™ process efficiencies so that results can be used in future heat flow and solidification modeling studies. There are three main dimensionless process efficiencies that can be measured for this process: laser energy transfer efficiency, melting efficiency, and deposition efficiency. Laser energy transfer efficiency, is a parameter that is used to describe the fraction of energy that is actually absorbed by the workpiece from the total laser output energy. In past research, there have been studies in which the laser energy transfer efficiency was measured for

2

laser welding processes as a function of laser beam irradiance and travel speed by means of calorimetry; however, there have been no studies conducted that directly measure energy transfer efficiency specifically for the LENS™ process. What sets the LENS™ process apart from other laser welding process is that powder mass additions are incorporated into the weld pool to fabricate a component, i.e. by laser deposition. Powder mass additions may have an effect on the energy transfer efficiency: either by increasing laser beam absorption or by decreasing absorption by reflective losses off of the powder particles.

The second process efficiency to be measured is the melting efficiency, which is a parameter used to describe the amount of energy that is utilized to create a molten pool from the total energy absorbed by the workpiece. Several models have been developed that predict melting efficiency from knowledge of processing parameters (laser power and travel speed), heat flow geometry, and base metal thermophysical properties. These models can be compared to experimental measurements of actual laser deposits to determine if these predictive models can be applicable to the LENS™ process.

Lastly, deposition efficiency is a parameter that is used to describe the ratio of the actual deposition rate to the output powder mass flow rate. From a processing standpoint, the deposition efficiency is an important quantity to recognize because only a small fraction is actually fused to the substrate leaving a large amount to be recycled or scrapped. It is thus essential to understand what roles processing parameters have on the joining of powder material to the workpiece so as to avoid excess costs attributed to wasted powder.

2.0 LITERATURE REVIEW

2.1 Solid Freeform Fabrication

2.1.1 Introduction

A recent advancement in automated manufacturing has been the development of solid freeform fabrication (SFF). In this approach, dense, three-dimensional, near net-shaped parts are produced directly from computer-aided drawings (CAD) without the need for molding or additional tooling. This fabrication process has evolved from a combination of conventional manufacturing techniques that utilize the following processes to achieve the desired part geometry: near-net shape, subtractive, and additive.[1] Near net-shaped processes are distinct forms of forging, molding, or casting. The component is formed through the use of molds and dies whereby the final product takes on the geometry of the mold or die. The subtractive processes are commonly performed when a component is initially created by methods such as casting, but then must undergo subsequent machining operations to remove any unwanted material from the structure in order to achieve final part tolerance. Additive processes usually take on some form of joining or welding to create structures with more complex shapes than the original. The limiting steps in conventional manufacturing techniques are the design and fabrication of molds and dies, machining, and welding. A significant amount of time and labor must be invested to manufacture a product from start to finish. For example, in forgings and/or castings, several weeks to a year can elapse in the development and testing of a mold or die before it can even be employed in a manufacturing process.[2]

The desire to reduce manufacturing times, cost, and the multi-step processing associated with the movement of a part from the initial design stages to full scale

4

manufacturing has been the driving force for the development of SFF. One such method of solid freeform fabrication is laser engineered net shaping (LENS™), developed by Sandia National Laboratories and commercialized by Optomec Design Company.[3-6] The following section gives an introduction to the components that comprise the LENS™ system and how they are employed to fabricate near net-shaped, 3-D structures.

2.1.2 Laser Engineered Net Shaping (LENS™)

The LENS™ workstation in itself consists of a Nd:YAG laser, controlled atmosphere glovebox, a 3-axis (or 5axis) computer controlled positioning system, and multiple powder feed assemblies. To produce a structure using the LENS™ workstation, a computer-aided drawing (CAD) is first developed of the desired part geometry using 3-D solid modeling software having a stereolithography (.stl) file format. After the CAD model has been created it is sent through a file-slicing program (decomposition package) where it is subdivided into discrete planar cross sections of a finite thickness yielding a .sli file format.[1] The cross sections are in turn converted into machine code (.dmc), which is used to direct the movement of a multi-axis motion control system through a sequence of binary ASCII commands. The component is constructed by the laser deposition of powder material in a line-by-line, layer-by-layer manner in a shape that is dictated by the CAD model.

The molten pool is created when the continuous wave Nd:YAG laser beam is focused onto the substrate. Powder material is then delivered directly into the molten pool by the powder feed mechanism through a series of four copper nozzles. Upon solidification a metallurgical bond is formed between the substrate and the powder material. The programmed part geometry (CAD model) controls the movement and direction of an X-Y

5

stage upon which the component resides and is continuously in motion when a part is being built. The nozzles, as well as the focusing lenses of the laser, are incremented in the (+) z-direction to begin the deposition process of subsequent layers thereby building the three-dimensional form of the component. Successive layers are deposited atop one another until the three-dimensional part is completed in a layer-by-layer manner. A schematic illustration of the LENS™ process can be seen in Figure 2-1. Powders that have not been fused to the workpiece and fall into the catch tray may be recycled since the entire process is performed in an inert, contamination free environment but must be sifted in order to remove unwanted contaminants and agglomerated powder particles.
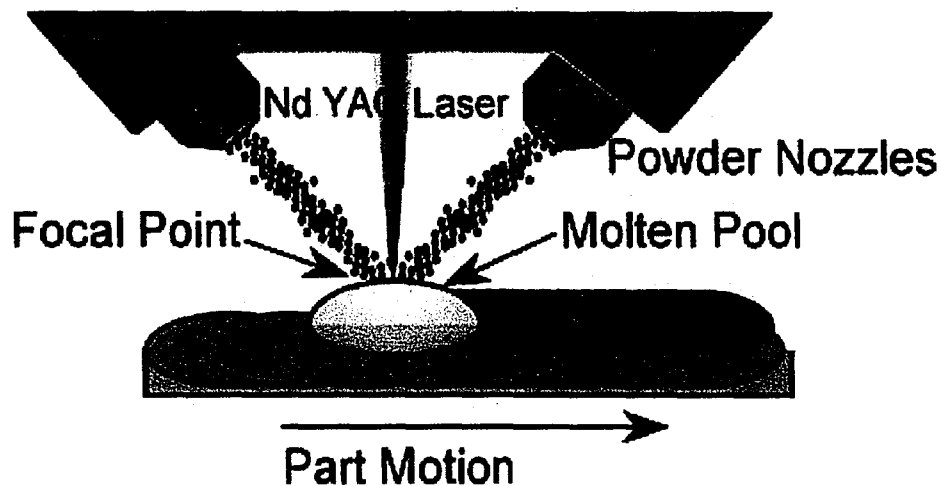
Figure 2- 1. Schematic illustration of the LENS™ laser deposition process.

The LENS™ process has gained interest throughout industry where the goal is to move this proof of stage concept into full-scale manufacturing, prototyping, and/or repair implementation. In order for this to occur, it is important to conduct research on what effects processing parameters have on microstructure and mechanical properties and overall part integrity.

6

2.1.3 LENS™ Processing Parameters

A fundamental understanding of the effect of LENS™ processing parameters on microstructure and mechanical properties are essential in that the results can be used to develop process optimization models, which will enable LENS™ operators to choose an optimal set of parameters to rapidly produce a nearly defect free structure for a given class of materials. LENS™ processing parameters can be divided into two discrete areas. The first set of parameters deals primarily with the computer workstation, CAD model decomposition process, and the machine codes that dictate stage movement. The purpose of these parameters are to control the CAD model slicing algorithms and slice file conversion into machine code, which in turn directs the deposition sequence. The second set of parameters affect heat transfer and solidification behavior of each deposited layer. These parameters form the basis of the present research and thus will be discussed in detail.

There are three main processing parameters that can be controlled by the LENS™ process that in combination with one another, affect heat transfer, thermal cycling, solidification behavior, and layer build height. The parameters are laser input power, travel speed, and powder mass flow rate and they will be discussed in the following sections.

2.1.3.1 Laser Input Power

Laser input power is the amount of energy that is transferred from the laser head into the work piece. The input laser power and travel speed, are extremely important processing parameter in that they control the temperature gradient, cooling rate, and mode of solidification which will in turn affect the resultant microstructure. The

7

temperature gradient of a single point source can be derived based on the principles of 2-D and 3-D heat flow and knowledge of the laser input power, travel speed, and material thermophysical properties. 2-D heat flow exists when the substrate thickness is on the same order of the weld depth as depicted in Figure 2- 2. 3-D heat flow occurs when the substrate thickness is much larger than the weld depth as illustrated Figure 2- 3. In the LENS™ process, heat flow can either be 3-D or 2-D. During the deposition of the first few layers of a solid object, heat flow is predominately 3-D because heat is conducted in the substrate radially in all directions because the substrate thickness is significantly larger than the depth of penetration. If however, a thin walled structure is being deposited heat flow is initially 3-D, because the heat is conducted through the substrate in a 3-D manner, but becomes 2-D when the heat can escape only in the downward and forward/backward directions away from the molten pool. This is attributed to the high depth to width ratio of the thin walled structure.

Figure 2- 2. Schematic illustration of 2-D heat flow conditions that exists when the plate thickness is on the same order as the weld depth.
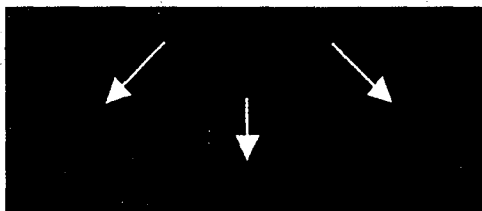
Figure 2- 3. Schematic illustration of 3-D heat flow conditions that exists when the plate thickness is much larger than the weld depth.

Heat flow is affected by base metal thickness, thermal properties of the base material, and process variables such as: power and travel speed of the heat source. The effects were examined by Rosenthal.[7] Analytical solutions for 2-D and 3-D conduction heat flow were developed and are presented in Equations [2-1] and [2-2] respectively.

$$T - T_o = \frac{\eta_a P}{2\pi k d} \exp\left(\frac{-Sx}{2\alpha}\right) K_o\left(\frac{Sr}{2\alpha}\right) \qquad \text{[2-1]}$$

$$T - T_o = \frac{\eta_a P}{2\pi k r} \exp\left(\frac{-S(r-x)}{2\alpha}\right) \qquad \text{[2-2]}$$

Where:

T = Temperature (°C)
T_o = Initial Temperature of the Workpiece (°C)
P = Power (Watts)
η_a = Energy Transfer Efficiency (Unitless)
S = Travel Speed (mm/s)
K_o = Modified Bessel function.
d = Plate Thickness (mm)
r^2 = Radial distance from origin of heat source ($x^2+y^2+z^2$) (mm^2)
k = Thermal Conductivity (W/mm-°C)
α = Thermal Diffusivity (mm^2/s)

Rosenthal's equation takes into account several assumptions which include: a point heat source, no melting, heat flow by conduction only, constant thermal properties, and no heat loss from the work piece surface. A point to inject about the equations above is that the model used in the development of these solutions does not take into account any mass additions into the melt pool. Information on thermal conduction with powder mass

additions is key for accurate predictions of temperature gradients and cooling rates for the LENS™ process.

The general form of Rosenthal's heat flow solutions can be modified so that equations relating thermal conduction heat flow conditions to the temperature gradient and cooling rate can be formulated.[8] The temperature gradient is given as the change in temperature with respect to a change in position. To determine the temperature gradient along the weld centerline (y=0 and z=0) at a distance from the heat source along the x-axis, Equation [2-2] can be reduced to yield the following equation:

$$G = \frac{dT}{dx} = -2\pi k \frac{(T - T_o)^2}{\eta_a P} \qquad [2\text{-}3]$$

From this equation it can be seen that the temperature gradient decreases with a decrease in preheat temperature, a decrease in thermal conductivity, and an increase in the net input power ($\eta_a P$). Travel speed will also have an affect on the temperature gradient. If the travel speed of the heat source is increased, holding all other welding variables constant, there is less time available for heat to be conducted away from the locally heated region. This will lead to a decrease in the temperature gradient and will inevitably change the temperature gradient along specific distances of the weld pool.

High-speed thermal imaging was used to deduce temperature gradient information from the vicinity of the molten pool as a function of laser input power by Hofmeister et al.[9] A digital 64x64 CCD video camera was used to capture images of the laser and 316

10

stainless steel powder interactions in the molten weld pool at 990 frames per second. The thermal imaging system was calibrated using a tungsten-strip lamp radiance source obtained from National Institute of Standards and Technology (NIST). A thermal image from the molten pool can be seen in Figure 2- 4. As seen from this image, the weld pool and surrounding areas were colorized and converted to a temperature scale. The images convey information on the maximum temperature of the molten pool as well as the temperature profile within its vicinity.
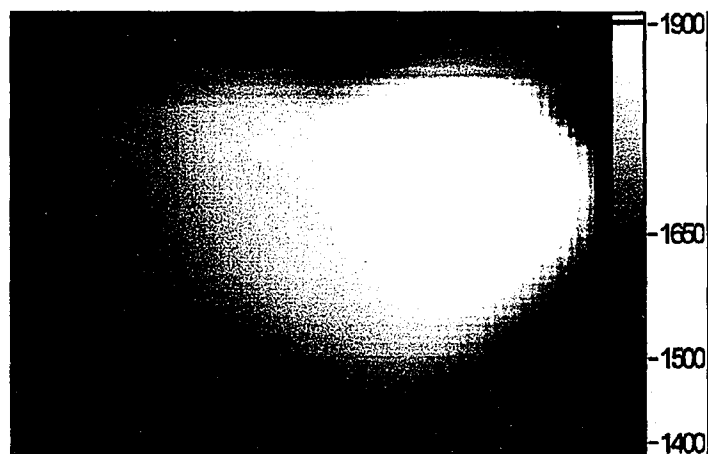
Figure 2- 4. Thermal image taken from the molten pool of a LENS™ deposit using a color CCD thermal imaging camera.

From this, Hofmeister et al were able to study the effects of laser beam input power on the temperature gradient.[9] In their study line deposits of 316 stainless steel were made at a travel speed of 7.62mm/s. Powder mass flow rates, however, were not specified so it is impossible to decipher what effects powder mass additions had on the temperature gradient for a given laser power and travel speed. Figure 2- 5 depicts how the temperature profile varies across the molten pool as a function of laser input power.

11
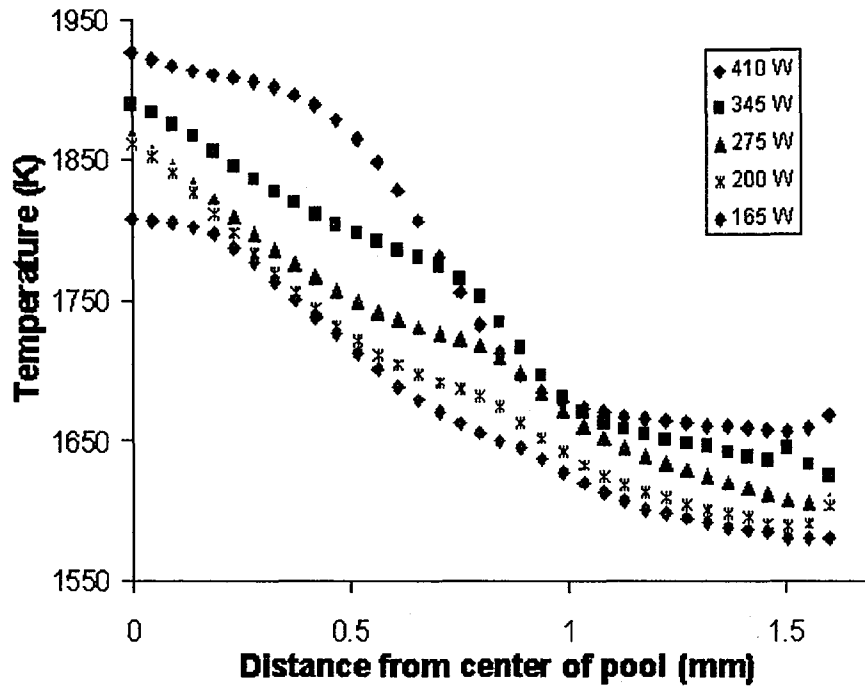
Figure 2-5. Thermal profile at distances from the center of the molten pool at varying laser powers.

In this figure, the maximum temperature reached for each laser input power is shown for laser powers of 165, 200, 275, 345, and 410 watts. There was no mention of whether or not the laser powers used in this study were the actual power absorbed by the workpiece or simply the output power of the laser. The region, at x=0, corresponds to the zone directly underneath the heat source. A high initial temperature is observed then it appears to taper off the further away it is from the heat source. At the highest laser power (410 watts), the slope of the temperature profile abruptly decreases at a distance of x=0.5mm. This region corresponds to the length of the molten weld pool in the x-direction. A gradual decrease in the temperature profile follows in wake of the weld pool corresponding to the temperature gradient in the solidified weld metal. The length of the weld pool was observed to decrease for lower laser power settings. On the low laser

power end, 165 watts, the length of the weld pool is approximately 0.25mm. The information gained from this research is that for a given material and travel speed, the size of the weld pool is predominately controlled by the laser input power.

2.1.3.2 Travel Speed

Cooling rate can be described as the change in temperature with respect to time. The same factors, which affect the temperature gradient, will also affect the cooling rate; however, the cooling rate is also largely dependent upon the travel speed of the heat source. By multiplying the temperature gradient Equation [2-3] with the travel speed (dx/dt) of the heat source it is possible to calculate the cooling rate:

$$\frac{dT}{dt} = -2\pi \ kS \frac{(T - T_o)}{\eta_a P}$$

[2- 4]

Where S is the travel speed of the heat source. It should be noted that Equations [2-3] and [2-4] are not general expressions of the temperature gradient and cooling rate but rather specific expressions for estimating the temperature gradient and cooling rate along the weld centerline at distances away from the heat source in the x-direction. Examination of Equation [2-4] reveals that the same factors that affect the temperature gradient also affect the cooling rate; however, an increase in the travel speed will result in an increase in the cooling rate.

Cooling rate measurements were also conducted by Hofmeister et al.[9] Thermal profile information were collected by the same methods described in Section 2.1.3.1. From the thermal gradient information the authors were able to calculate cooling rates at

13

the solid-liquid interface for different laser powers. Since the travel speed (dx/dt) was fixed at 7.62mm/s the cooling rates (dT/dt) were calculated by multiplying this quantity by the temperature gradient (dT/dx). The results of cooling rate measurements as a function of laser power are displayed in Figure 2-6.
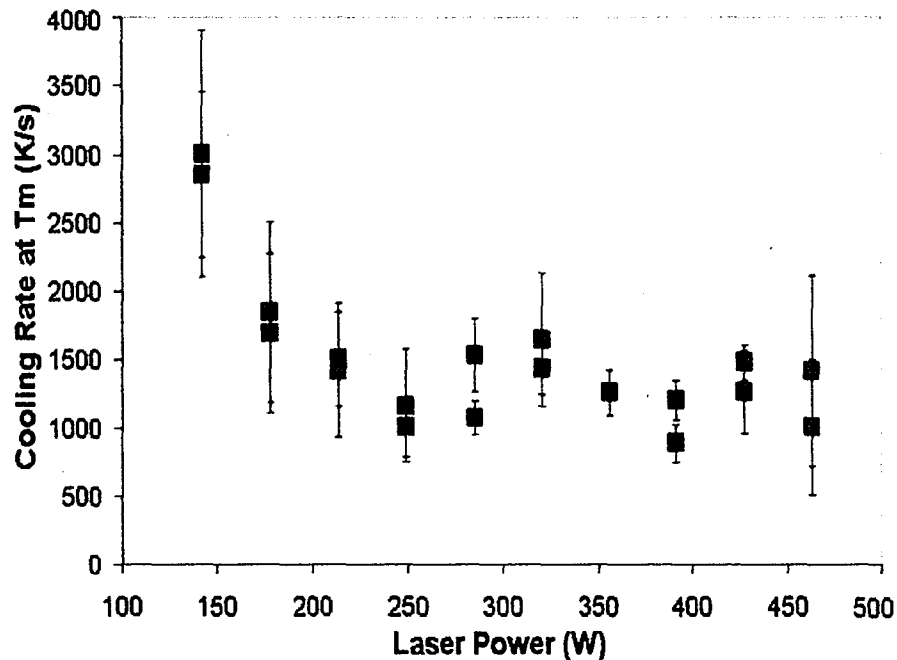
Figure 2- 6. Cooling rate as a function laser power for LENS™ deposits of 316 stainless steel.

From this figure it can be deduced that at lower energy inputs high cooling rates result, while at higher energy inputs the cooling rates fairly remain constant. The high cooling rates at low heat inputs occur mainly because the molten pool is small when compared to the molten pool of high heat inputs. The smaller molten pools allow for heat to be extracted by conduction through the surrounding base metal due to high thermal gradients. A high energy input is associated with a lower temperature gradient because there is less of a driving force for heat removal and thus the cooling rates in turn become low. From Figures 2-5 and 2-6 it has been shown that the input power of the laser beam

14

has a vital impact on the temperature gradient and cooling rate and hence, the solidification behavior of the component.

2.1.3.3 Powder Mass Flow Rate

Layer build height is influenced by the combination of laser power, travel speed, and powder flow rate. The combination of powder flow rate and the travel speed govern the amount of material that can be deposited per unit time (i.e. deposition rate) for a given laser power. Powder mass flow rate is the amount of powder, typically expressed as a mass per unit time, which is delivered to the molten pool. This differs from the deposition rate in that deposition rate is the amount of material that is deposited on the substrate per unit time. The laser power comes into effect since it controls the amount of energy that is available to melt the filler material and the underlying substrate.

The influence of laser power, travel speed, and powder mass flow rate variables were studied by McLean et al in a laser deposition process similar to that of LENS™.[10] Their results show that at constant laser power, the build height is mainly dependent upon travel speed (process velocity) and powder mass flow rate. The effect of travel speed and powder flow rate on deposition rate can be observed in Figure 2- 7. An interesting point to make about this graph is that the deposition rate appears to scale linearly with the powder flow rate.

An ideal deposition process would be to have all of the powder that is delivered to the molten pool be used to form a metallurgical bond. In actual laser deposition processes, a majority of the powder will not be fused to the workpiece because 1) the size of the molten pool is either too small to accommodate a large flux of powder, 2) there is not enough melting power available in the localized melt region to effectively melt the

substrate and the incoming powder material, and/or 3) powder is injected at such a high velocity that a particles will have a sufficient amount of momentum that when impinged upon the surface it is deflected away from the melt pool. A term used to describe this phenomenon is deposition efficiency and it is a dimensionless parameter of the ratio between the actual deposition rate (i.e. powder that is fused into the melt pool) to the total mass flow rate of powder. Deposition efficiency will be discussed in more detail in Section 2.2.4.
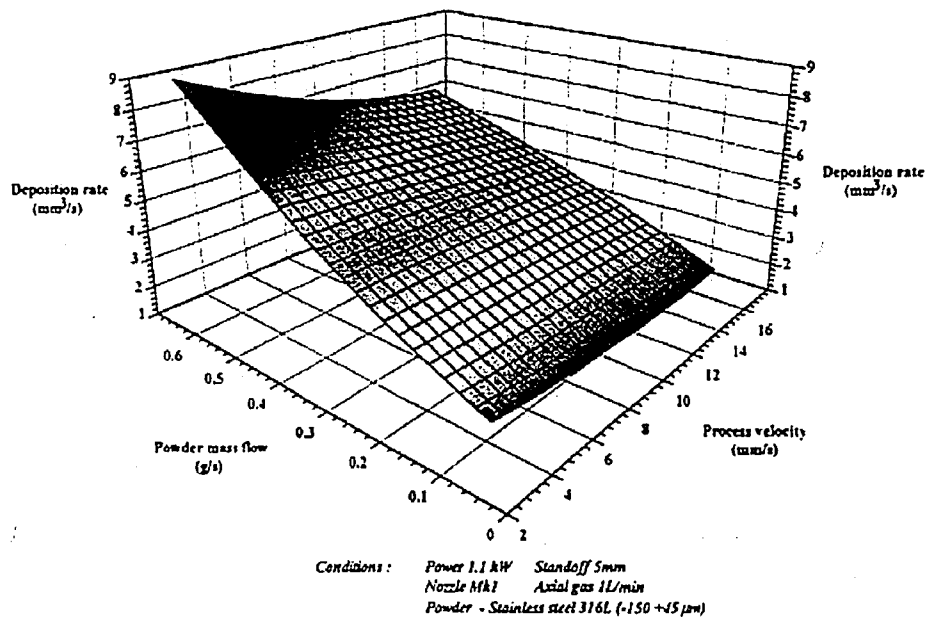
Figure 2- 7. Effect of powder mass flow rate and travel speed on deposition rate.

2.2 Process Efficiencies

2.2.1 Introduction

As described above in Sections 2.1.3.1-2.1.3.3, knowledge of LENS™ processing parameters are essential in that they affect the temperature gradient, cooling rate, and mode of solidification, which in turn has an affect on the microstructure and mechanical

16

properties of the work piece for the duration of melting, solidification, and subsequent thermal cycling. In the following sections, an attempt has been made to review current research that has been conducted on the efficiencies of related arc welding and laser welding processes to determine how they can be used to measure and/or predict the process efficiencies of the LENS™ process since the LENS™ process can be envisioned as a combination of laser welding and consumable arc welding process where filler material is added to the weld joint. There has been a significant amount of research that has been conducted on well established welding and joining processes dealing primarily with energy transfer, melting, and deposition efficiencies.

More recently, attention has been focused upon the use of these efficiency measurements to select process variables that give optimal joining results and for compositional control of consumable filler metal processes. This research can be extended to the LENS™ process to develop optimal processing parameters.

2.2.2 Laser Energy Transfer Efficiency

Energy transfer efficiencies of arc welding and laser welding have been extensively studied for a variety of welding processes and under a range of processing parameters in order to determine the amount of energy that absorbed by the workpiece. A term used to describe this is energy transfer efficiency and it is a dimensionless parameter that is defined as the fraction of energy transferred into the work piece over the energy generated by the heat source:

$$\eta_a = \frac{Energy\ Transferred\ to\ the\ Work\ Piece}{Energy\ Generated\ by\ the\ Heat\ Source} \qquad [2\text{-}5]$$

17

In the case of laser welding, the transfer efficiency can be defined as the ratio of heat absorbed by the work piece to the incident laser energy.[11] This fraction is always less than unity because not all of the energy generated by the heat source makes it to the workpiece. In laser welding, a fraction of the laser light is reflected by surface of a material. This will be discussed in more detail in Section 2.2.2.1.

The transfer efficiency factor is an important quantity to recognize for any given welding or joining process as it governs how much energy is delivered into the workpiece under a specific set processing parameters. An equation used to describe the net heat input of conventional arc welding and laser welding processes can be applied to calculate the net heat input of the LENS™ process through knowledge of the energy transfer efficiency. This equation is given in Equation [2-6]:

$$H_{Net} = \frac{\eta_a P}{S}$$

[2- 6]

Where:

H_{Net} = Net Input (J/mm)
η_a = Energy Transfer Efficiency (Unitless)
P   = Laser Output Power (Watts)
S   = Travel Speed (mm/s)

Note: In the LENS™ process the travel speed (S) is implied to be the crosshead velocity of the moveable X-Y stage because of the fixed optics in the laser delivery system. The two terms are interchangeable. Power has units of Watts (J/s) and the travel speed S has the units of mm/s; therefore, the unit for heat input into the work piece is energy per unit length, or J/mm.

18

2.2.2.1 Factors Affecting Laser Energy Transfer Efficiency

The mechanism by which laser energy is absorbed by the work piece is complex as there are many factors that influence absorption. For laser beam welding processes, energy transfer efficiency typically range from 20-90% which is dependent mainly upon: 1) angle of incidence, 2) wavelength of the laser beam, 3) optical reflectivity of the material surface conditions of the work piece, and 4) laser beam irradiance. These four major factors that effect laser energy transfer will be discussed in the following sections and will be presented in a manner that is general to laser beam processing and if possible, specific to the LENS™ process.

The first two factors that affect laser beam coupling, angle of incidence and laser beam wavelength, are fixed for the LENS™ process because the angle of incidence is perpendicular to the x-y stage upon which with substrate resides and type of laser used is an Nd:YAG laser with a fixed wavelength of 1064nm (1.06μm). The laser beam wavelength also has a profound affect on laser absorption. This is evident when welding the same material at the same parameters but with a different laser. The wavelength of a CO_2 laser at 10.6μm is ten times greater than the wavelength of a Nd:YAG laser is at 1.06μm. Laser beam absorption is directly related to the wavelength of the incident laser light. At shorter wavelengths, such as in the Nd:YAG laser, the more energetic photons can be readily absorbed by a greater number of bound electrons in the material which decreases the reflectivity and thereby increasing the absorptivity of the laser beam into the workpiece.[12]

Laser beam coupling is highly material dependent as some materials are more optically reflective than others. For example at the Nd:YAG laser beam wavelength

19

(1.06μm), highly reflective materials such as copper and aluminum reflect approximately 99% and 91% of the incident laser beam energy.[13] This is significantly higher than materials such as iron and nickel, which is 64% and 74% reflective, respectively.

Surface roughness will also have an effect on laser beam absorption. Surface roughness will vary from one material to another depending on the manufacturing method and whether or not any surface preparation was done to remove surface irregularities. Surface roughness is measured with a profilometer and is commonly expressed as a root-mean-square roughness. A decrease in laser beam absorption is associated with a rougher surface since the laser light can be reflected from the material off of the local peaks and valleys In general, a surface is optically smooth if the surface roughness is less than the wavelength of the laser beam.[14]

Besides laser beam characteristics, material reflectivity, and surface roughness, processing parameters will also have a profound effect on laser beam absorption. Processing parameters such as laser power and travel speed are controllable and by varying these parameters it is possible to alter the transfer of laser energy into the workpiece. When referring to the laser power processing parameter, two terms are commonly used in place of laser power: laser beam irradiance and laser beam intensity. Laser beam irradiance is simply the ratio of laser output power per unit area (power density) and its value is found by dividing the laser output power by the laser beam focused spot area while laser beam intensity is the ratio of the laser output power to the focused laser spot diameter.

In a study of laser energy transfer efficiency of CO_2 laser welding process Fuerschbach observed the effects of processing parameters on laser beam absorption for

304 stainless steel, 1018 steel, and tin. The objective of his research was to observe what effects laser output power, travel speed, and focus spot size had on transfer efficiency.[11] Travel speed was found to have no effect on transfer efficiency. The level of irradiance however did affect the transfer efficiency. Transfer efficiencies were shown to increase with the level of irradiance (Refer to Figure 2- 8).
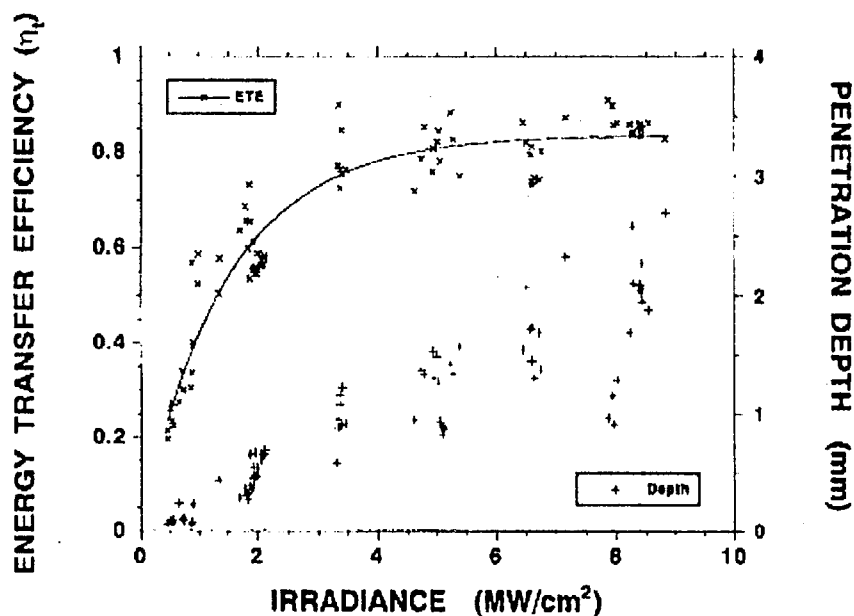
Figure 2- 8. Variation of energy transfer efficiency with laser beam irradiance.

After an irradiance level of approximately $3MW/cm^2$ the transfer efficiency begins to plateau where a further increase in irradiance causes no change significant in transfer efficiency. The information gained from this graph was that laser energy transfer efficiency varied from 20%-90%. The higher end values are of interest from a processing standpoint because it entails that most of the energy is absorbed by the workpiece with minimal loss of laser beam energy. An interesting point to note in the results is the dramatic increase in transfer efficiency from approximately $1MW/cm^2$-$3MW/cm^2$. This

region can be explained by the keyhole cavity formation, which is characteristic to laser beam welding.

The creation of the keyhole like cavity occurs at high levels of irradiance. At low irradiance levels, a small amount of heat is delivered to the substrate causing some surface heating and a small amount of localized melting; however, much of the incident light energy is reflected from the surface (Figure 2- 9a). At even higher irradiance levels a keyhole is formed (Figure 2- 9b). When the laser beam creates the keyhole cavity energy is absorbed and multiple internal reflections of the laser light occurs within the cavity. The series of beam deflections within the keyhole minimize light being reflected out of the keyhole and thereby maximizing laser absorption into the workpiece. This has been concluded as the main reason why laser processing can attain 90% energy transfer efficiency.[11]
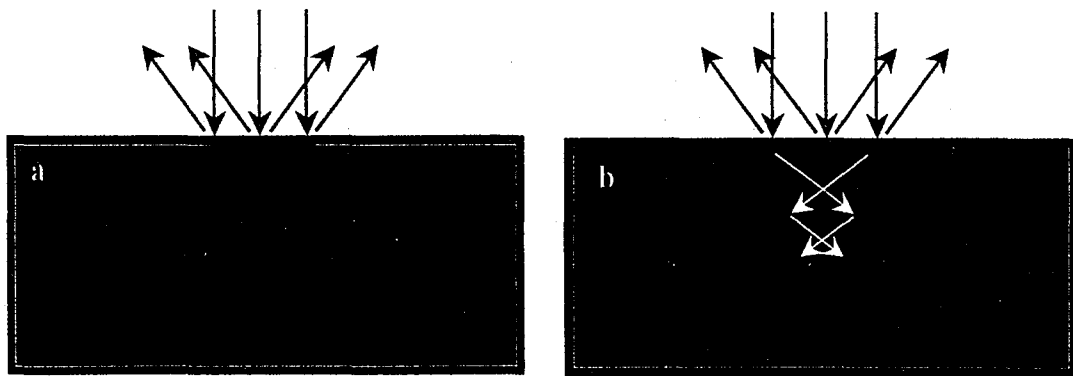
Figure 2- 9. Schematic illustration of a) laser beam reflective losses at low laser beam irradiance and b) keyhole cavity formation at high laser beam irradiance.

For the LENS™ process, the transfer of energy from the laser beam to the substrate is slightly different than that of other laser fabrication processes because of the addition of powder material into the melt pool and the lower levels of irradiance used in

the deposition process. In the above paragraph it was stated that the maximum attainable transfer efficiency for laser beam welding was 90%, corresponding to high levels of irradiance and keyhole cavity formation. In laser deposition processes, the keyhole mode is rarely ever achieved since the purpose of the laser beam is to create a small molten weld pool into which powder material is injected. Creation of a keyhole cavity would prove detrimental to part build up since previously deposited layers will be destroyed and part tolerance will subsequently be unattainable. Energy transfer efficiency may be affected by powder additions transferred to the weld pool in laser deposition processes. To date, there has been no published research in the open literature that has dealt with measuring transfer efficiencies as a function of power, travel speed, and powder mass flow rate in laser deposition process. Powder additions into the weld pool are envisioned to have some effect on transfer efficiency values.

2.2.2.2 Measuring Laser Energy Transfer Efficiency

Energy transfer efficiencies have been measured for various arc and laser welding processes using a gradient layer type calorimeter. Validation of arc efficiency measurements by the Seebeck envelope calorimeter was conducted by Geidt et al.[15] In their study, DC straight polarity gas tungsten arc welding was used to produce bead on plate welds under a matrix of arc currents and arc voltages on 304 stainless steel base material. The sample was placed in the calorimeter and after each weldment was made, the calorimeter lid was immediately closed to measure the heat content evolved from the workpiece. The calorimeter works on the gradient layer principle whereby a voltage output signal is generated by a temperature difference through a series of heat flux transducers that line the inner chamber walls of the calorimeter. The resultant output

voltage signal is integrated, and then multiplied by a calibration constant (units of WV^{-1}) to yield the amount of heat that is absorbed by the work piece from the welding process (i.e. the net heat input). By measuring the total heat content evolved from the sample (E_{cal}), it is possible to determine the transfer efficiency for a specific set of welding variables through the use of the following equation:

$$\eta_a = \frac{E_{cal}}{VIt} \qquad [2\text{-} 7]$$

Where:

V = Voltage (Volts)
I = Current (Amperes)
t = Welding "on time" (seconds)

The units for E_{cal} are joules and the unit of the product in the denominator (VIt) is in joules as well. The results of welding calorimetric measurements by the gradient layer approach, was compared to that of other calorimeter-type measurements to prove that this method of measuring transfer efficiencies is feasible.[15] Measured transfer efficiencies of 80% for the gas tungsten arc welding process were consistent with results of other calorimeter type devices (liquid nitrogen calorimeter and water-cooled copper anode measurements) under the same processing conditions.

Through the proven feasibility of energy transfer measurements by calorimetry, research has been extended for arc welding processes. DuPont et al has conducted research on arc efficiency measurements for four arc welding processes using this approach.[16] The four arc welding processes that were studied can be subdivided into two

types of processes: consumable and non-consumable. In consumable arc welding processes, the electrode is used as filler material to fill the weld joint and/or for alloying purposes. These processes are gas metal arc welding (GMAW) and submerged arc welding (SAW). The non-consumable electrode processes are plasma arc welding (PAW) and gas tungsten arc welding (GTAW). Consumable processes were found to yield higher arc efficiencies because there is a high rate of net energy transfer from the electrode to the substrate.

2.2.3 Melting Efficiency

From Section 2.2.2 it was shown that it is possible to measure the amount of energy that is transferred into the work piece. By knowing this quantity it is possible to determine how much of the energy that actually makes it to the workpiece is used for melting. Only a small portion of the energy is actually used for melting the fusion zone; the rest is dissipated to the surrounding area by thermal conduction. The term used to describe this is melting efficiency (η_m) and it is defined as the ratio of energy used for melting to that which is delivered to the substrate:

$$\eta_m = \frac{Heat\ Required\ For\ Melting}{Heat\ Delivered\ to\ the\ Substrate} \qquad \text{[2-8]}$$

The heat required to melt the material can be calculated from the following equation:

$$\Delta H_m = V_s \left(\int_{T_o}^{T} C_p(T)dT + \Delta H_f \right) \qquad \text{[2-9]}$$

Where:

ΔH_m = Melting Enthalpy (J)
V_s = Total Volume of Melted Substrate (mm^3)
T = Temperature (°C)
T_o = Initial Temperature (°C)
C_p = Heat Capacity (J/mm^3-°C)
ΔH_f = Latent Heat of Fusion (J/mm^3)

Equation [2-9] can be incorporated into Equation [2-8] to yield the following:

$$\eta_m = \frac{V_s \left(\int_{T_o}^{T} C_p(T)dT + \Delta H_f \right)}{\eta_a VIt} \qquad \text{[2-10]}$$

Where $\eta_a VIt$ is the energy delivered to the substrate. Notice that the transfer efficiency term comes into effect in the denominator as it governs the amount of energy delivered to the substrate. This illustrates how an accurate value of energy transfer efficiency is necessary in order to accurately estimate the melting efficiency.

2.2.3.1 Factors Affecting Melting Efficiency

Through examination of 2-D and 3-D conduction heat flow conditions, as described in Section 2.1.3.1, it is possible to observe which parameters will have the most effect on melting efficiency. These "process controlled" parameters are the magnitude of the power from the heat source and the travel speed. Several researchers have formulated

theoretical equations that can be used to predict the melting efficiency.[17-19] These

equations incorporate heat flow conditions, processing parameters, and thermophysical

properties of the materials in use.

Melting efficiency equations were developed to predict the melting efficiency

behavior for the 2-D and 3-D heat flow conditions. For the 2-D heat flow case, Wells[17]

developed an analytical expression to predict melting efficiency in terms of base metal

thermophysical properties and processing properties:

$$\eta_m = \frac{1}{\left(\dfrac{8\alpha}{5Sd} + 2\right)}$$

[2- 11]

Where:

α = Thermal Diffusivity of the Base Metal (mm^2/s)
S = Travel Speed (mm/s)
d = Weld Width (mm)

Okada[18] also formulated an expression of melting efficiency for the 3-D case as shown in

Equation [2-12].

$$\eta_m = \frac{1}{1.35\left(1 + \left(1 + \dfrac{10.4\alpha^2}{(Sd)^2}\right)^{\frac{1}{2}}\right)}$$

[2- 12]

27

In the 2-D case, the theoretical melting efficiency maximum is 0.48 whereas the theoretical maximum for the 3-D case 0.37. From the equations stated above, the sole processing parameter that has an effect on the melting efficiency is the travel speed. Continued research on melting efficiency revealed that this quantity is not dependent solely upon travel speed but it is also dependent upon on the power that is delivered to the base metal as well.[11, 17-19] Okada also proposed another formula, which accounts for the power delivered to the base metal:

$$\eta_m = \exp\left[-\left(1 + \frac{\alpha^2 \Delta H_m}{1.14 \eta_a VIS}\right)\right]$$

[2-13]

Where E is the enthalpy change due to melting. Fuerschbach and Knorovsky later developed an equation that relates the melting efficiency to welding parameters and material properties.[20]

$$\eta_m = A \exp\left(\frac{-B}{\eta_a VIS / \Delta H_m \alpha \upsilon}\right)$$

[2-14]

Where A and B are constants that can be extracted from a plot of $\ln(\eta_m)$ against $(\eta_a VIS / E\alpha \upsilon)^{-1}$ and υ is the kinematic viscosity at the melting point.

More recently a model has been developed to estimate the melting efficiency using dimensionless parameters.[21] To represent the heat transfer mechanism in arc and

28

laser welding processes, the dimensionless parameters Ry and Ch incorporate welding

input parameters and base metal properties.

$$Ry = \frac{\eta_a PS}{\alpha^2 \Delta H_m}$$

[2- 15]

$$Ch = \frac{S^2 A}{\alpha^2}$$

[2- 16]

Where:

η_a = Energy Transfer Efficiency (Unitless)
P = Laser Power (Watts)
S = Travel Speed (mm/s)
α = Thermal Diffusivity at the Liquidus Temperature (mm^2/s)
ΔH_m = Enthalpy of Melting (J/mm^3)
A = Weld Cross Sectional Area (mm^2)

The ratio of Ry/Ch yields the melting efficiency:

$$\eta_m = \frac{Ch}{Ry} = \frac{SA\Delta H_m}{\eta_a P}$$

[2- 17]

Good correlation has been shown to exist between the dimensionless parameter model

and experimental results. From the theoretical equations described above, it is important

to understand how each of the processing parameters and thermophysical properties of

the material affect melting efficiency; therefore, the effects of laser input power, travel

speed, base metal geometry, and base metal properties will be discussed in the following sections.

2.2.3.1.1 Laser Input Power

The input power has a profound effect on the melting efficiency. The melting efficiency was shown to increase with an increase in the amount of power delivered to the substrate. Figure 2- 10 depicts the gradual increase of melting efficiency with increasing power for several arc welding processes. This trend can also be seen in Figure 2- 11 for laser beam welding. An explanation of this effect is as follows: if heat is delivered to the substrate at a faster rate (i.e. higher laser input power) then there would be a lesser amount of time available for heat to be dissipated away and thus heat can effectively be used to increase melting in the fusion zone. For this reason, the combinations of laser power and travel speed are processing parameters that govern that amount and rate of heat delivered to the workpiece.
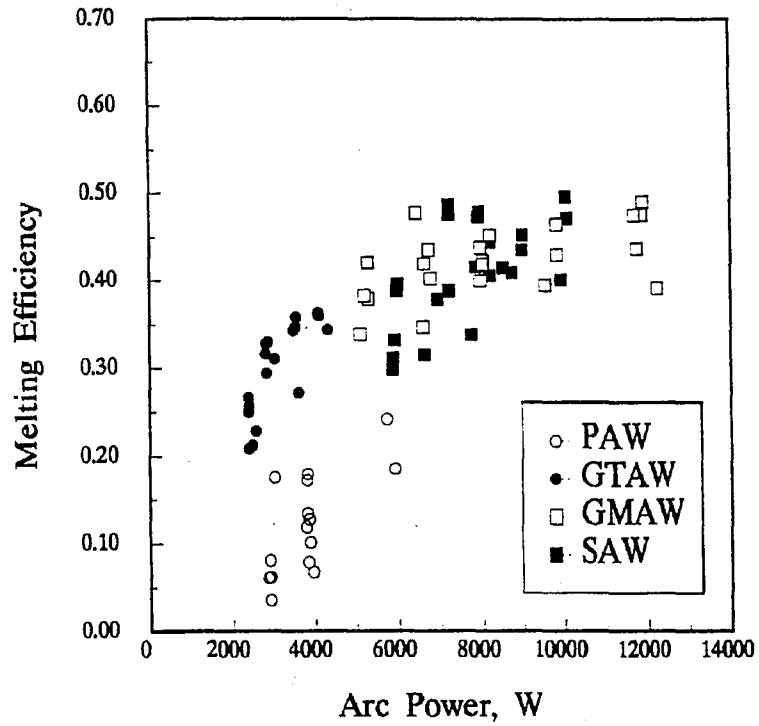
Figure 2-10. Effect of arc power on melting efficiency for arc welding processes.
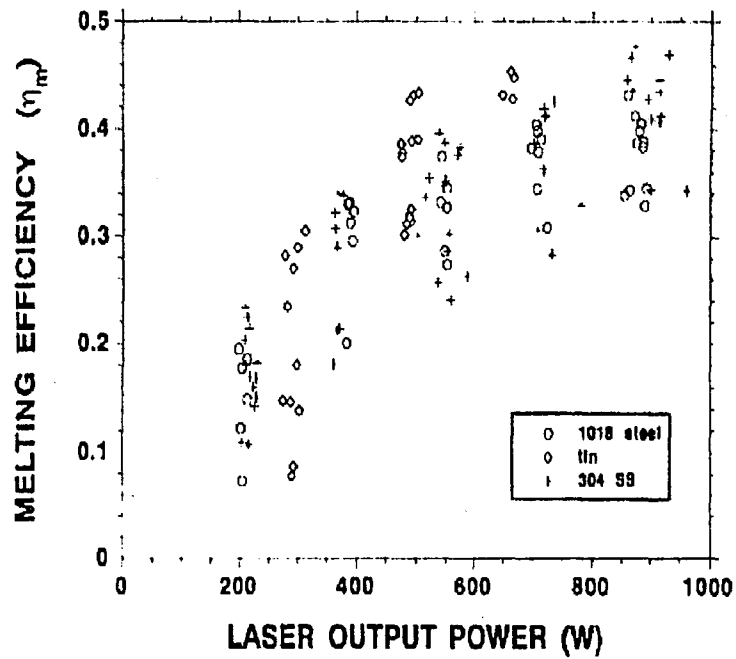
Figure 2-11. Effect of laser power on melting efficiency for CO_2 laser beam welding.

31

2.2.3.1.2 Travel Speed

The net heat input to the base metal is governed by the travel speed as indicated in Equation [2-6]. Travel speed would then have an impact on the melting efficiency. Examination of the melting efficiency equations shows that the travel speed term is located in the numerator. Therefore, when the travel speed is increased one would expect the melting efficiency to increase as well. The physical explanation for this is as follows: if travel speed is increased, energy would be delivered to the work piece at a much faster rate than it can be dissipated. Under these circumstances, the energy is effectively used to melt the material rather than being dissipated away by conduction. (i.e. more melting would occur). The effect of travel speed on melting efficiency has been studied for a variety of arc and laser welding processes while keeping power constant.

In a study conducted by DuPont et al, the melting efficiencies were examined as a function of travel speed for four arc welding processes.[16] The results of this work are presented in Figure 2- 12. The trend of increasing melting efficiency with travel speed is apparent for each of the processes examined. Another observation that can be made when examining this graph is that the melting efficiency reaches the theoretical maximum value of 0.48 for GMAW and SAW and not for PAW or GTAW. The discrepancies arise because GMAW and SAW processes can attain far greater travel speeds when compared to PAW and GTAW. Melting efficiency in laser beam welding showed results similar to that of arc welding. Fuerschbach measured the melting efficiency for laser beam welding on 1018 steel, tin, and 304 stainless steel using a CO_2 laser. The results are presented in Figure 2- 13. As with DuPont et al with conventional arc welding processes, Fuerschbach

observed that the maximum attainable melting efficiency was 0.48 for laser beam welding under 2-D heat flow conditions.
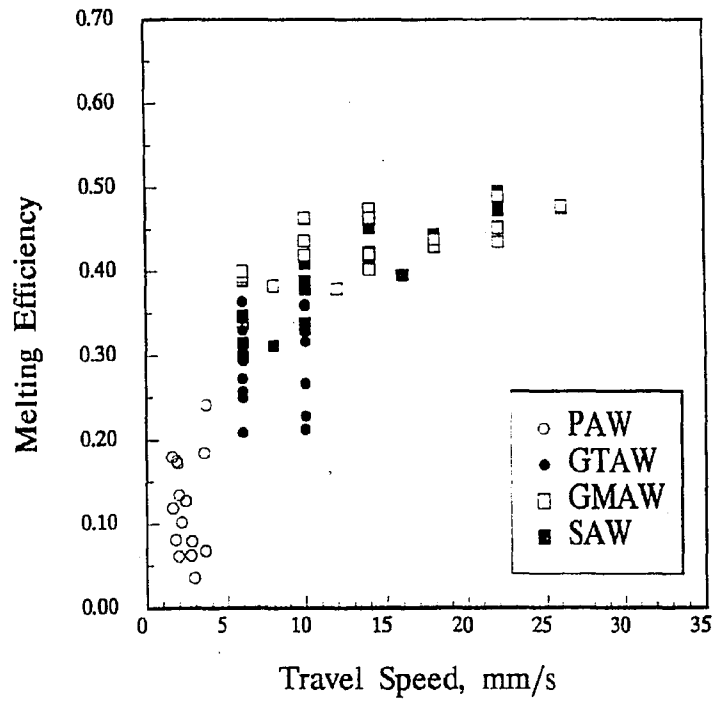
Figure 2- 12. Variation of melting efficiency with travel speed for arc welding processes.
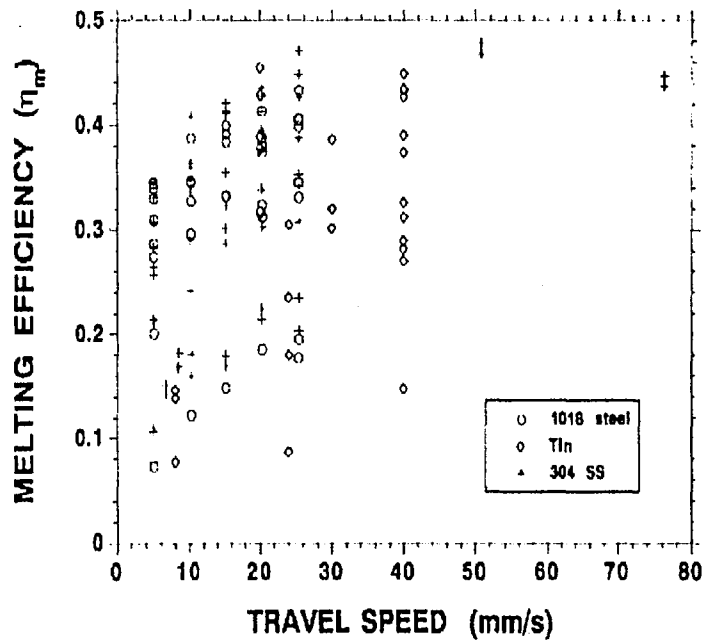
Figure 2- 13. Variation of melting efficiency with travel speed for CO_2 laser beam welding.

2.2.3.1.3 Base Metal Geometry

In order for researchers to formulate theoretical melting efficiency equations, it was important for them consider the cases of 2-D and 3-D heat flow because these heat conditions exist for varying weld joint geometries. The effect of melting efficiency on base metal geometry can be seen in Figure 2- 14. Okada generated this graph from an approximation of melting efficiencies, which were based on Rosenthal's heat flow solutions.[22] The differences can be explained by the 2-D and 3-D heat flow geometry of the substrate. It is apparent the 3-D heat flow condition is more effective in removing heat away from the heat source because there are more avenues for heat conduction when compared to that of the 2-D case. Because there are more heat conduction avenues, the melting efficiency is effectively lowered because heat is rapidly dissipated away from the fusion zone at a much faster rate than it can be used for melting.
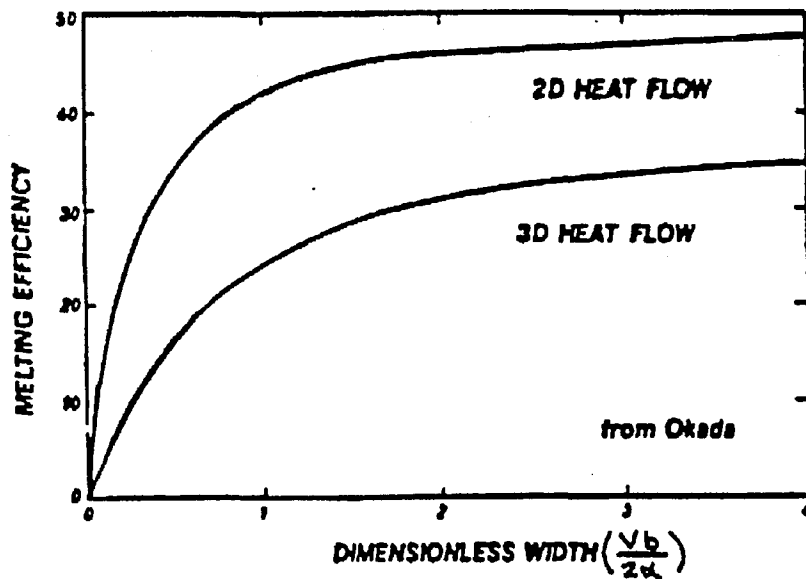
Figure 2- 14. Variation of melting efficiency with 2-D and 3-D heat flow geometry.

2.2.3.1.4 Base Metal Properties

From the examination of Equations [2-11] – [2-17], it is apparent that base metal properties have a strong influence on melting efficiency. Each of these equations incorporates the term α, which is the thermal diffusivity of the base metal. Thermal diffusivity is defined as the ratio of thermal conductivity to the specific heat per unit volume and is an indicator of how effective a material is in transferring energy by conduction rather than storing energy.[22] When welding on materials with a high thermal diffusivity it is expected that greater travel speeds and higher heat inputs are required to attain a high level of melting efficiency. The reason for this is that heat would be transported away from the fusion zone at a faster rate by thermal conduction thereby causing a decrease in melting efficiency if not compensated by the higher heat inputs and higher travel speeds. The effect of base metal diffusivity on melting efficiency can be seen in (Figure 2- 15) for GTAW of 304L stainless steel and Ni 200. The thermal diffusivity of Ni 200 (α=0.220cm/s) is much greater than that of 304L SS (α=0.041cm/s) and thus has a lower melting efficiency for the same processing parameter.
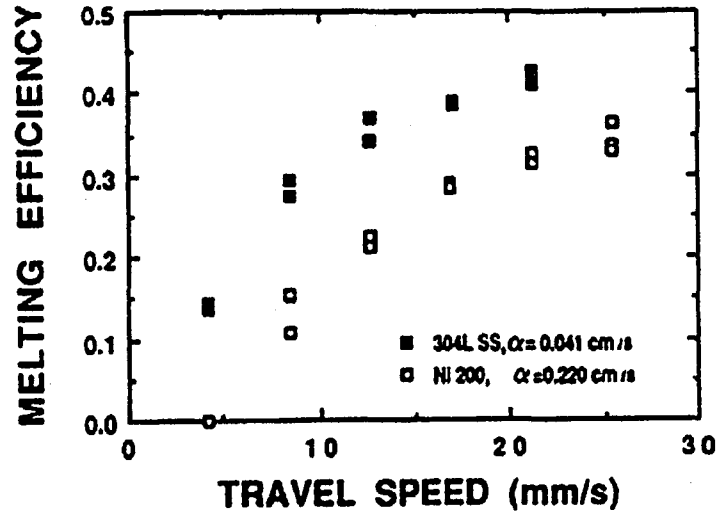
Figure 2- 15. Effect of travel speed and base metal thermal diffusivity on melting efficiency for 304L SS and Ni 200 base metal.

2.2.3.2 Measuring Melting Efficiency

Once the energy transfer efficiency is known for a given set of process variables it is possible to experimentally measure the melting efficiency. This is done through measurements of the cross sectional area of the weld deposit. The cross sectional area of the deposited filler material is multiplied by the total length of the deposit and vise versa for the cross sectional area of the melted substrate. Equation [2-10] can then be manipulated to include terms for melting of the substrate and filler material:

$$\eta_m = \frac{(V_f)\left(\int_{T_o}^{T} C_p(T)dT + \Delta H_f\right)_f + (V_s)\left(\int_{T_o}^{T} C_p(T)dT + \Delta H_f\right)_s}{\eta_a VIt}$$ [2- 18]

36

Where V_f and V_s is the total volume of the melted filler metal and substrate (mm^3). The terms directly adjacent to V_f and V_s correspond to the enthalpy terms for the filler material and the substrate, respectively.

2.2.4 Deposition Efficiency

For consumable welding processes there is a need to know the rate at which filler metal can be deposited to the weld pool under a given set of process parameters. (i.e. deposition rate) Typical deposition rates for the LENS™ system range from 0.25in^3/hr-1in^3/hr.[23] Only a fraction of the powder material that is delivered to the weld pool is actually fused to the substrate to create a metallurgical bond. A term used to describe the ratio of actual deposition rate (i.e., powder that is fused into the melt pool) to the total mass flow rate of powder delivered to the melt pool is the deposition efficiency. Deposition efficiency is given in the following equation as:

$$\eta_d = \frac{A_d}{\left(\dot{V}_{fm} \middle/ S \right)}$$

[2-19]

Where:

A_d = Cross Sectional Area of the Deposit (mm^2)
$\dot{V}_{fm}$ = Volumetric Powder Material Feed Rate (mm^3/s)
S = Travel Speed (mm/s)

This equation explains how to determine the deposition efficiency experimentally; however, it doesn't explain what physically controls the deposition efficiency. Processing parameters such as powder feed rate, melting power ($\eta_a\eta_mP$), and travel speed have a large effect on deposition efficiencies and thus there is a need for an analytical equation

37

to be developed that relates these variables to the deposition efficiency. The deposition efficiency term can be formulated through an energy and mass balance approach, incorporating the use of process efficiency terms, filler metal/substrate material properties, and process variables including: filler metal feed rate, travel speed, and power.

Processing parameters affect the deposition rate because they govern the amount of material that is delivered to the work piece and the quantity of energy that is available to melt the filler material and the substrate to form a metallurgical bond. Figure 2- 16 depicts the effect of powder mass flow rate on deposition/catchment efficiency. For a given laser power and gas flow rate, the deposition efficiency increases with an increase in powder mass flow rate. The researchers from which this work was reviewed indicated that the low values for deposition efficiencies was attributed to poor nozzle and high powder stream divergence.[10]
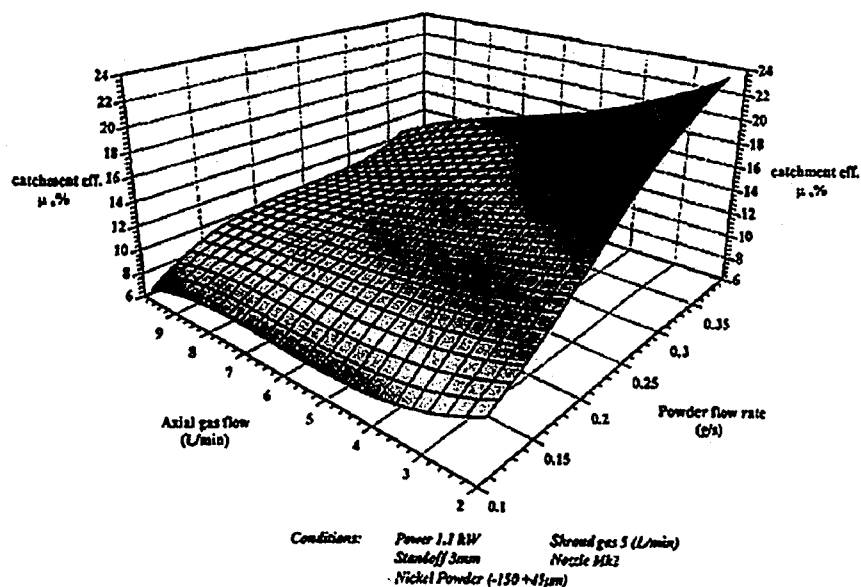
Figure 2- 16. Effect of powder flow rate and axial gas flow on deposition/catchment efficiency.

Further studies have suggested that deposition efficiencies can achieve values as high as 85% under optimal processing conditions and efficient nozzle design. However, a simple factor that may have been overlooked is the ratio of the molten weld pool area to that of the impingement area of the incoming flux of powder. If this ratio is small, a lesser amount of powder can be fused to the workpiece because there is an insufficient amount of energy available to melt the powder. Moreover, a larger weld pool area could conceivably melt more powder material because there is more energy available to melt the incoming powder.

2.2.4.1 Factors Affecting Deposition Efficiency

There are several factors that have an effect on the deposition efficiency for the LENS™ system. The design of the powder delivery system has a large impact on deposition efficiency in that it directs the flow of powder into the weld pool. If for example the nozzles are misaligned, then a fraction of the powders will not be fused to the substrate because a majority of the powder will not even come in contact with the weld pool; thereby causing a decrease in the deposition efficiency.[24] Deposition efficiency can also decrease when particles do not adhere to the substrate in which case they ricochet from the surface of the substrate as depicted in Figure 2- 17. This figure depicts a laser deposition process similar to LENS™ with one main difference: there is only one main powder feed nozzle instead of four. What can be observed from this figure is that the powder is flowing at such high velocities that when it does impinge upon the molten weld pool it still has enough momentum to be deflected from the surface.

Figure 2- 17. Powder deflection from substrate during laser deposition.

2.2.4.2 Measuring Deposition Efficiency

Experimentally, the deposition efficiency can be determined by measuring the cross sectional area of deposited material (A_d) and dividing it by the ideal value of deposited cross sectional overlay given by the ratio of $\dot{V}_{fm}$ /S. Where $\dot{V}_{fm}$ is the volumetric filler metal feed rate and S is the travel speed.

2.2.5 Composition Control

Solid freeform fabrication processes have demonstrated the feasibility of producing functionally graded structures for improved mechanical properties and microstructural tailoring by selectively depositing the powder material that is injected into the molten pool.[25-30] The LENS™ process is one such method. The adaptation of multiple powder feeders in the LENS™ system makes this feasible. Dissimilar powder materials can be placed into separate powder hoppers. Computer software, which is

Figure 2- 17. Powder deflection from substrate during laser deposition.

2.2.4.2 Measuring Deposition Efficiency

Experimentally, the deposition efficiency can be determined by measuring the cross sectional area of deposited material (A_d) and dividing it by the ideal value of deposited cross sectional overlay given by the ratio of $\dot{V}_{fm}$/S. Where $\dot{V}_{fm}$ is the volumetric filler metal feed rate and S is the travel speed.

2.2.5 Composition Control

Solid freeform fabrication processes have demonstrated the feasibility of producing functionally graded structures for improved mechanical properties and microstructural tailoring by selectively depositing the powder material that is injected into the molten pool.[25-30] The LENS™ process is one such method. The adaptation of multiple powder feeders in the LENS™ system makes this feasible. Dissimilar powder materials can be placed into separate powder hoppers. Computer software, which is

40

integrated into the powder feed system, enables the user to precisely control the deposit composition as a function of position. Research on controlling the composition in functionally graded materials is essential. To date, there has been no such research that has been conducted that deals primarily on composition control in the LENS™ process from a process parameter standpoint. Composition in multi-layered fabrication processes can be by controlling the dilution in each pass of the deposit.

2.2.5.1 Dilution

For any welding or surfacing operation that involves the addition of filler metal in the form of an electrode or powder, it is important to select optimal processing parameters to control the properties of the fusion zone and surrounding heat affected zone. A scheme used to control weld metal composition, which incorporates the use of process efficiency terms described in Sections 2.2.2-2.2.4 will be discussed in this section. In welding, filler material is generally added to a weld joint for two reasons: 1) to fill joint geometry and 2) for alloying additions. A term used to describe the degree of base metal and filler metal amalgamation during welding is dilution and it is defined as:

$$D = \frac{A_s}{A_s + A_d} \times 100\%$$

[2-20]

Where:

D $\quad$ = Dilution
A_s = Cross Sectional Area of Melted Substrate (mm^2)
A_d = Cross Sectional Area of Deposited Filler Metal (mm^2)

41

For constant length weld deposits the cross-sectional areas can be multiplied by the weld length to obtain percentage of dilution in terms of weld volumes.

2.2.5.2 Factors Affecting Dilution

The ability to predict dilution levels depends mainly on the ability to predict and control process efficiencies. This concept was the focus of research conducted by DuPont et al.[19] Through a series of power balance equations, DuPont was able to estimate dilution for single pass arc welds in terms of filler metal feed rate, melting enthalpy, power, and process efficiencies. The results are presented below in Equation [2-21].

$$Pct\ D = \left[1 + \frac{\dot{V}_{fm}\Delta H_{m,s}}{\eta_a \eta_m VI - \Delta H_{m,f}\dot{V}_{fm}} \right]^{-1} \times 100 \qquad \text{[2-21]}$$

Where:

$\dot{V}_{fm}$ = Volumetric Melting Rate of the Filler Metal (mm^3/s)
$\Delta H_{m,s}$ = Melting Enthalpy of the Substrate Material (J/mm^3)
$\Delta H_{m,f}$ = Melting Enthalpy of the Filler Metal (J/mm^3)
$\eta_a \eta_m VI$ = Melting Power (Watts)

By analyzing this equation, it is possible to determine the effects of processing parameters on dilution. Both $\Delta H_{m,s}$ and $\Delta H_{m,f}$ are materials properties and thus the only other variables are $\dot{V}_{fm}$ and $\eta_a \eta_m VI$. Let's examine the cases when we hold one constant over the other. If $\dot{V}_{fm}$ were increased, while $\eta_a \eta_m VI$ was held constant, then the level of dilution would decrease. The reason for this is that the filler metal consumes more of the melting energy and less energy is available for melting the substrate. If on the other hand,

$\dot{V}_{fm}$ was held constant and the melting power were increased, there would be enough power to adequately melt the filler metal and the substrate causing an increase in the level of dilution. This effect is shown in Figure 2- 18.
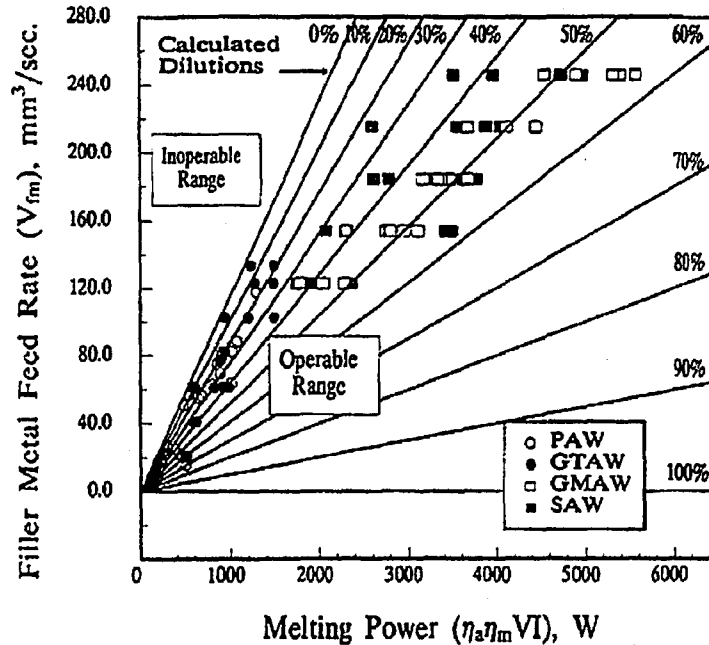
Figure 2- 18. Effect of processing parameters on dilution for conventional arc welding processes.

The diagram in Figure 2- 18 depicts how the level of dilution can be altered for different arc welding processes by varying filler metal feed rate and melting power. Included with the figure are regions, which were deemed operable and inoperable. The operable region indicates the range of melting powers that can be used to create a metallurgical bond for a given filler metal feed rate. Dilution increases with increasing melting power under a fixed filler metal feed rate.[19] For fixed melting power, dilution will decrease when there is an increase in filler metal feed rate. The inoperable region exists when no bonding occurs because there is not enough melting power to adequately form an adhesion between the filler metal and the substrate. In this region there will be no dilution.

Tailoring processing parameters to yield low levels of dilution will increase the build height and the deposition rate. This is key from a manufacturing standpoint whereby more components can be fabrication is a shorter period of time.

2.3 Literature Review Summary

Laser engineered net shaping (LENS™) is a newly emerging rapid prototyping process that has the capability of producing dense, three dimensional, near net-shaped components through the use of CAD models. In an effort to understand the combined effects of LENS™ processing parameters (laser power, travel speed, and powder mass flow rate) on energy transfer efficiency, melting efficiency, deposition efficiency, and dilution it is important know how processing parameters influence process efficiencies. A summary of the effects of laser output power, travel speed, and powder mass flow rate on dilution and process efficiencies can be seen in Table 2- 1.

Table 2- 1. Process Parameter Effects on Process Efficiencies.

Process Variable	η_a	η_m	η_d	Dilution
Laser Input Power (W)	S	S	M	S
Travel Speed (mm/s)	N	S	S	S
Powder Mass Flow Rate (g/min)	U	U	S	S

S= Strong Effect, M=Moderate Effect, N=No Significant Effect, U=Unknown Effect

Travel speed was found to have no effect on energy transfer efficiency for laser beam welding. The level of irradiance (power density) however did affect the transfer

efficiency. Transfer efficiencies were shown to increase with increasing levels of irradiance. No information in the open literature was found on what effects, if any, powder additions into the weld pool had on transfer efficiency. Melting efficiency is dependent upon thermo-physical properties of the substrate as well as laser power and travel speed. The melting efficiency was shown to increase with an increase in the amount of power delivered to the substrate because more energy is made available to melt the underlying substrate. When travel speed is increased, energy is delivered to the work piece at a faster rate than it can be dissipated by thermal conduction, which causes an increase in the melting efficiency. Powder mass flow rate has an unknown effect on melting efficiency. On the other hand, the deposition efficiency is heavily dependent upon powder mass flow rate and travel speed since these process variables govern how much material is deposited over time. Dilution was found to be strongly dependent upon the combination of laser power, travel speed, and powder mass flow rate processing parameters.

2.4 Research Objectives

The objectives of this research are as follows:

- Measure laser energy transfer efficiency (η_a), melting efficiency (η_m), deposition efficiency (η_d), and dilution under a matrix of operating parameters.

- Develop a semi-empirical model that can be used to predict melting efficiency for the LENS™ process.

- Compare melting efficiency data to the semi-empirical model and available predictive models found in literature.

- Develop an analytical expression that relates the deposition efficiency to processing parameters such as powder mass flow rate, melting power ($\eta_a\eta_m P$), and travel speed.

- Compare dilution data to available predictive models.

- Develop a scheme to model dilution in multipass LENS™ deposits.

3.0 EXPERIMENTAL PROCEDURE

The following experimental procedure section is subdivided into four sections: 1) materials selection, 2) equipment, 3) experimental design matrix/methodology, and 4) measurement techniques. The first section describes the selection of materials used in this study. The second section describes the components of the laser deposition equipment and how it was used to fabricate samples for process efficiency measurements. The third section describes the experimental design matrix as well as the manner in which it was generated. Lastly, the laboratory techniques used to measure laser energy transfer efficiency, melting efficiency, deposition efficiency, and dilution is presented.

3.1 Materials Selection

A metal-metal functionally graded material that has gained interest in the tool and die industry is H-13 tool steel to copper. The main applications are injection molding tools and dies with tool steel contributing to wear resistance and toughness whereas copper facilitates heat removal from the part during production. The microstructure and properties of laser deposited H-13 tool steel has been studied by Mazumder et al.[31] Their results indicate that the microstructure of the solidified structure consists primarily of tempered martensite with some retained austenite. Maziasz has shown similar results.[32] Further research is however needed for microstructural characterization of the graded H-13/Cu structure. From the past research conducted on the laser deposition of H-13 tool steel for injection molding dies, H-13 tool steel and copper were selected as a model material system in the examination of processing parameter effects on process efficiencies and composition control of functionally graded structures.

47

3.2 Laser Deposition Equipment

The laser deposition equipment used in this study was the LENS™ 750 Directed

Metal Deposition System (DMDS) manufactured by Optomec Design Company. The

LENS™ 750 equipment is shown in Figure 3- 1. The LENS™ system utilizes a 750 watt,

continuous wave (CW), Nd:YAG laser as its energy source to create a molten pool into

which powder material is deposited.

Figure 3- 1. LENS™ 750 Directed Metal Deposition System (DMDS) laser deposition
equipment used in this study of process efficiencies at Lehigh University.

Powder material is delivered to the molten weld pool via two separate powder feeders

which can be operated one at a time or simultaneously. To fabricate a component, a CAD

model is first developed of a given part geometry. A substrate is fastened to the fixture

plate on the x-y stage and the component is built in a line-by-line, layer-by-layer manner that is dictated by the geometry of the CAD model.

3.3 Experimental Design Matrix/Methodology

To evaluate the effects of processing parameters on LENS™ process efficiencies, an experimental design matrix was developed in order to test the full processing capabilities of the LENS™ 750 system. The processing parameters were chosen based on the capability limits of the system.

The maximum attainable laser power at the substrate's surface was measured to be approximately 500 watts (W) with a laser power meter from Kentek. Note: the laser power meter from Kentek is accurate within ± 5%. The working envelope of this system is thus laser powers up to 500W. The specifications for laser output power of the Nd:YAG laser used in this study is 750W. The nearly 66% loss in laser power from the laser head to the substrate is attributed to power losses through the optics of the laser beam delivery system. Four laser output powers were used in this study and they were chosen in 125W increments, yielding the following laser powers to be tested: 125W, 250W, 375W, and 500W.

In the LENS™ system travel speed refers to the traverse velocity of the x-y stage. Preliminary testing has shown that above 35mm/s an unsuitable deposit is formed regardless of the laser input power and powder mass flow rate. Four travel speeds were chosen in 5mm/s increments, yielding the following travel speeds to be tested: 5, 15, 25, and 35mm/s.

The powder feed mechanism consists of a vertical, gravity fed powder hopper that feeds powder material to a rotating disc which in turn lifts the powder to a constant

supply of argon carrier gas that delivers the powder to the nozzles and then on to the melt pool. Controlling the motor speed of the rotating disc controls powder mass flow rates. The range of motor speeds was from 0-20 RPM. Different powders flow differently because of particle size distribution and density; therefore, for the H-13 tool steel and copper powder used in this study powder mass flow rates were calibrated to the motor speed RPM.

3.4 Laser Energy Transfer Efficiency Measurements

Laser energy transfer efficiency was measured for the LENS™ process using a Thermonetics Seebeck envelope calorimeter. The calorimeter works on the gradient layer principle whereby a voltage output signal is generated by a temperature difference through a series of heat flux transducers that line the inner chamber walls of the calorimeter. The experimental setup of the Thermonetics Seebeck envelope calorimeter inside of the LENS™ workstation can be seen in Figure 3- 2. The calorimeter itself is labeled **a** in the figure.

After a sample is prepared, it is quickly placed in the calorimeter and the lid is immediately closed. The sample is allowed to equilibrate to the temperature of the constant temperature water bath. For this study, a NESLAB HX300 recirculating chiller was used to flow a constant supply (flow rate of 100cc/min) of water at 25°C. A National Instruments data acquisition (DAQ) system, utilizing LabVIEW 6.0i, an instrumentation amplifier, and a PC was interfaced with the calorimeter to acquire the output voltage signal as a function of time. A typical output signal during an actual measurement is shown in Figure 3-3.
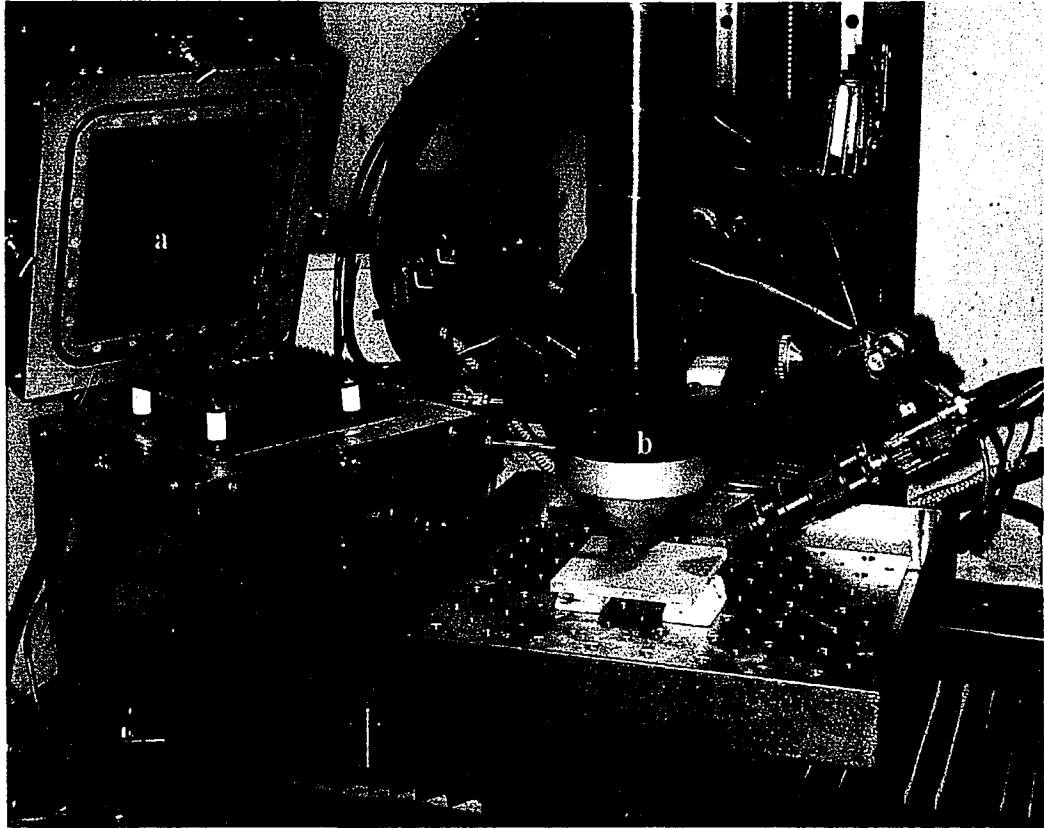
Figure 3- 2. Experimental setup of Seebeck envelope calorimeter used for energy transfer efficiency measurements. a) Seebeck envelope calorimeter, b) laser delivery system, c) substrate, and d) ccd camera for weld pool monitoring.
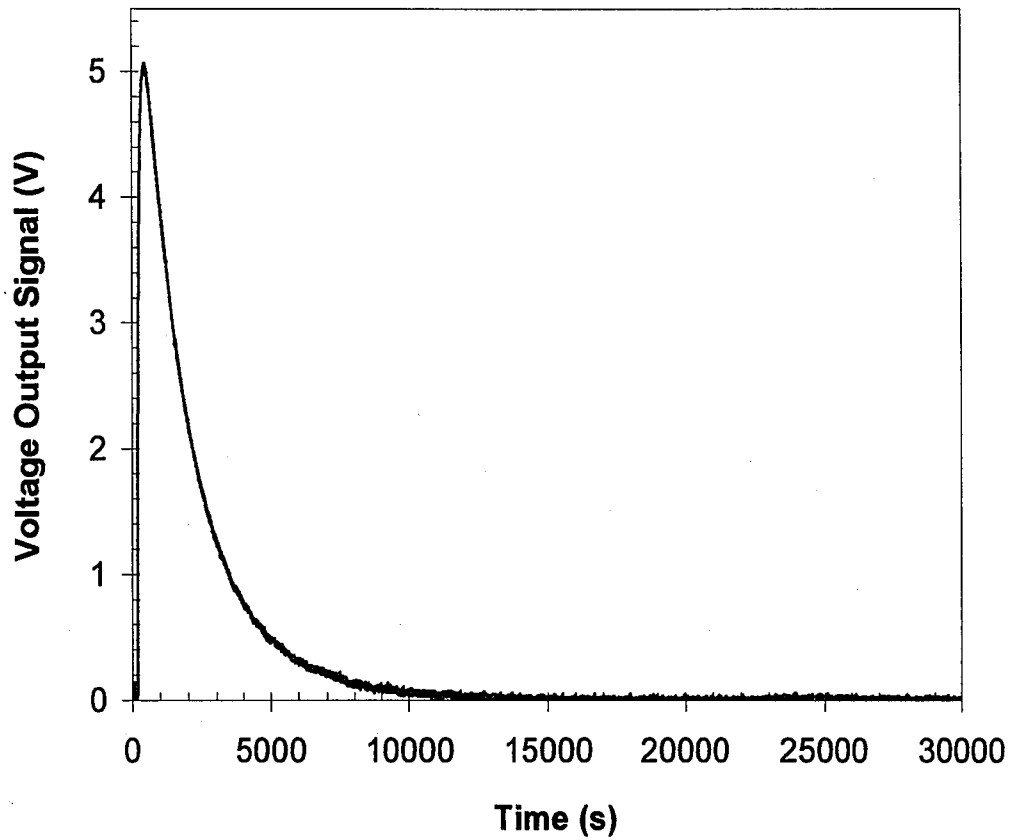
Figure 3- 3. Typical output voltage signal from the Seebeck envelope calorimeter during energy transfer efficiency measurements.

The calorimeter was calibrated by placing a resistive heater inside the calorimeter and inducing a known voltage across the heating element with a constant voltage power supply. An ammeter was placed in series with the circuit to measure the resultant current that was imposed on the heater by the constant voltage power supply. By knowing the voltage and current it was possible to calculate the input power across the resistive heater. Different input powers were used to measure the output voltage signal from the calorimeter at steady state. A plot of input power versus output voltage can be seen in Figure 3- 4. The slope of the plot yields the calibration constant that, when multiplied by the voltage output signal, yields the corresponding output voltage value in watts.
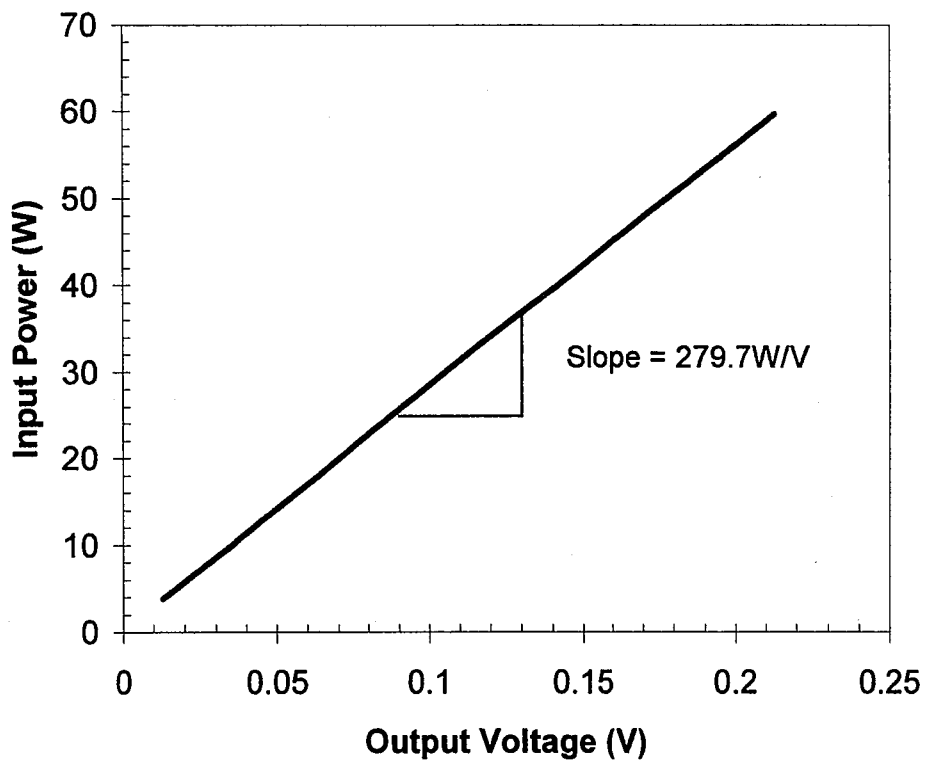
Figure 3- 4. Plot of input power versus output voltage for calorimeter calibration
Note: With amplifier calibration constant was 0.598W/V

To measure the amount of energy that is transferred from the laser beam and absorbed by the substrate, the LENS™ process was used to produce single pass 1) bead on plate autogenous welds, 2) deposits of H-13 tool steel, and 3) deposits of copper powder under the combination of processing parameters shown in Table 3-1.

Table 3- 1. Experimental test matrix of processing parameters used in laser energy transfer efficiency measurements.

Material	Laser Power (W)	Travel Speed (mm/s)	Powder Flow Rate (g/s)
Autogenous	125-500	5,15	---
H-13 Tool Steel	125-500	5,15	0.08-0.33
Copper	250-500	5,15	0.11-0.22

The substrate material upon which laser welds and deposits were made was ¼ inch thick H-13 tool steel substrates that were cut into 4 x 4 inch test specimens. The test specimens were placed upon insulating ceramic bricks during welding/deposition so as to avoid heat loss from the sample through the metal fixture plate. By doing this, it is possible to retain the heat absorbed by the substrate so that more accurate measurements may be obtained. Also, by depositing single pass "bead on plate" deposits it was possible to simplify the layer additive process by concentrating on only the main variables (laser power, travel speed, and powder mass flow rate) while disregarding other processing variables such as hatch angle, hatch spacing, beam offset, etc. of which are used to deposit larger 3-D structures.

After the weld/deposit was made on the substrate, the test specimen was immediately placed into the calorimeter and allowed to cool to the temperature of the

constant supply of cooling water. Average transfer times of 2-3 seconds elapsed between welding/deposition and the placement of the sample into the calorimeter. The total heat content absorbed by the substrate (E_{cal}) was determined by integrating the resultant output voltage vs. time signal then multiplying that quantity by the calibration constant. Laser energy transfer efficiency (η_a) was then calculated by the following equation.

$$\eta_a = \frac{E_{cal}}{Pt}$$
[3- 1]

Where:
    E_{cal} = Total Energy Absorbed by the Workpiece (J)
    P   = Laser Output Power (W or J/s)
    t   = Laser "on time" (s)

Prior to each energy transfer efficiency measurement; the laser power was measured using a laser power meter by Kentek to have an accurate value of the laser output power. Laser "on time" was found by dividing the total deposit length by the travel speed. The deposition pattern was in the shape of a rectangular with a total length of 7 inches. This was done to increase the heat input into the test specimen so a greater output voltage signal could be measured with the amplifier at maximum gain. Energy losses due to convection, radiation, and evaporation were found to be less than 1% for this type of calorimetry experiments.[15]

As previously mentioned in Section 2.2.2.1, surface conditions have an affect on laser energy transfer efficiency; therefore, in order to examine the effects of surface roughness on laser beam absorption the H-13 tool steel substrates were prepared by first

performing a grinding operation with 120 grit sandpaper to remove mill scale, surface scratches, and any other irregularities that were present on the outer extremities of the material in the as received condition. The substrates were then grit blasted with 120 grit Al_2O_3 to obtain a more uniform surface finish. These substrates were then used for energy transfer efficiency measurements. A select set of substrates were set aside and prepared in such a manner that mimics the surface topography of an actual LENS™ deposit. This was accomplished by cladding an entire substrate with H-13 tool steel powder in a single layer then energy transfer efficiency measurements were made by rastering the laser 90° to the cladding direction. An optical profilometer was used to measure the root-mean-square (σ_m) surface roughness of the 120 grit blasted substrates as well as the cladded substrates. A 3x3mm area was scanned across representative grit blasted and clad substrates at a step size of 5μm to measure height fluctuations. From the resulting profiles, σ_m was measured.

3.5 Melting Efficiency Measurements

Single pass H-13 tool steel and copper deposits were made on the grit blasted substrates under the matrix of processing parameters presented in Table 3-2 and Table 3-3, respectively.

Table 3- 2. Experimental test matrix of processing parameters used in melting efficiency measurements of H-13 tool steel deposits on H-13 tool steel substrates.

Power (W)	Travel Speed (mm/s)	Powder Flow Rate (g/s)	Volumetric Flow Rate (mm^3/s)
125-500	5-35	0.08-0.33	11.2-42.5

Table 3- 3. Experimental test matrix of processing parameters used in melting efficiency measurements of copper deposits on H-13 tool steel substrates.

Power (W)	Travel Speed (mm/s)	Powder Flow Rate (g/s)	Volumetric Flow Rate (mm^3/s)
250-500	5-15	0.11-0.22	12.4-24.7

Macroscopic observations of the 3.5 inch deposits showed that they were uniform and thus sectioning the deposit perpendicular to the deposit direction at 1.75 inches into the deposit yielded a cross section that would be representative of the entire deposit length. The weld cross sections were mounted in epoxy, polished to a 1μm diamond finish, then etched with 2% Nital. Image analysis was then performed with the LECO 3001 Quantitative Image Analysis (QIA) system to measure the cross sectional area of the deposit (A_d) and melted substrate (A_s) as shown in Figure 3- 5.
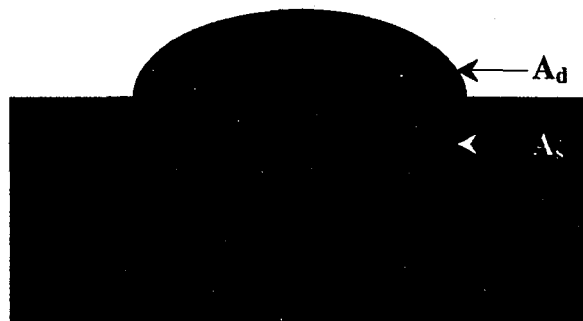
Figure 3- 5. Schematic illustration of weld cross sectional area for dilution measurements. (A_d-deposit cross sectional area. A_s- melted substrate cross sectional area)

57

From the deposit cross sectional areas of the melted substrate and the deposit, the melting efficiency (η_m) was calculated from the following equation:

$$\eta_m = \frac{(V_d)\left(\int_{T_o}^{T} C_p(T)dT + \Delta H_f\right)_d + (V_s)\left(\int_{T_o}^{T} C_p(T)dT + \Delta H_f\right)_s}{\eta_a Pt}$$ [3-2]

Where V_d and V_s is the total volume of the deposited filler metal and substrate (mm^3), respectively. V_d and V_s were determined by multiplying the cross sectional area of the deposit and the substrate by the deposit length. The terms directly adjacent to V_d and V_s in parentheses correspond to the melting enthalpy terms for the deposit and the substrate, respectively, where C_p is the specific heat and ΔH_f is the latent heat of fusion. For the H-13 tool steel powder deposited on the H-13 tool steel substrate the melting enthalpy (which is defined as the energy required to raise the temperature of the material above its melting temperature plus the latent heat of fusion) of the deposit and the substrate are the same since they are of the same material, 10.5 J/mm^3.[33] The copper deposits on the H-13 tool steel substrates on the other hand, have different melting enthalpies because they are different materials. Therefore, values of 10.5 J/mm^3 and 5.9J/mm^3 were used to calculate melting efficiency for the H-13 tool steel substrate and copper deposits, respectively.[33]

Note that the laser energy transfer efficiency term is incorporated into the denominator of Equation [3-2]. To make melting efficiency measurements accurate, it is important to have values of laser energy transfer efficiency for the same set of processing

58

variables. Therefore, the results of energy transfer efficiency measurements, as described in Section 3.4, were used for melting efficiency calculations.

3.6 Deposition Efficiency Measurements

Deposition efficiency (η_d) was experimentally determined from measurements of deposit cross sectional areas by quantitative image analysis as described in Section 3.5. The deposition efficiency was then calculated from the following equation:

$$\eta_d = \frac{A_d}{\left(\dfrac{\dot{V}_{fm}}{S}\right)}$$

[3- 3]

The deposits cross sectional area A_d term was divided by the ideal value of material deposited, which is given by the ratio $\dot{V}_{fm}/S$, where $\dot{V}_{fm}$ is the volumetric filler metal feed rate and S is the travel speed. The ideal value is indicative of the total weld deposited assuming that all of the powder delivered to the weld pool adheres to the substrate.

During the deposition of each deposit in the experimental matrix, a color CCD camera was used to record images of the interaction between the powder material and the molten weld pool. This information was then used to observe the manner in which powder material is fused to the substrate to form a deposit.

3.7 Dilution Measurements

Single pass dilution measurements were conducted on samples of the H-13 tool steel and copper deposits used in melting efficiency and deposition efficiency

59

measurements. Dilution was calculated from geometric measurements of deposit cross sectional areas and melted substrate cross sectional areas by the following equation:

$$\%D = \frac{A_s}{A_s + A_d} \times 100$$

[3-4]

Where:

D = Dilution
A_s = Melted Substrate Cross Sectional Area (mm^2)
A_d = Deposit Cross Sectional Area (mm^2)

4.0 RESULTS & DISCUSSION

4.1 Laser Energy Transfer Efficiency

The results of laser energy transfer efficiency measurements are shown in plots of laser energy transfer efficiency as a function of laser output power for autogenous laser welds and deposits of H-13 tool steel and copper powder on grit blasted H-13 tool steel substrates. Figures 4-1 and 4-2 correspond to weld/deposits made at travel speeds of 5mm/s and 15mm/s, respectively. Within each plot there are several energy transfer efficiency measurements for each value of laser output power tested. At the lowest laser output power (125W), there are only three measurements and they correspond to autogenous laser welds and deposits of H-13 tool steel powder at two different powder mass flow rates (0.08g/s and 0.17g/s). The remaining laser output powers (250, 375, and 500W) tested each have five energy transfer efficiency measurements, corresponding to autogenous laser welds, deposits of H-13 tool steel powder at two different powder mass flow rates (0.08g/s and 0.17g/s), and deposits of copper powder at two different powder mass flow rates as well (0.11g/s and 0.17g/s). Autogenous laser welding was used to establish baseline values of η_a solely as a function of laser output power and travel speed for the cw Nd:YAG laser used in the study. From that, a comparison was made between the baseline measurements and measurements that incorporate powder material into the weld pool in order to determine what effect, if any, powder mass additions have on laser energy transfer efficiency.

61
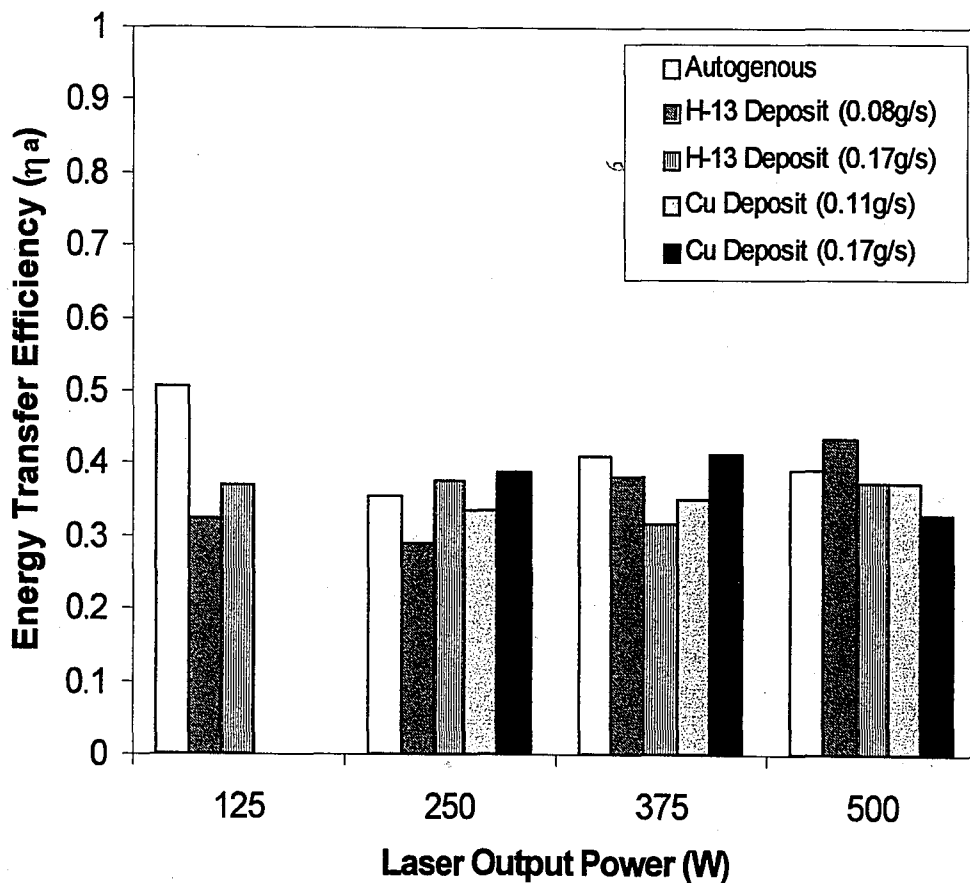
Figure 4- 1. Plot of energy transfer efficiency measurements as a function of laser beam irradiance for autogenous laser welds and H-13 tool steel and copper powder deposits on grit blasted H-13 tool steel substrates. (Travel Speed 5mm/s)
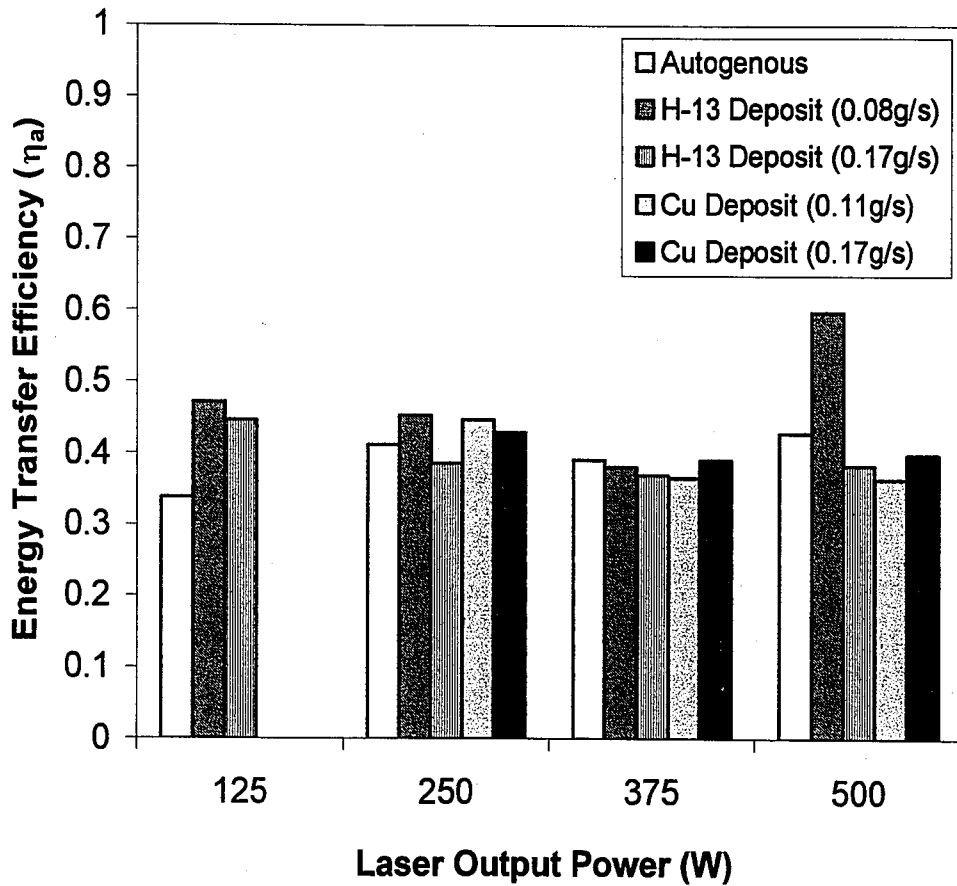
Figure 4- 2. Plot of energy transfer efficiency measurements as a function of laser beam irradiance for autogenous laser welds and H-13 tool steel and copper powder deposits on grit blasted H-13 tool steel substrates. (Travel Speed 15mm/s)

From the range of processing parameters tested, the resulting laser energy transfer efficiency measurements ranged between 30 and 50%. This indicated that more than half of the incident laser energy is never transferred to the substrate. A direct comparison between results found in this study and published results in the open literature could not be made since there have been no reported results of energy transfer efficiency measurements on a Nd:YAG or laser deposition process that include powder mass additions into the molten pool. As indicated in the introduction section, there are many factors that can affect laser beam absorption. The following sections highlight some probable causes of laser beam loss from a materials and processing standpoint.

4.1.1 Effect of Processing Parameters on Energy Transfer Efficiency

Laser beam irradiance is known to have a large effect on energy transfer efficiency. At higher levels of beam irradiance increased absorption occurs by the formation of a depressed keyhole like cavity. This absorption mechanism yields high η_a because laser light is effectively absorbed by the vapour column and weld pool cavity, which minimizes laser beam reflective losses because of the occurrence of multiple internal reflections within the cavity.[11] Laser deposition under these conditions would prove to be detrimental to part build up during LENS™ processing since previously deposited layers will be destroyed and part tolerance will subsequently be unattainable. Laser beam irradiance is determined by dividing the laser power by the laser beam spot size. The deposits were all made at the same focal length; therefore, the spot size is the same for each. Thus, increasing laser beam irradiance is the same as increasing laser output power.

From Figures 4-1 and 4-2, it can be seen that under the range of laser output powers/irradiance tested, there was no dramatic increase in energy transfer efficiency. This suggested that the levels of irradiance used in the laser deposition process are less than that required to initiate keyhole cavity formation. Further examination of the weld pool geometries by light optical microscopy of weld cross sections showed a semi-circular weld pool geometry, which is indicative of conduction mode and not keyhole mode of welding. A representative photomicrograph can be seen in Figure 4- 3 for a deposit made at a laser output power of 500W, travel speed of 5mm/s, and powder mass flow rate of 0.08g/s.

Figure 4- 3. Photomicrograph of H-13 tool steel deposited on an H-13 tool steel substrate.

Travel speed has been shown to have no effect on energy transfer efficiency.[11] Fuerschbach indicated that precision error was the probable cause of scatter since no discernible trend could be found as travel speed was varied. Some scatter did however exist in this study when energy transfer efficiency was measured at travel speeds of 5mm/s and 15mm/s, while holding all other variables constant. The variances may be the result of the time it took to process the samples before they were placed in the calorimeter

From Figures 4-1 and 4-2, it can be seen that under the range of laser output powers/irradiance tested, there was no dramatic increase in energy transfer efficiency. This suggested that the levels of irradiance used in the laser deposition process are less than that required to initiate keyhole cavity formation. Further examination of the weld pool geometries by light optical microscopy of weld cross sections showed a semi-circular weld pool geometry, which is indicative of conduction mode and not keyhole mode of welding. A representative photomicrograph can be seen in Figure 4- 3 for a deposit made at a laser output power of 500W, travel speed of 5mm/s, and powder mass flow rate of 0.08g/s.

Figure 4- 3. Photomicrograph of H-13 tool steel deposited on an H-13 tool steel substrate.

Travel speed has been shown to have no effect on energy transfer efficiency.[11] Fuerschbach indicated that precision error was the probable cause of scatter since no discernible trend could be found as travel speed was varied. Some scatter did however exist in this study when energy transfer efficiency was measured at travel speeds of 5mm/s and 15mm/s, while holding all other variables constant. The variances may be the result of the time it took to process the samples before they were placed in the calorimeter

for measurements. At the higher travel speed the total laser on time was approximately 11.85 second, while at the lower travel speed the total on time was 35.56 seconds. At the slower travel speed, it took nearly 3x as much time to produce a sample. During this time, heat that is transferred throughout the sample by conduction may escape from the sample's surface by convection. Although a significant amount of heat is retained within the sample, it stands to reason that slight deviations among data points may be attributed to the loss of heat from the sample before it can be measured. However, calorimetric studies done on energy transfer efficiency measurements indicate that there is only about a 1% loss in heat from the time the sample is welded to the time it is placed within the calorimeter.[15] From this standpoint, it was concluded that variance among data points is the result of precision error and not due to changes as a result of varying travel speed.

The LENS™ system is unique to other laser welding processes in that powder material is incorporated into the weld pool for laser deposition. An increase in laser beam absorption would indicate that the incoming powder is readily absorbed by the laser beam and the energy is effectively transferred to the workpiece with minimal losses to the surroundings. Moreover, a decrease in laser beam absorption would indicate that the laser light is reflected off of the powder particles and thus energy would not be efficiently transferred to the substrate. Laser energy transfer efficiency values appear to be relatively insensitive to changes in powder mass flow rates. This can be seen in Figure 4- 4 in a plot of energy transfer efficiency as a function of heat input for autogenous laser welds and H-13 tool steel and copper powder deposits at two different powder flow rates. Heat input is defined as the quantity of energy incident upon the workpiece per unit length of deposit and is given by the ratio of input power to travel

speed. Energy transfer efficiency was plotted as a function of heat input so as to normalize the effects of power and travel speed. No trend is observed that would suggest any influence of powder additions on laser beam absorption
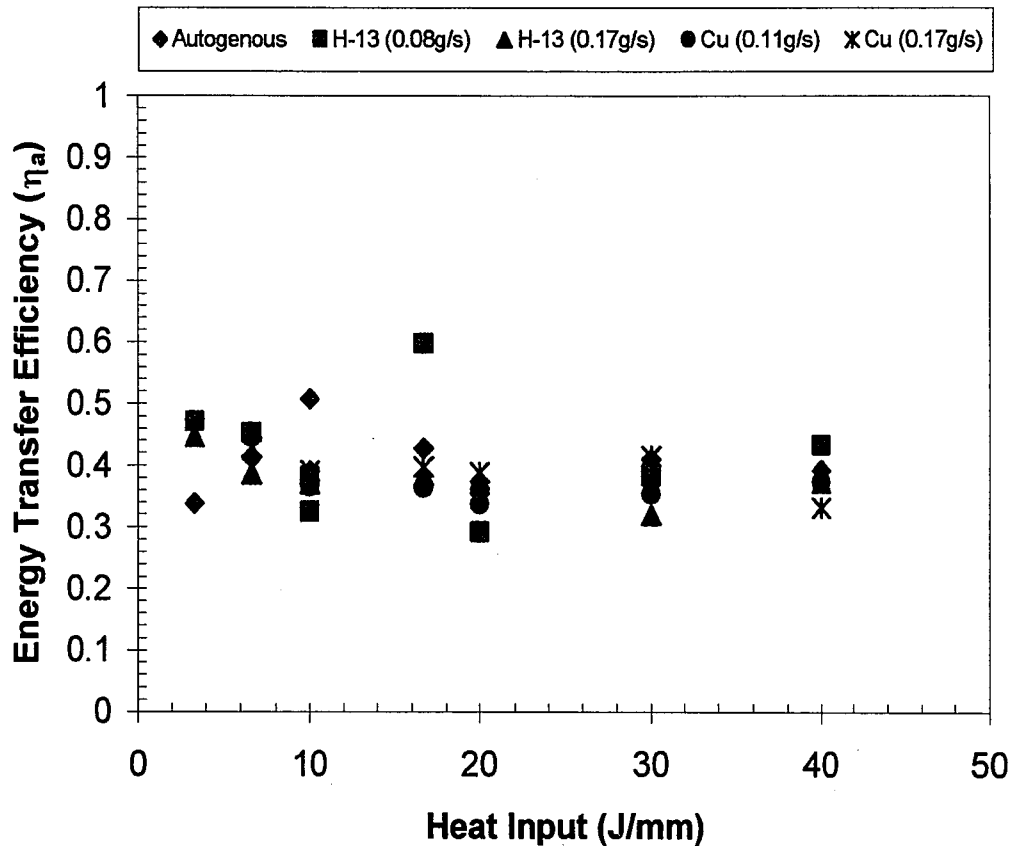
Figure 4- 4. Plot of energy transfer efficiency as a function of heat input for varying powder mass flow rates.

4.1.2 Material Effects on Energy Transfer Efficiency

Aside from processing parameters, laser beam absorption is also heavily dependent upon the type of material that is to be deposited. The materials used in this study have varying optical reflectivity. Copper has a higher reflectivity than the tool steel; therefore, one would expect that depositing copper powder would decrease the energy transfer efficiency if laser light could reflect off the surfaces of the individual powder particles that come in contact with the laser beam. The section above showed how

powder mass additions had no effect on energy transfer efficiency. The type of powder delivered to the weld pool also appeared to have no effect on energy transfer efficiency. This can also be seen in

Figure 4- 4, where energy transfer efficiency is plotted as a function of heat input at the same powder mass flow rate for the H-13 tool steel powder and the copper powder. These results suggest that powder mass flow rate and the type of powder delivered to the weld pool have no significant effect on energy transfer efficiency. Thus, it appears that only the substrate material governs energy transfer efficiency because a larger portion of laser light actually interacts with the substrate material rather than with the individual powder particles. If for example, copper substrates were used in this study, it is expected that the energy transfer efficiency would be significantly lower than what was measured for the steel substrates regardless of the type of powder deposited. This is due to the inherently high optical reflectivity of copper.

4.1.3 Effect of Surface Roughness on Energy Transfer Efficiency

3-D images taken from surfaces of the grit (120 grit Al_2O_3) blasted and clad H-13 tool steel substrates with the optical profilometer are shown in Figures 4-5 and Figures 4-6, respectively. The surface profile from the grit blasted substrate shows a uniform dimpled appearance, which corresponds to surface depressions that occurred from the impact of the 120 grit Al_2O_3 particles as they impinged upon the substrate. The clad substrate on the other hand shows a series of peaks and valleys, corresponding to the outline of deposit traces. The measured root-mean-square surface roughness of the grit blasted and clad substrates were 220μm and 330μm, respectively.
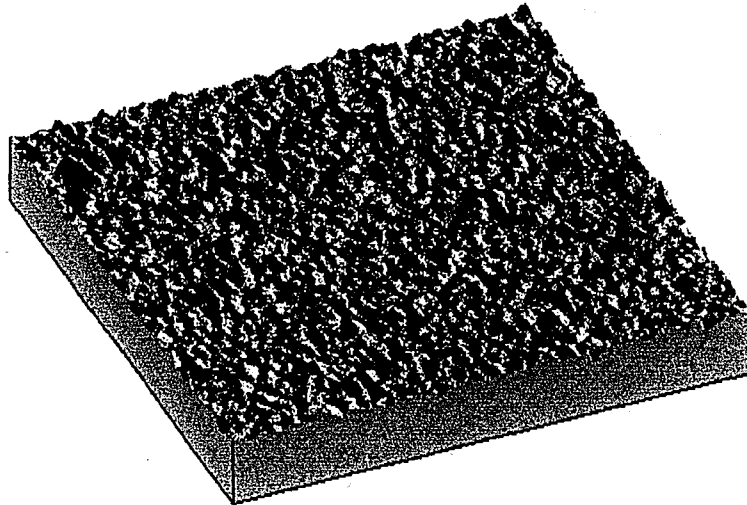
Figure 4- 5. 3-D image from the surface of grit (120 grit Al_2O_3) blasted H-13 tool steel substrates used in the measurement of energy transfer efficiency in the LENS™ process. (σ_m=220μm)
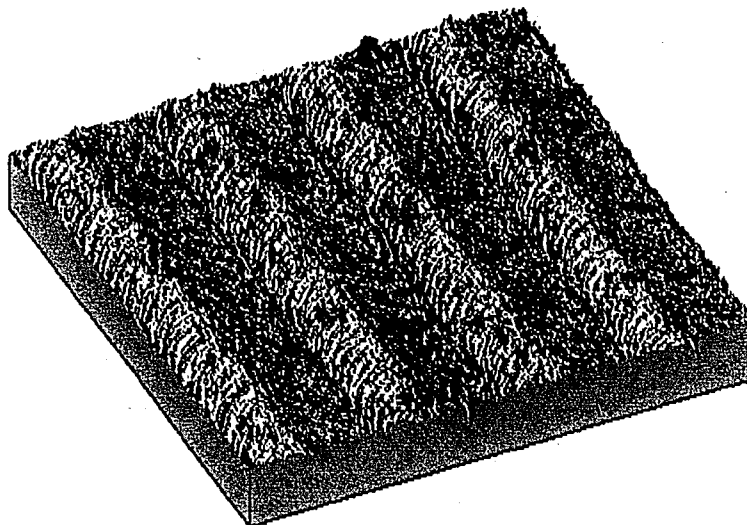
Figure 4- 6. 3-D image from the surface of H-13 tool steel powder clad onto a H-13 tool steel substrates used to evaluate surface roughness effects on energy transfer efficiency in the LENS™ process. (σ_m=330μm)

To evaluate the effect of surface roughness on energy transfer efficiency, autogenous laser welds were made on the substrates at 5mm/s while varying laser output power. Powder deposition was not used in the study so as to eliminate one more variable. The results of energy transfer efficiency measurements of the clad and unclad substrates are shown in Figure 4- 7. While the energy transfer efficiency measurements for the grit blasted substrates were slightly higher than the clad substrates, the differences are small. The results are expected to be similar because once a stable weld pool is formed; surface roughness should have no effect on laser beam absorption. From that in itself, it stands to reason that the energy transfer efficiency of the clad and unclad substrates should be relatively equal for each laser beam irradiance tested. The largest difference (37%) occurred at a laser power of 375W while the smallest difference (4%) occurred at the highest beam irradiance tested 500W. An average difference for all measurements was 15%. Since there were only four data points to compare to no finite conclusion about the effects of surface roughness on laser beam coupling can be made without further experimentation.
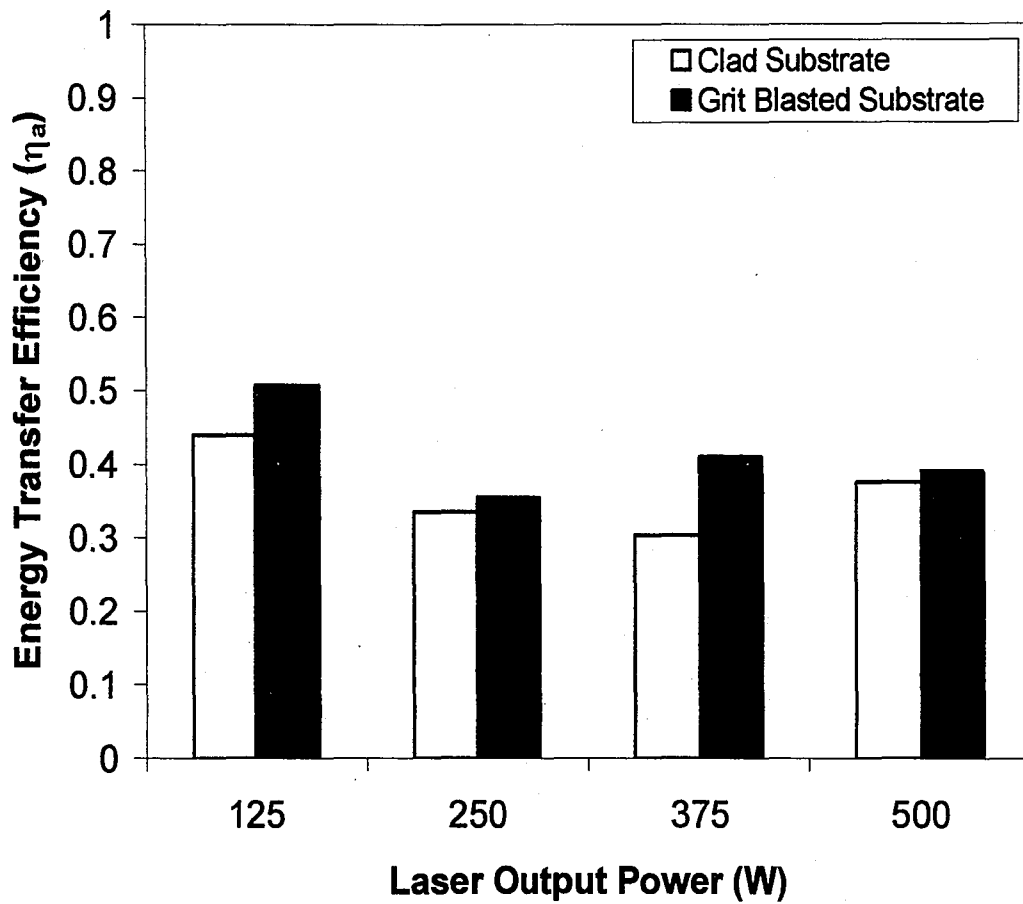
Figure 4- 7. Plot of energy transfer efficiency as a function of laser output power for clad and unclad substrates that were used to evaluate the effect of surface roughness on laser beam coupling.

4.2 Melting Efficiency

From the total energy that is transferred to the workpiece, only a small fraction of it is used to create and maintain a molten pool by melting a localized region of the workpiece (i.e. melting efficiency). For laser deposition processes to be efficient, the total energy transferred from the energy source to the workpiece must posses enough energy to melt the underlying substrate and the incoming powder flux. The melting efficiency is affected by processing parameters, material thermophysical properties, and heat flow conditions. In this study, the heat flow conditions were entirely 3-D since the weld pool penetration depths of the deposits were significantly less than the substrate thickness. Results from the calorimetric study on energy transfer efficiency indicated that laser absorption was relatively insensitive to the range of processing parameters tested. Therefore, an average laser energy transfer efficiency value of 0.4 was used to determine melting efficiency from geometric cross sectional area measurements and Equation [3-2].

4.2.1 Effect of Processing Parameters on Melting Efficiency

The effect of processing parameters on melting efficiency was examined for the entire test matrix of H-13 tool steel single pass deposits. The effect of laser input power on melting efficiency is displayed in Figure 4- 8. It should be noted that the laser input power is implied to be the actual power delivered to and absorbed by the workpiece. Thus, the laser input power was calculated by multiplying laser output power by an average value of energy transfer efficiency, 0.4. A trend is revealed which shows how melting efficiency increases with increasing laser input power. A maximum is reached at a melting efficiency of approximately 0.33 and then tapers off at the highest input power.

72

These results are to be expected since the theoretical maximum for 3-D heat flow conditions is 0.37.[18]
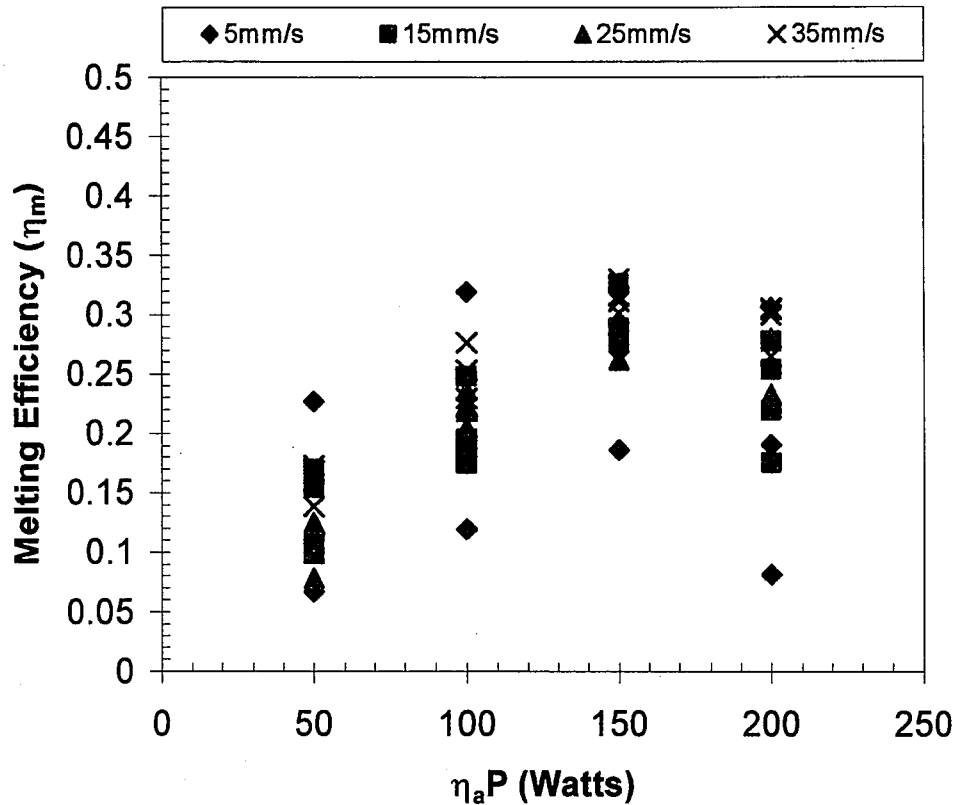
Figure 4- 8. Melting efficiency as a function of laser input power for varying travel speeds and powder mass flow rates.

Melting efficiency increases with the increasing rate of energy (i.e. laser input power) delivered to the workpiece. When energy is distributed to a localized region at a faster rate, there is less time available for the energy to be transported away from the weld region by thermal conduction to the surrounding material. If all other processing variables were held constant, then increasing the laser power alone would cause an increase in melting efficiency because there is a greater amount of energy available to melt the incoming powder and the underlying substrate. This can be seen in Figure 4- 9 a-c, which displays deposit cross sectional micrographs for varying laser input powers at a

constant travel speed (5mm/s) and powder mass flow rate (0.17g/s). Note: melting efficiency and deposit cross sectional area increase as laser input power increases.

a)

$\eta_a P = 50W$
$\eta_m = 0.16$
$A = 0.05mm^2$

b)

$\eta_a P = 100W$
$\eta_m = 0.25$
$A = 0.11mm^2$

c)

$\eta_a P = 150W$
$\eta_m = 0.27$
$A = 0.27mm^2$
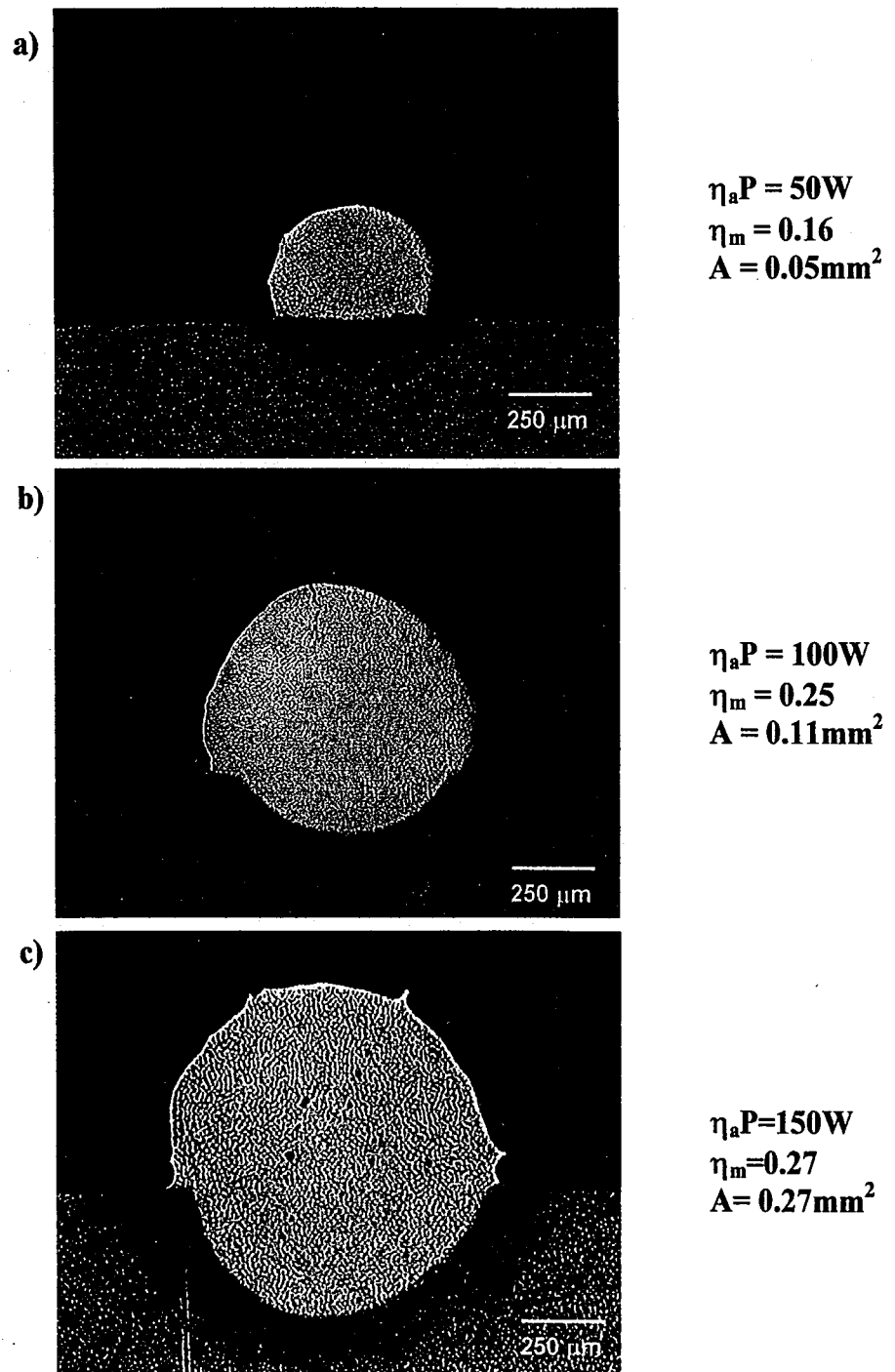
Figure 4- 9. Effect of laser input power on melting efficiency and deposit cross sectional area. (Travel speed of 5mm/s and powder mass flow rate of 0.17g/s)

constant travel speed (5mm/s) and powder mass flow rate (0.17g/s). Note: melting efficiency and deposit cross sectional area increase as laser input power increases.

a)

$\eta_a P = 50W$
$\eta_m = 0.16$
$A = 0.05mm^2$

b)

$\eta_a P = 100W$
$\eta_m = 0.25$
$A = 0.11mm^2$

c)

$\eta_a P = 150W$
$\eta_m = 0.27$
$A = 0.27mm^2$
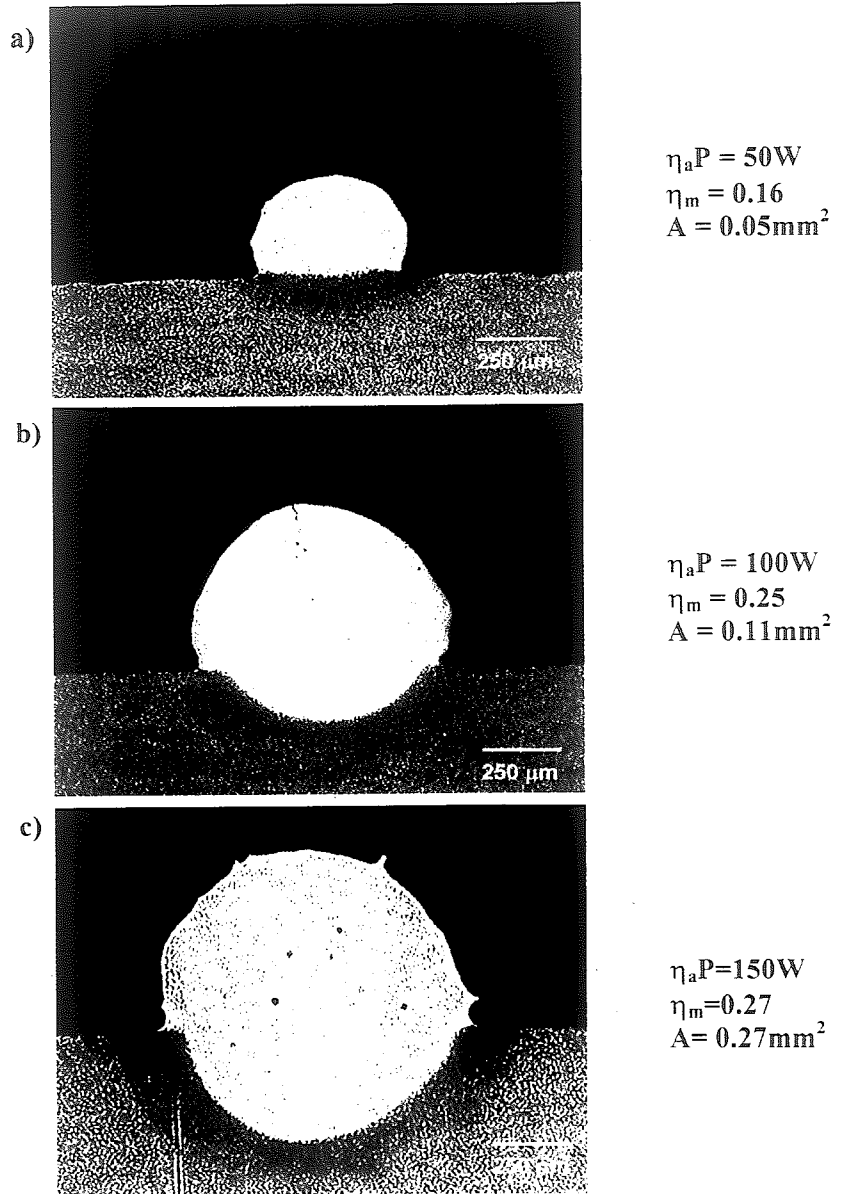
Figure 4- 9. Effect of laser input power on melting efficiency and deposit cross sectional area. (Travel speed of 5mm/s and powder mass flow rate of 0.17g/s)

To determine the rate at which energy is delivered to the workpiece, it is important to examine the effects of travel speed. It is known that an increase in travel speed will increase melting efficiency.[34] The reason being that when melting occurs at faster heat source travel speeds, less time is available for heat to be transported away from the localized melted region. Therefore, more total energy is used to create and maintain the molten weld pool.[35] Travel speed was also included in Figure 4- 8 to show the dependence of travel speed on melting efficiency. Results show that there is a slight increase with an increase in travel speed for the range of travel speeds tested. A plot of melting efficiency as a function of travel speed for varying laser powers (125, 250, 375, and 500W) can be seen in Figure 4- 10.

Figure 4- 10. Melting efficiency as a function of travel speed for varying laser powers.

75

Under closer examination of this plot, it can be seen that the there is an increase in melting efficiency with an increase in both laser power and travel speed. Figure 4- 11 a-d also depicts the dependence of melting efficiency on travel speed and laser input power for constant powder mass flow rates. Melting efficiency is not solely dependent upon travel speed but rather it is codependent with laser power and powder mass additions into the weld pool. Visually, the effect of travel speed (while holding all other variables constant) on melting efficiency and deposit cross sectional area can be seen in Figure 4- 12a-c. The influence of travel speed on melting efficiency can clearly be seen in Figure 4- 13, which shows a plot of meltin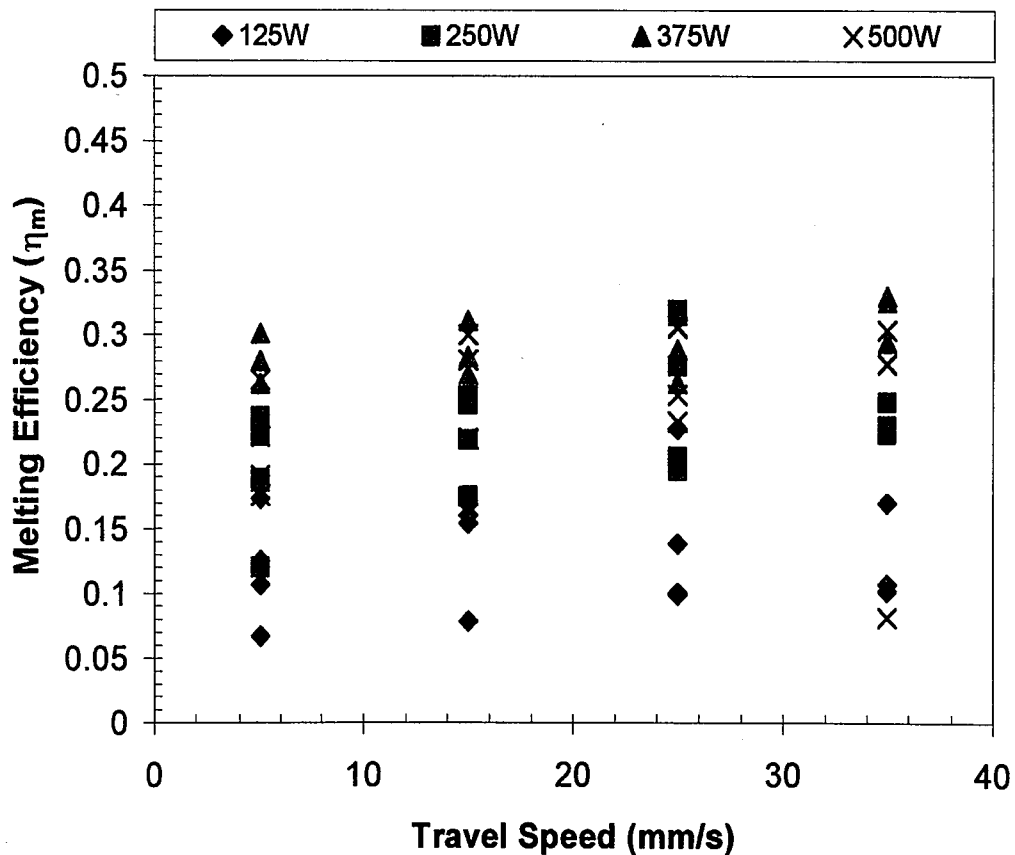g efficiency as a function of laser input power for travel speeds of 5 and 35 mm/s under a fixed powder mass flow rate. For each data point, the higher travel speed corresponds to a higher melting efficiency.

Previous work has shown that the combination of the laser input power and travel speed governs the rate at which energy is transported to the workpiece and when both processing parameters increase, either independently or together, melting efficiency increases as well.[34] This trend can be seen in Figure 4- 14 where melting efficiency is plotted as a function of the product between laser input power and travel speed. At higher travel speeds, while holding laser power constant, a larger fraction of the total energy is retained to melt the underlying substrate and vice versa for higher laser power with a fixed travel speed. At some point, travel speed can become too high to cause further melting of the material because there is less time available for transferring energy to the workpiece.[34]

a)

Powder Mass Flow Rate 0.08g/s

b)

Powder Mass Flow Rate 0.17g/s
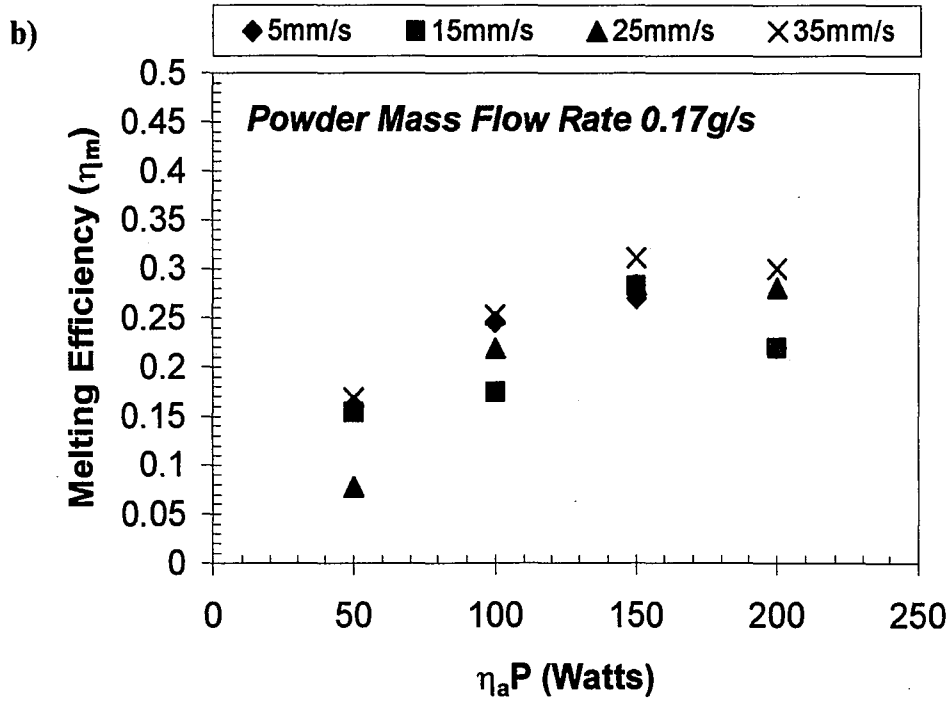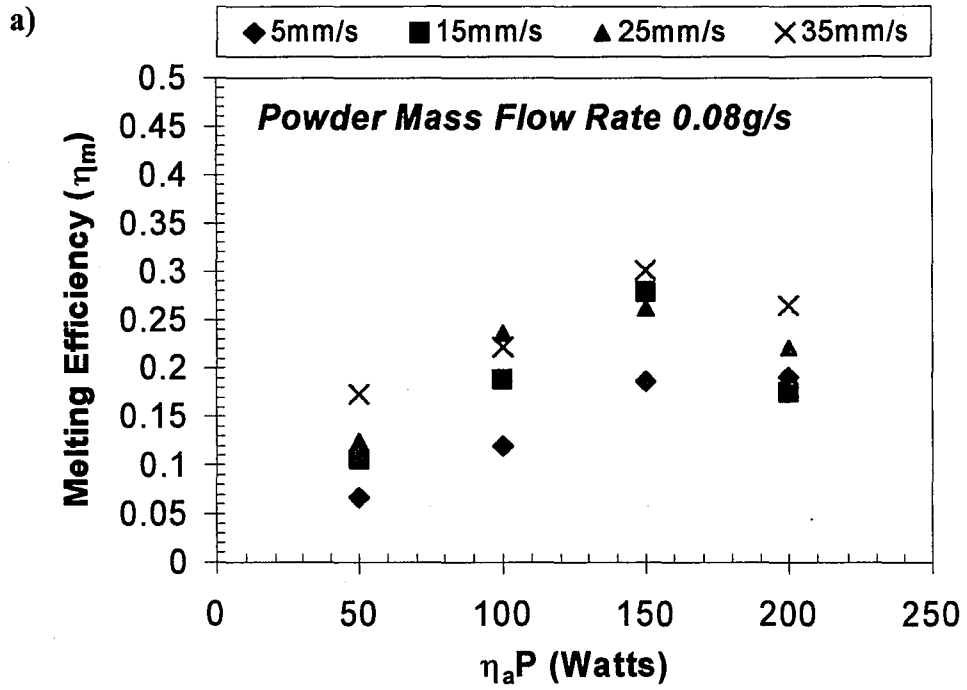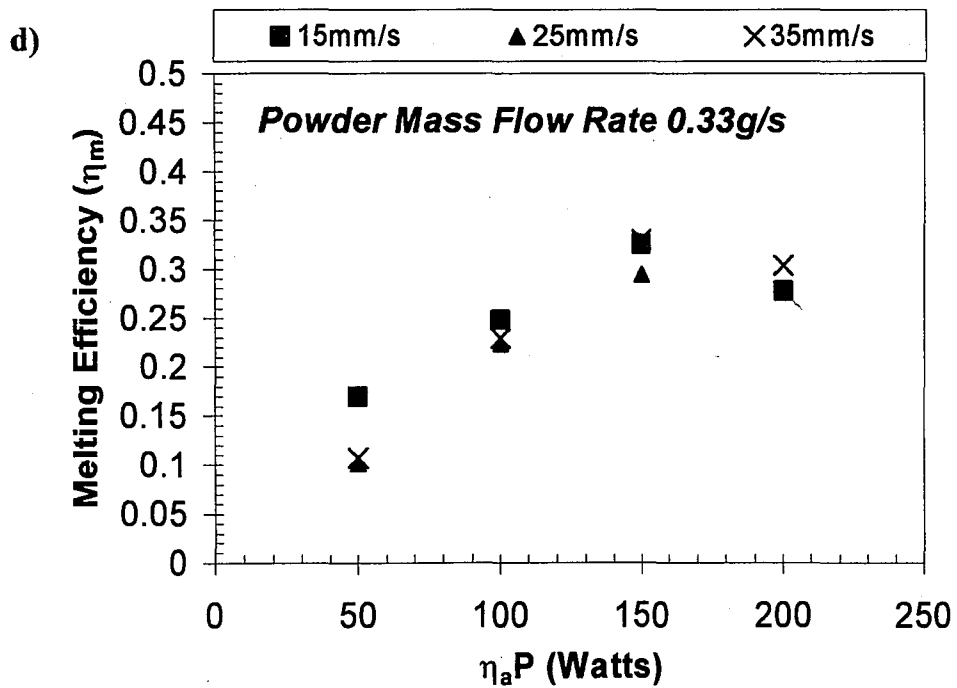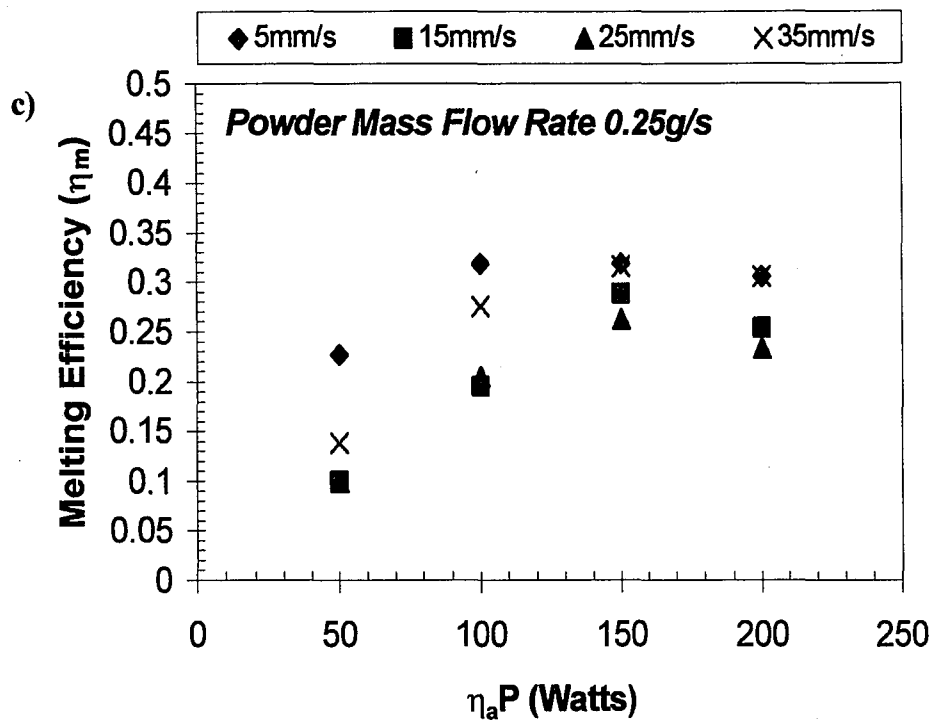
Figure 4- 11. Effect of melting efficiency on laser input power and travel speed for powder mass flow rates of a) 0.08, b) 0.17, c) 0.25, and d) 0.33g/s.
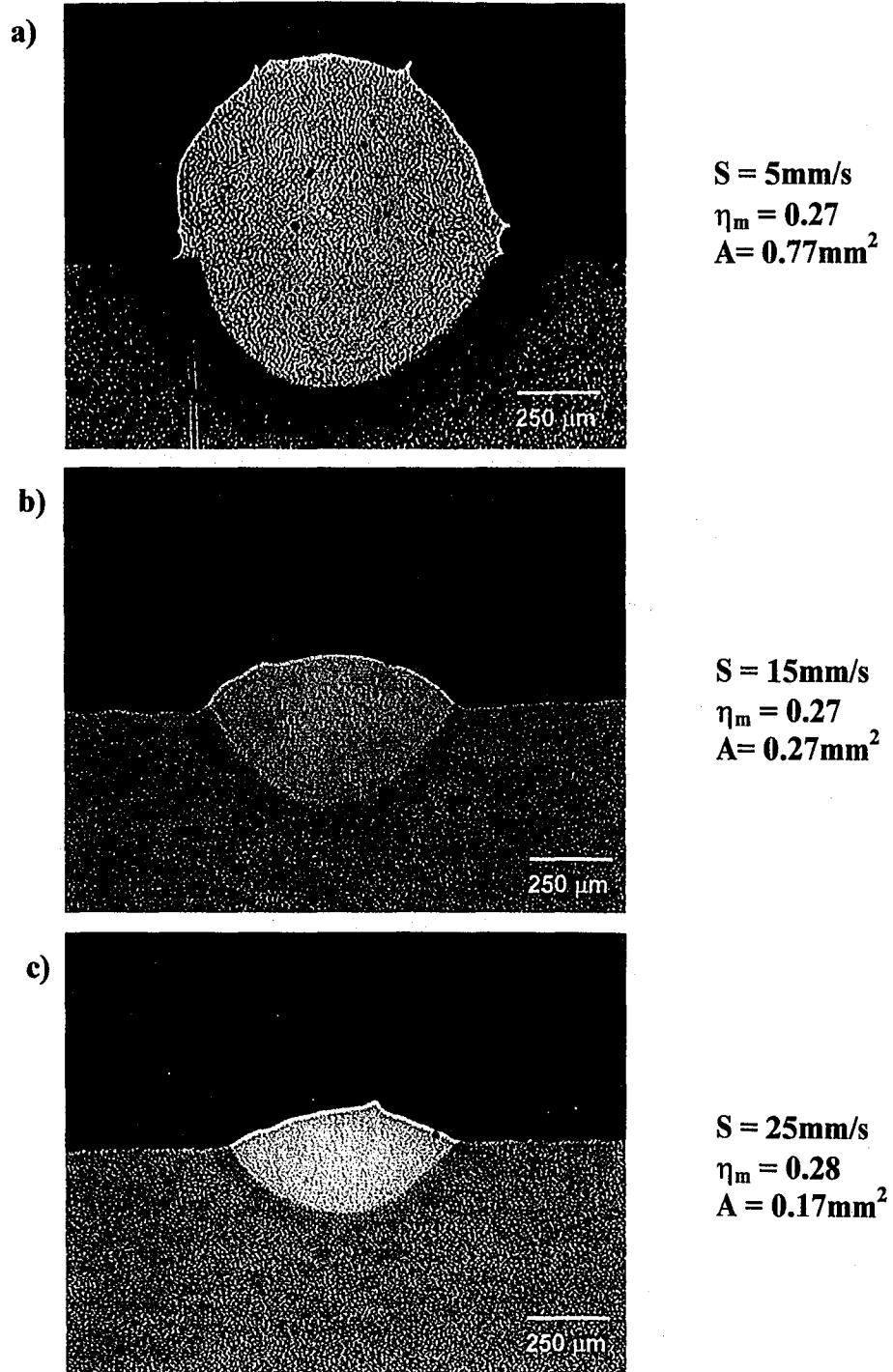
a) S = 5mm/s
η_m = 0.27
A= 0.77mm^2

b) S = 15mm/s
η_m = 0.27
A= 0.27mm^2

c) S = 25mm/s
η_m = 0.28
A = 0.17mm^2

Figure 4- 12.Effect of travel speed on melting efficiency and deposit cross sectional area. (Laser input power of 150W and powder mass flow rate of 0.17g/s)

a)

S = 5mm/s
η_m = 0.27
A= 0.77mm^2

b)

S = 15mm/s
η_m = 0.27
A= 0.27mm^2

c)

S = 25mm/s
η_m = 0.28
A = 0.17mm^2

Figure 4- 12.Effect of travel speed on melting efficiency and deposit cross sectional area. (Laser input power of 150W and powder mass flow rate of 0.17g/s)

79
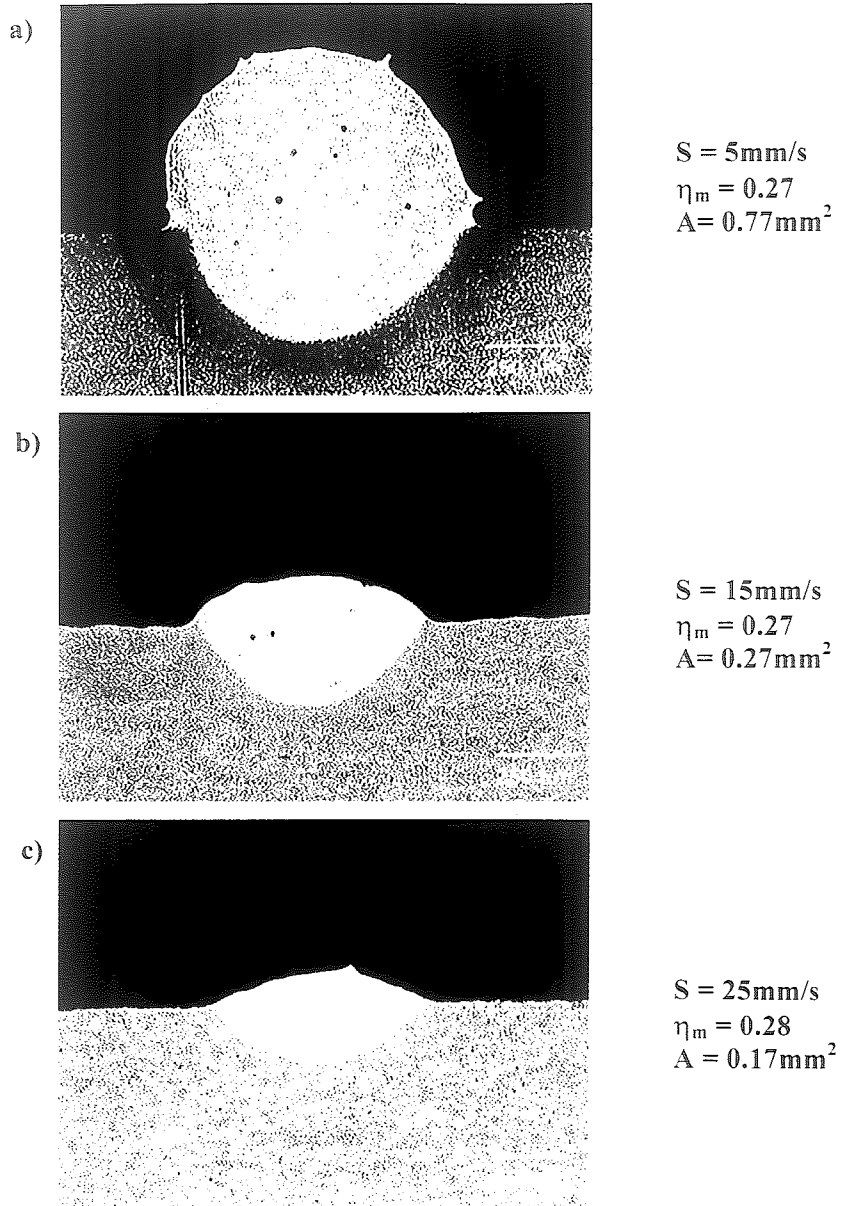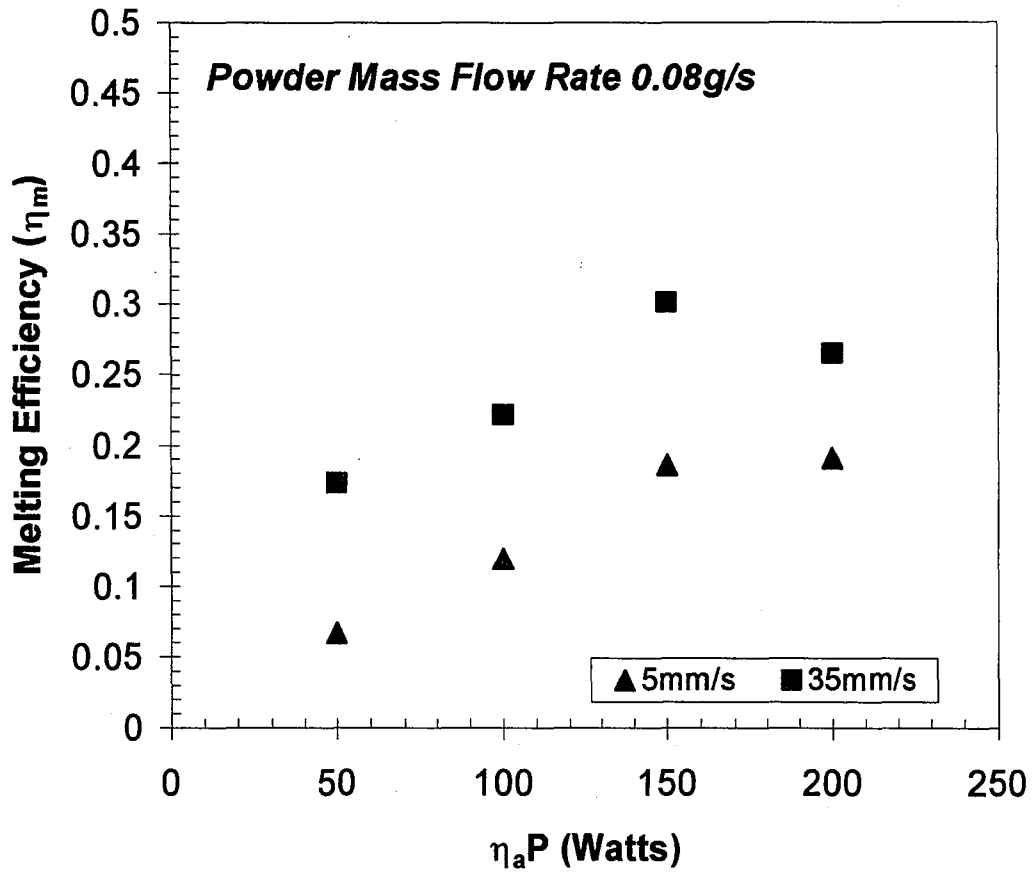
Figure 4- 13. Plot of melting efficiency as a function of laser input power for travel speeds of 5 and 15mm/s for fixed powder mass flow rate. (0.08g/s)
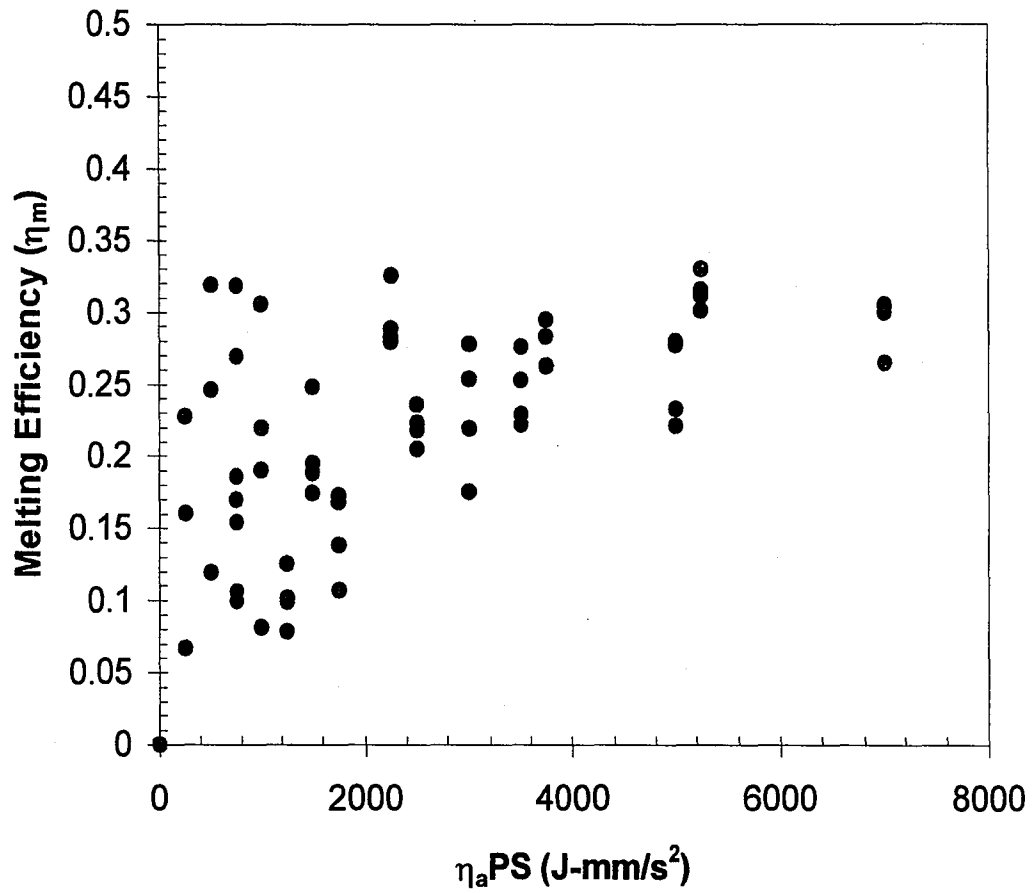
Figure 4- 14. Melting efficiency as a function of the product of laser input power and travel speed.

Powder mass additions into the molten pool was also observed to have an effect on melting efficiency. This was evident when melting efficiency was plotted as a function of laser input power at varying powder mass flow rates while holding travel speed constant. The results are presented in Figure 4- 15 a-d, which correspond to plots of melting efficiency as a function of laser input power and powder mass flow rate for travel speeds of 5, 15, 25, and 35mm/s, respectively. At the lowest travel speed of 5mm/s (Figure 4- 15 a), two distinguishable trends are immediately evident. The first trend depicts how melting efficiency increases with laser input power, as observed in the section above. The second noticeable trend clearly depicts an increase in melting efficiency with an increase in the amount of powder material that is delivered to the weld pool. At the higher travel speeds, (15, 25, and 35mm/s) these trends are also apparent although there is some overlap among data points. A pictorial representation showing the increasing effect of melting efficiency with increasing powder mass additions can be seen in Figure 4- 16 a-c.

The phenomenon of increased melting efficiency with the increased incorporation of powder material into the molten pool can be explained by examining the distribution of energy from the laser beam to the substrate and powder flux. As energy is transferred to the molten pool, a fraction of it is used to melt the underlying substrate while the rest is dissipated by thermal conduction to the surrounding material. When powder is distributed over the weld pool, the total energy available is utilized to create the molten pool and melt the incoming powder flux. The energy is effectively used to melt the underlying substrate and powder while leaving a lesser amount of energy to be dissipated away from

the localized melt region. Since a greater amount of energy is available and used for melting, it follows that melting efficiency will increase as well.

a)

b)
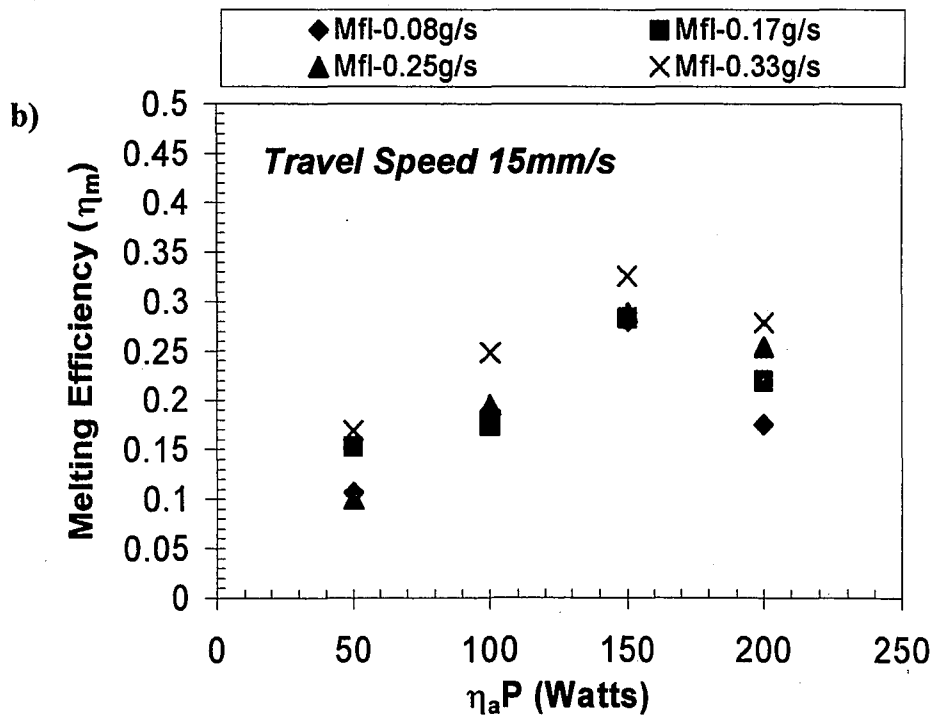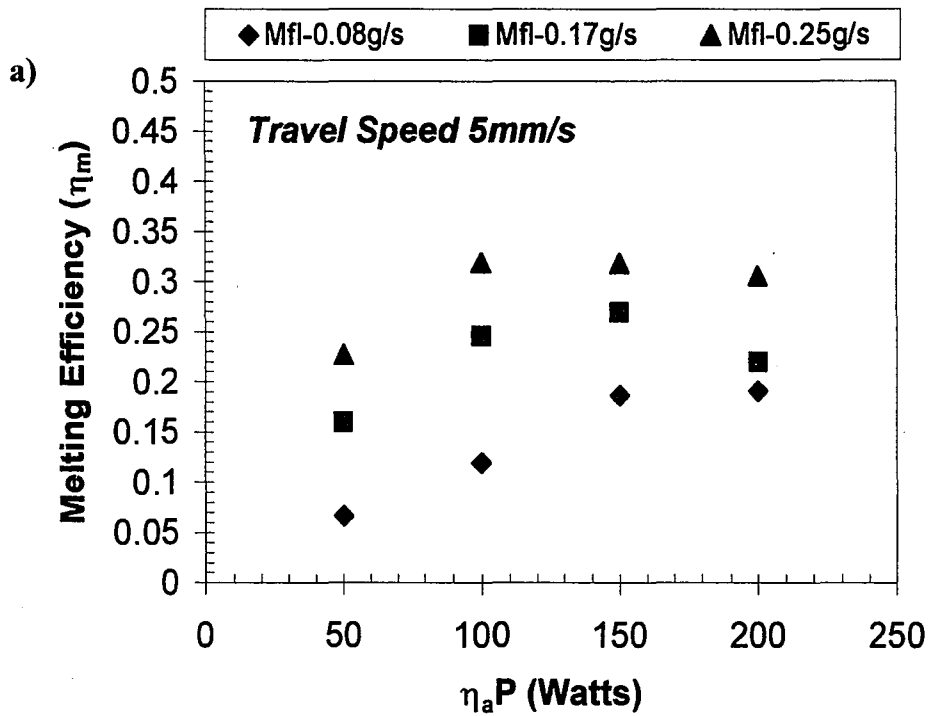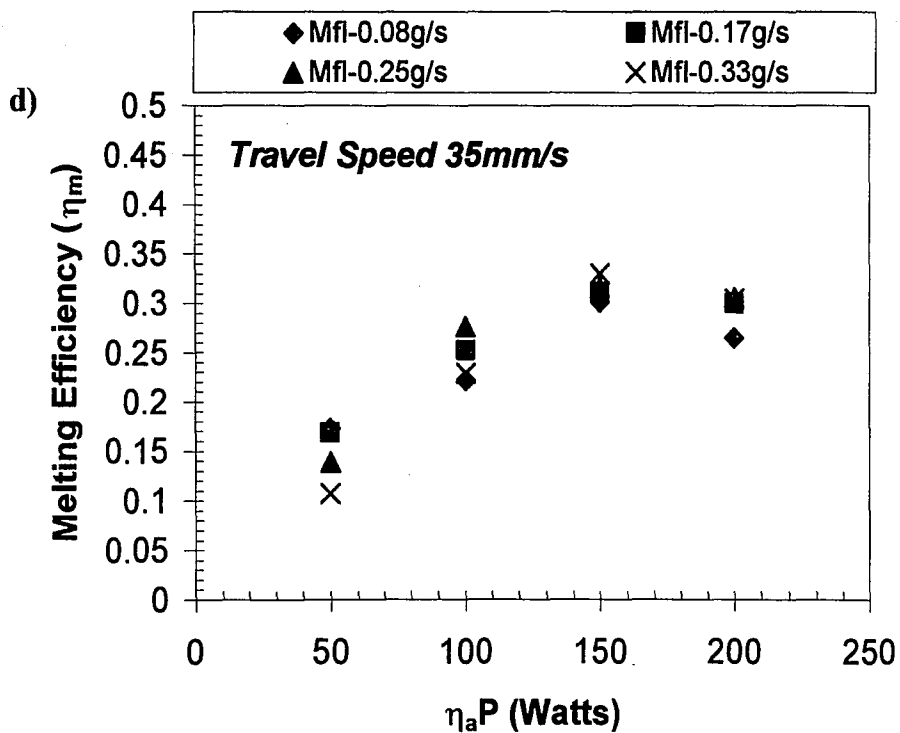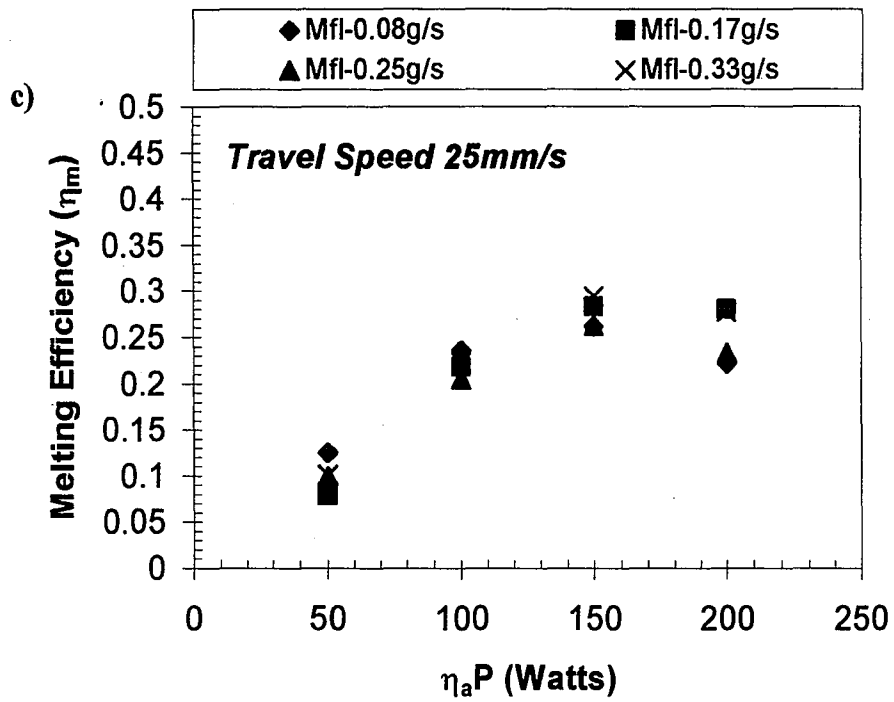
Figure 4- 15. Effect of laser input power on melting efficiency for varying powder mass flow rates and at travel speeds of a) 5, b) 15, c) 25, and d) 35mm/s.
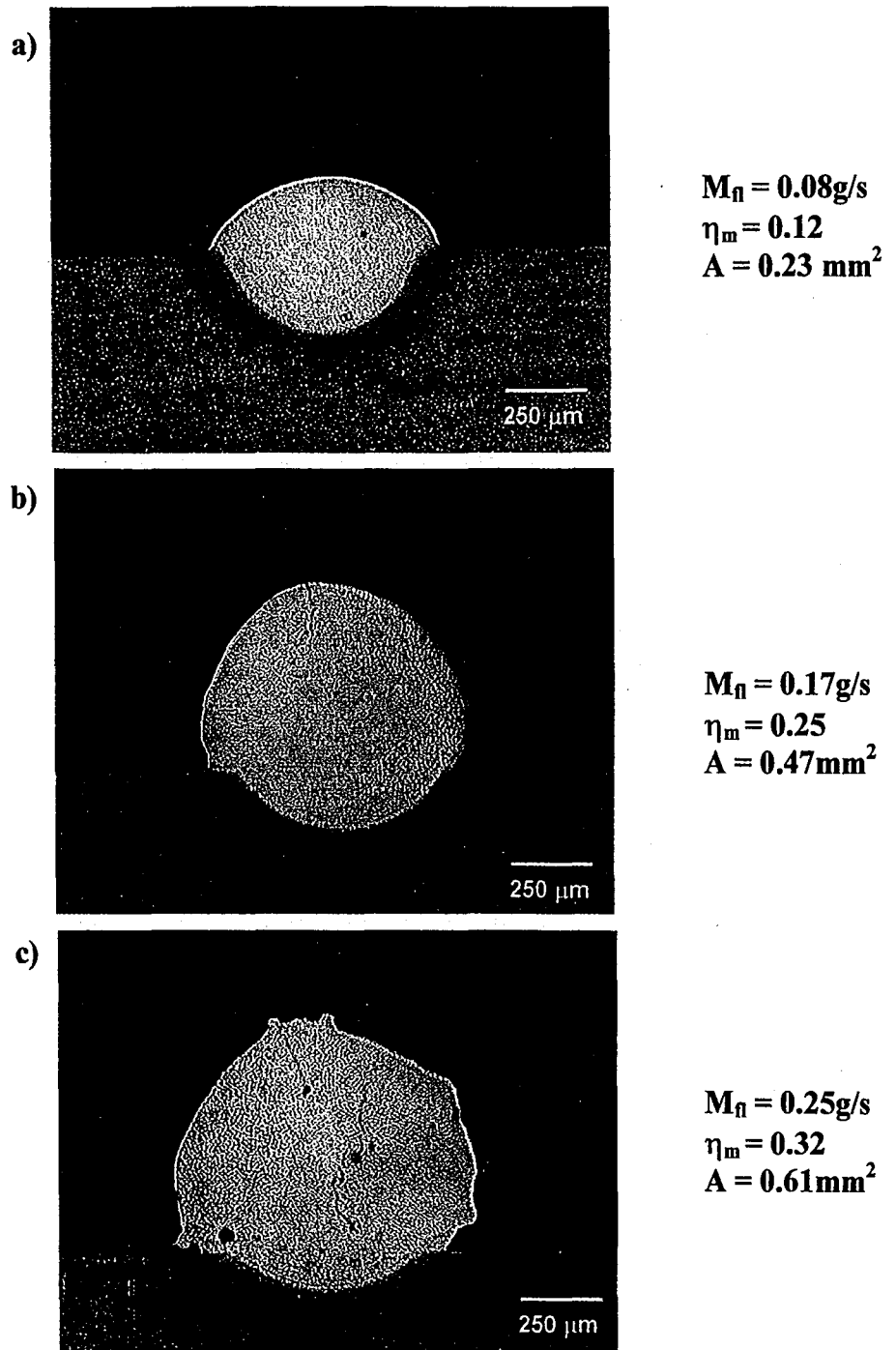
a)

$M_{fl} = 0.08g/s$
$\eta_m = 0.12$
$A = 0.23\ mm^2$

b)

$M_{fl} = 0.17g/s$
$\eta_m = 0.25$
$A = 0.47mm^2$

c)

$M_{fl} = 0.25g/s$
$\eta_m = 0.32$
$A = 0.61mm^2$

Figure 4- 16. Effect of powder mass flow rate on melting efficiency and deposit cross sectional area. (Laser input power of 100W and travel speed of 5mm/s)

85

a)

$M_{fl} = 0.08g/s$
$\eta_m = 0.12$
$A = 0.23 \ mm^2$

b)

$M_{fl} = 0.17g/s$
$\eta_m = 0.25$
$A = 0.47mm^2$

250 µm

c)

$M_{fl} = 0.25g/s$
$\eta_m = 0.32$
$A = 0.61mm^2$

250 µm

Figure 4- 16.Effect of powder mass flow rate on melting efficiency and deposit cross sectional area. (Laser input power of 100W and travel speed of 5mm/s)

85
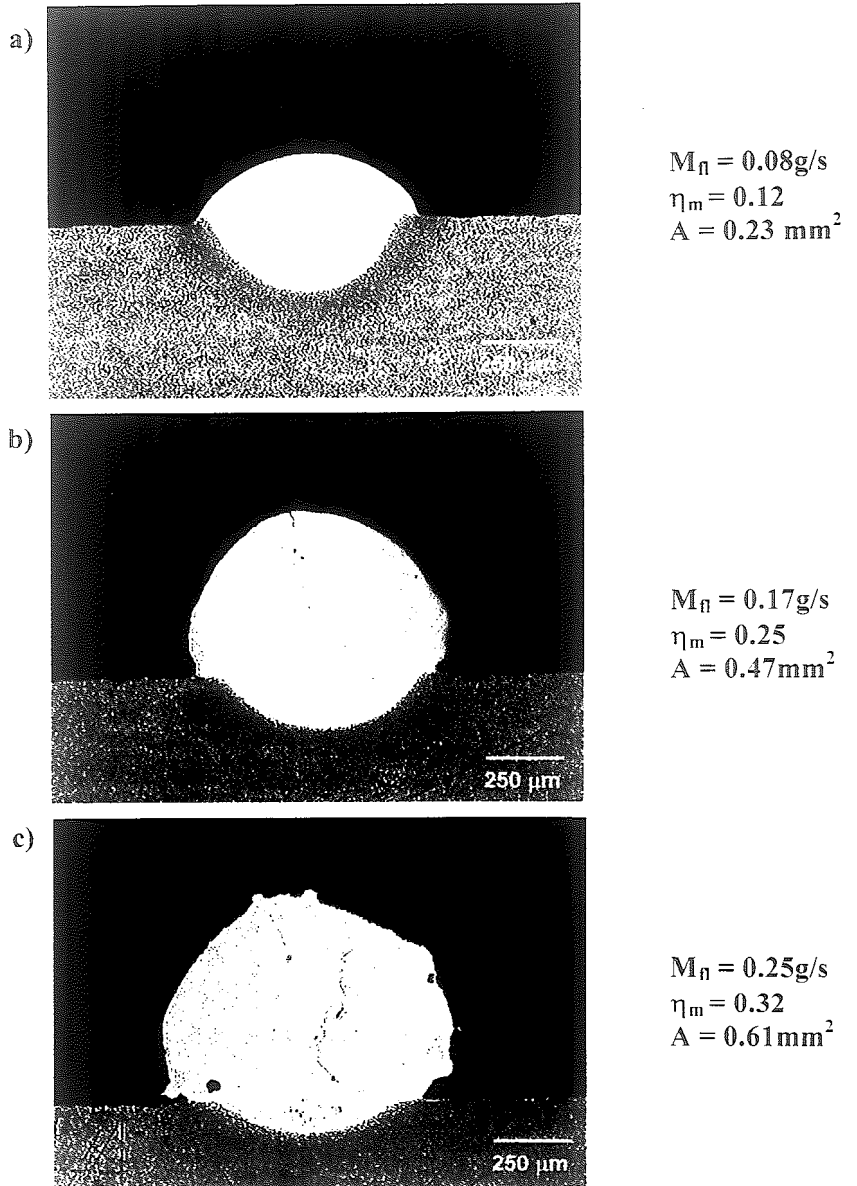
4.2.2 Predicting Melting Efficiency from Processing Parameters

Attempts have been made to predict melting efficiency through knowledge of process variables and material thermophysical properties.[17-19] The theoretical models are based upon steady state thermal conduction heat flow conditions first described by Rosenthal. The assumptions used by Rosenthal include a point heat source, constant thermal properties, no melting/negligible heat of fusion, and no heat loss from the workpiece surface.[7] More recently a model has been developed for arc welding and CO_2 laser welding processes to predict melting efficiency as a function of dimensionless parameters.[21] Dimensionless parameters were used to correlate the weld size to processing parameters and they are defined as follows:

$$Ry = \frac{\eta_a PS}{\alpha^2 \Delta H_m}$$

[4-1]

$$Ch = \frac{S^2 A}{\alpha^2}$$

[4-2]

Where η_a is the energy transfer efficiency (0.4), P is the laser power, S is the travel speed, α is the thermal diffusivity at the liquidus temperature (1018 Steel-5.5 mm^2/s and copper-42.1 mm^2/s),[36] ΔH_m is the melting enthalpy, and A is the weld cross sectional area. For copper powder deposits on the H-13 tool steel, the effect of thermal diffusivity should be controlled by the substrate material as previously shown by DuPont and Marder.[16]

86

Therefore, the value of thermal diffusivity should be that of the steel substrate. (5.5 mm^2/s) Since materials with dissimilar thermophysical properties have been deposited (i.e. copper deposited on tool steel), an average melting enthalpy value between tool steel and copper was used, 8.2 J/mm^3.[16] The ratio of Ch to Ry yields the melting efficiency as shown in the following equation:

$$\eta_m = \frac{Ch}{Ry} = \frac{SA\Delta H_m}{\eta_a P}$$

[4- 3]

To develop a relation between the two dimensionless parameters, Ch was plotted as a function of Ry for deposits of H-13 tool steel and copper powder on grit blasted H-13 tool steel substrates under a wide range of processing parameters. The results presented in Figure 4- 17 depicts a linear relationship between Ch and Ry and the data was fitted to a best-fit curve using linear regression analysis. The results yielded a correlation coefficient of 0.96 and the equation relating Ch to Ry is presented below:

$$Ch = 0.31 Ry - 0.47$$

[4- 4]

Since the ratio of Ch/Ry yields the melting efficiency, Equation [4-4] was manipulated to yield the following:

$$\eta_m = 0.31 - \frac{0.47}{Ry} = 0.31 - 0.47\left(\frac{\alpha^2 \Delta H_m}{\eta_a PS}\right) \qquad \text{[4-5]}$$

Equation [4-5] is thus a semi-empirically based, equation that can be used to estimate melting efficiency as a function of the dimensionless parameter Ry. Recall that Ry incorporates processing parameters (P and S) and thermal physical properties (α, ΔH_m), therefore Equation [4-5] can be used to predict melting efficiency when processing parameters and material thermophysical data are known. Melting efficiency data was plotted as a function of Ry so that it could be compared to calculated melting efficiency values using Equation [4-5]. (Refer to Figure 4- 18) From the plot it can be seen that there is not a tight correlation from data point to data point for the H-13 tool steel and copper data. A direct comparison between experimentally measured melting efficiency and melting efficiency calculated from Equation [4-5] can be seen in Figure 4- 19. At low values of melting efficiency there is poor correlation and the correlation generally improves at higher melting efficiencies. It has been shown that the deviations occur because of the inability to predict melting efficiency due to the exponential relation between melting efficiency and $\eta_a PS$.[19] At high values of melting efficiency, there is better correlation because melting efficiency asymptotically approaches the theoretical maximum of 0.37.

Figure 4- 17. Dimensionless parameter model Ch versus Ry for H-13 tool steel and copper powder deposits on H-13 tool steel substrates.

The chart shows melting efficiency data with the equation:

$$\eta_m = 0.31 - \frac{0.46}{Ry}$$

Legend:
- H-13 Tool Steel
- Copper
- Calculated

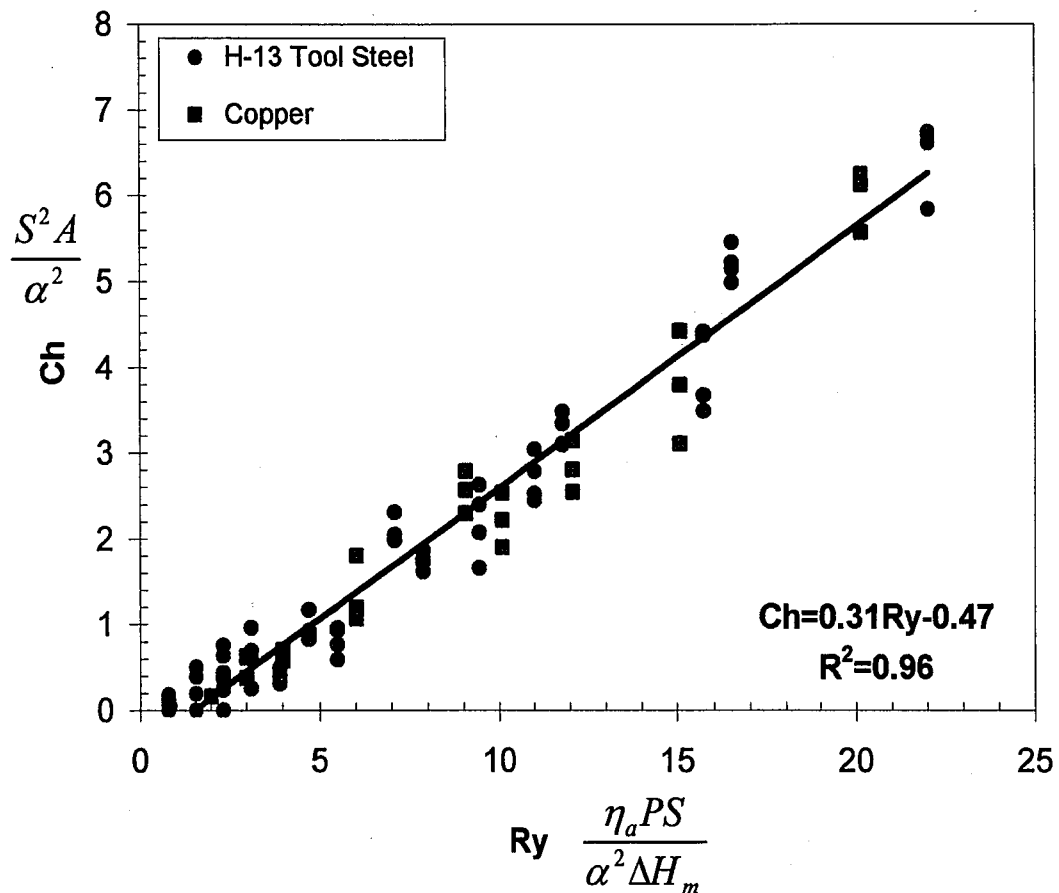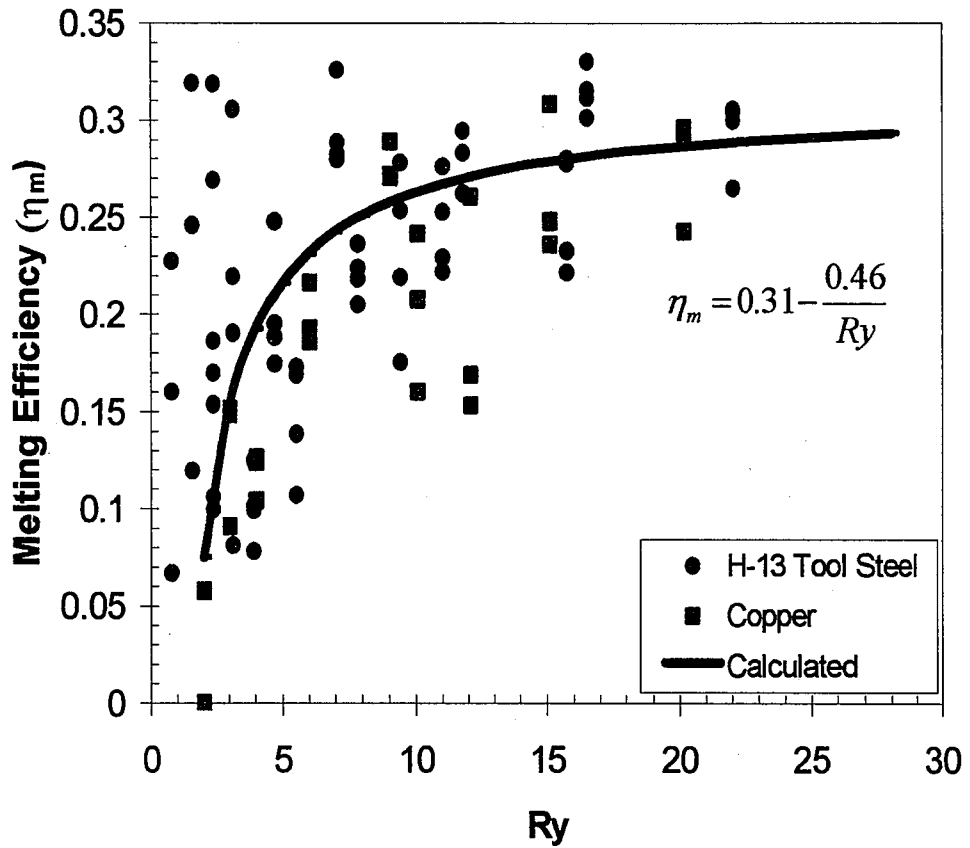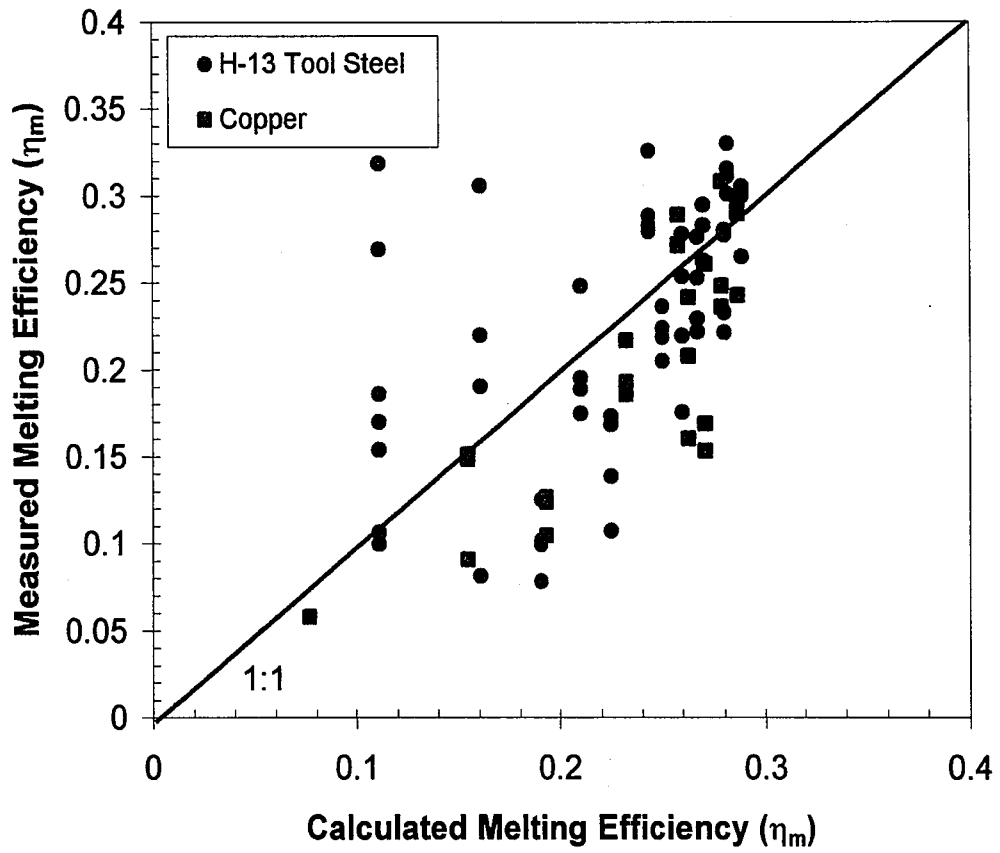**Figure 4- 18.** Melting efficiency as a function of the dimensionless parameter Ry for H-13 tool steel and copper powder deposits on H-13 tool steel substrates.

Figure 4- 19.Comparison between measured melting efficiency and melting efficiency calculated from Equation [4-5] for single pass deposits of H-13 tool steel and copper on grit blasted H-13 tool steel substrates.

4.3 Deposition Efficiency

From deposit cross sectional area measurements, the deposition efficiency was determined under a matrix of processing parameters. Deposition efficiency ranged from 0-14%. These results indicated that only a small fraction of powder delivered to the melt pool was actually fused to the substrate to form a metallurgical bond. The low deposition efficiency can be attributed to the following: 1) design of the powder delivery system and 2) an insufficient amount of energy available to melt the underlying substrate and incoming powder. Case 1 will be discussed in more detail in Section 4.3.1 while Case 2 will be discussed in more detail in Section 4.3.2.

4.3.1 Design of the Powder Delivery System

The design of the powder delivery system has a large impact on deposition efficiency in that it directs the flow of powder into the molten pool. If for example the nozzles are misaligned, then a large fraction of the powders will not be fused to the substrate because a majority of the powder will not even come in contact with the molten pool; thereby causing a decrease in the deposition efficiency. The laser beam focal point was set by the manufacturer, which resulted in a stand off distance between the tip of the nozzles and the substrate to be 8.89mm. At this distance, powder was evenly distributed over the molten pool in an area that was 16.26mm^2. Macroscopic images of single pass line deposits at a constant travel speed of 5mm/s and at laser powers of 250W and 500W can be seen in Figure 4- 20 a-b, respectively. The lighter area, sectioned off with dotted line, corresponds to the powder impingement area. As evident from these macrographs, the molten pool is significantly smaller than the total area that the powder is distributed over. Thus, it stands to reason that a larger amount of powder will not fuse to the

workpiece since the majority of it does not even come in contact with the molten pool. This gives one explanation as to why the deposition efficiency is so low. From the powder that does come in contact with the molten pool, the deposition efficiency would be dependent upon processing parameters since they control the size of the melt pool as well as the rate at which powder is delivered to the weld pool.
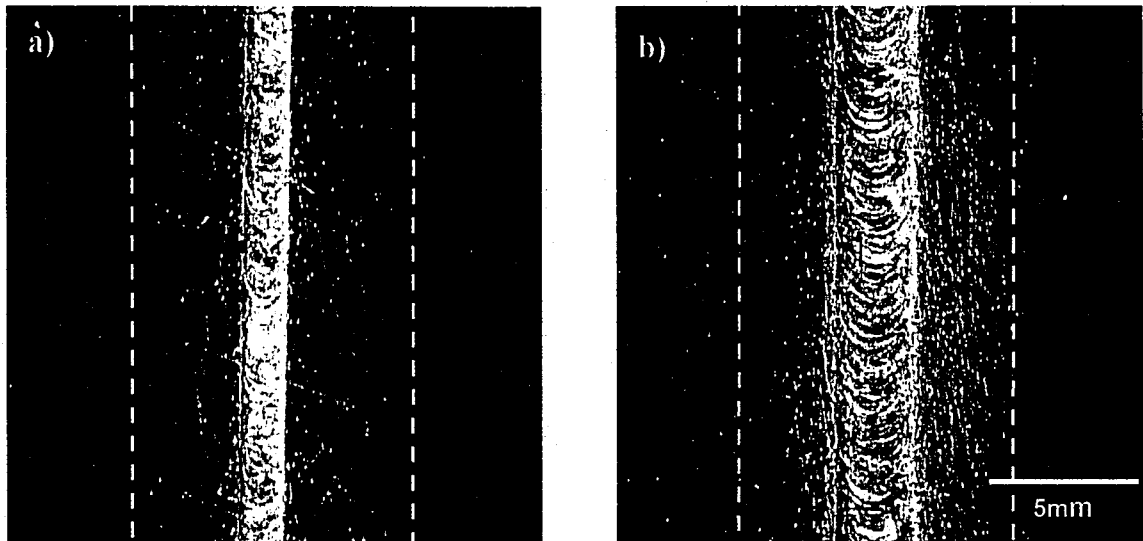
Figure 4- 20. Macrograph of powder convergent area for laser output powers of a) 250W and b) 500W.

4.3.2 Effect of Process Variables on Deposition Efficiency

Deposition efficiency is affected by the combination of laser power, travel speed, and powder mass flow rate. By examining the data that corresponds to $\eta_d(P,S,M_{fr})$ it is possible to observe general trends on how deposition efficiency varies with respect to one variable while holding all others constant. For example, the effect of laser power on deposition efficiency while holding travel speed and powder mass flow rate constant at 5mm/s and 0.08g/s, respectively can be seen in Figure 4- 21. From this figure, it is readily

93

apparent that deposition efficiency increases with an increase in laser power when examining corresponding micrographs for each data point. This trend can be explained by the fact that at higher laser powers a greater amount of energy is utilized for melting. Melting efficiency increases and a larger molten weld pool is created. Under these circumstances, there is a sufficient amount of energy available to melt the substrate and the powder, as evident in the size of the deposit cross sectional area. Travel speed also has an affect on deposition efficiency. (Refer to Figure 4- 22) With an increase in travel speed, while holding laser power and powder mass flow rate constant, deposition efficiency was shown to decrease. This occurs because at higher travel speeds, the size of the molten pool decreases. Lastly, the effect of powder mass flow rate on deposition efficiency (while holding laser power and travel speed constant) is shown in Figure 4- 23. From this it can be seen that there is little dependence on the rate at which powder is delivered to the molten pool. The small amount of powder that comes in contact with the molten pool will not fuse to the workpiece because powder is injected at such a high velocity such that the individual powder particles will have a sufficient amount of momentum to be deflected away from the weld pool and ricochet off of the substrate even when it gets heated by the molten weld pool.

Laser energy transfer and melting efficiency results from Sections 4.1 and 4.2 were used to examine the effects of melting power ($\eta_a\eta_mP$) on deposition efficiency. As melting power increases, a greater amount of energy is utilized for melting which will subsequently increases the size of the molten weld pool. This will in turn increase deposition efficiency, as more energy is available to melt the powder material over a larger area. Figure 4- 24 a-b depicts representative still images of the laser deposition

94

process taken with a color CCD camera. The images show the effect of melting power on deposition efficiency while holding all other variables constant. It can be seen in Figure 4- 24 a that there is an insufficient amount of energy available for melting and this powder that impinges upon the weld pool will not be effectively melted and fused to the substrate. When melting power increases as in Figure 4- 24 b the energy available for melting is effectively utilized for melting the powder material and thus a larger fraction of incident powder is fused to the workpiece.
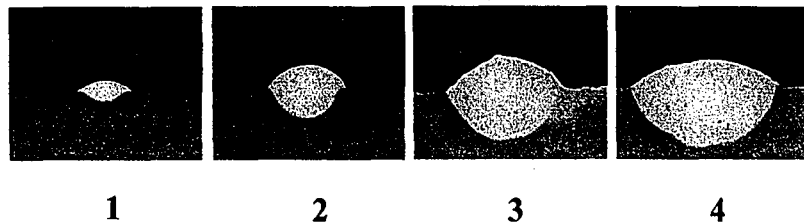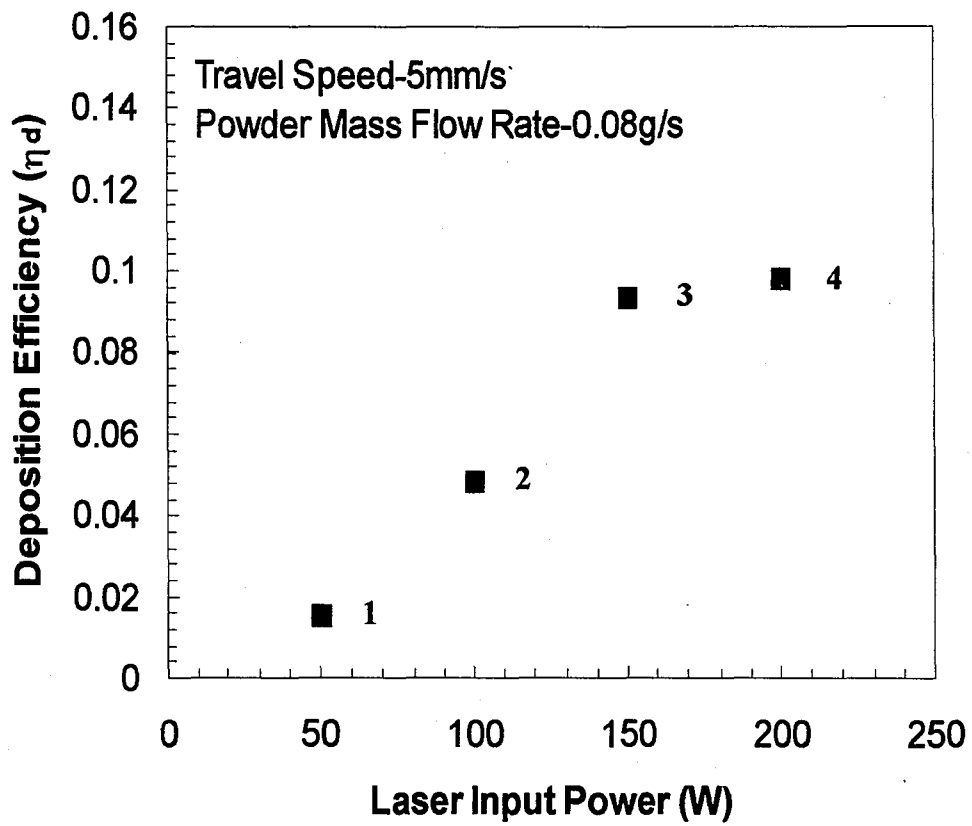
Figure 4- 21. Deposition efficiency as a function of laser input power for fixed travel speed and powder mass flow rate.
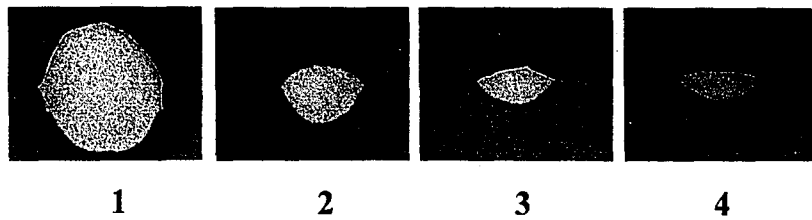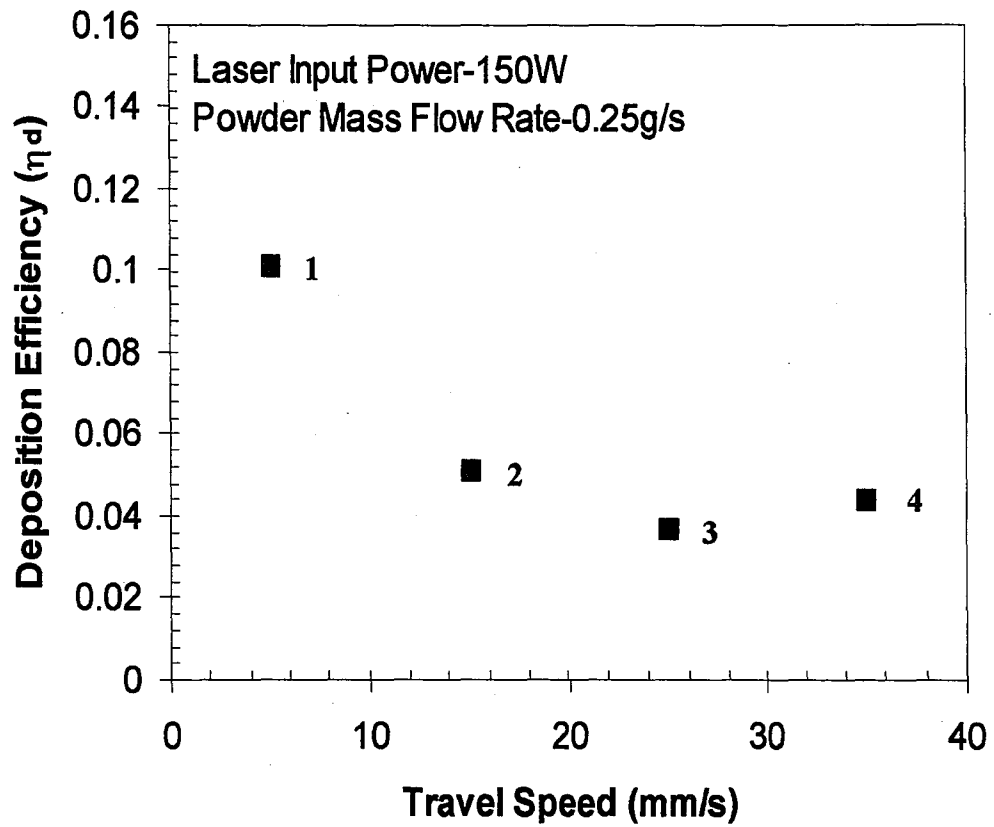
Figure 4- 22. Deposition efficiency as a function of travel speed for fixed laser input power and powder mass flow rate.
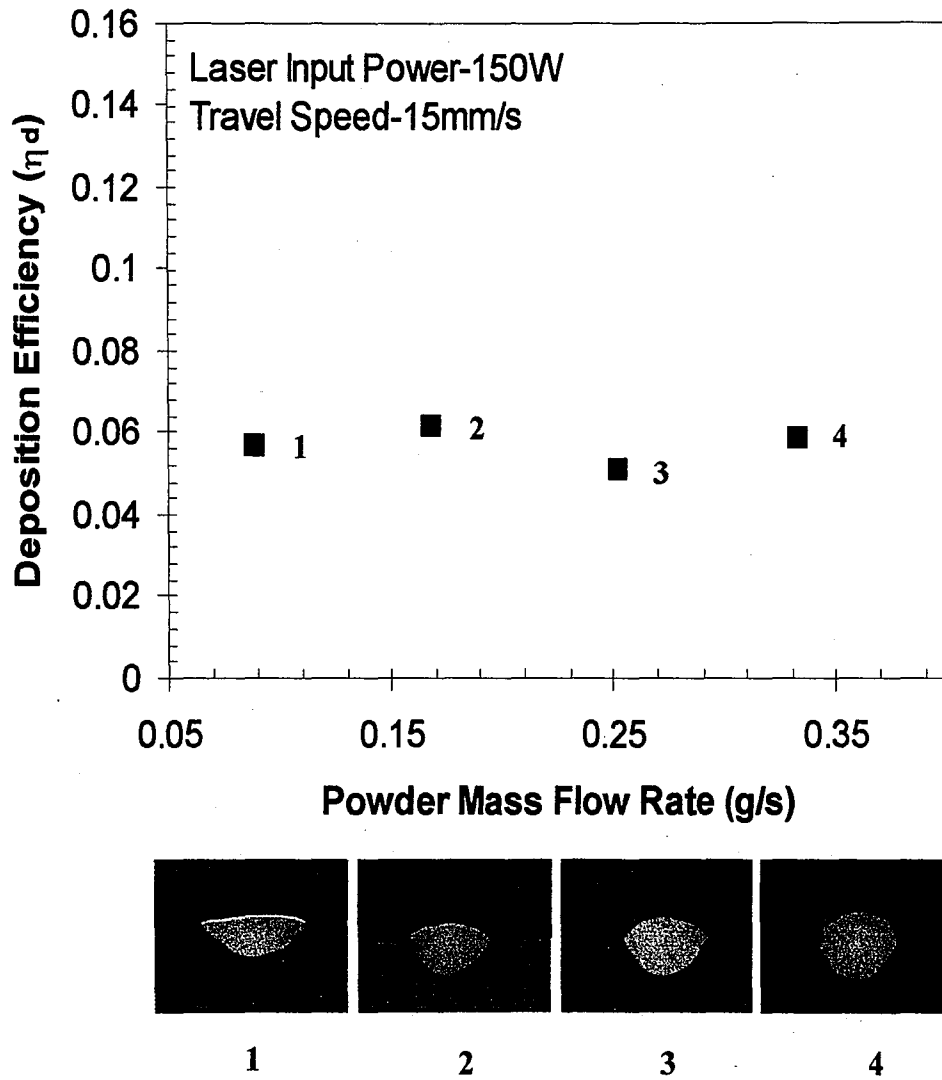
Figure 4- 23. Deposition efficiency as a function of powder mass flow rate for fixed laser input power and travel speed.

Figure 4- 24. Real time weld pool monitoring of laser deposition process at laser output powers
of a) 125W and b) 500W at constant travel speed (5mm/s) and powder mass flow
rate (0.08g/s).

4.3.3 Predicting Deposition Efficiency from Processing Parameters

The effect of processing parameters on deposition efficiency can be seen in a plot of deposition efficiency as a function of the parameter Γ for the H-13 tool steel and copper deposits (Refer to Figure 4- 25). The Γ parameter $[\dot{V}_{fm}/(\eta_a\eta_m P/S)]$ is a ratio of the volumetric filler metal feed rate $(\dot{V}_{fm})$ over the actual heat input that is used for melting $(\eta_a\eta_m P/S)$. The Γ parameter was used because it incorporates the main LENS™ processing variables that affect deposition. The volumetric powder feed rate is simply the volumetric amount of powder that is delivered to the molten pool. The melting heat input governs the size of the molten pool. When $\eta_a\eta_m P/S$ increases by increasing laser input power or decreasing travel speed, it follows that the size of the molten weld pool increases as well since there is a greater amount of energy that is utilized for melting. Conversely, when $\eta_a\eta_m P/S$ decreases, less energy is available for melting. When the Γ parameter is small (low $\dot{V}_{fm}$ and high $\eta_a\eta_m P/S$), deposition efficiency is high because the molten pool size increases and a greater amount of powder is incorporated into the melt pool. Moreover, when the Γ parameter is large (high $\dot{V}_{fm}$ and low $\eta_a\eta_m P/S$), deposition efficiency is low because there is an insufficient amount of energy available to melt the substrate and the large flux of incoming powder.

In order to develop a method of predicting deposition efficiency based on LENS™ efficiencies and processing parameters the data in Figure 4- 25 was fitted to a best-fit curve by regression analysis, which resulted in the development of equations relating deposition efficiency to Γ.

100

H-13 Tool Steel $\eta_d = -0.02 \ln(\Gamma) + 0.10$ [4- 6]

Copper $\eta_d = -0.07 \ln(\Gamma) + 0.30$ [4- 7]

Equation [4-6] and [4-7] are thus semi-empirical equations that can be used to estimate deposition efficiency as a function of Γ, which in turn is a function of process efficiencies and processing parameters such as laser power and travel speed. As can be seen in Figure 4- 25, there is a significant amount of scatter for the copper data.
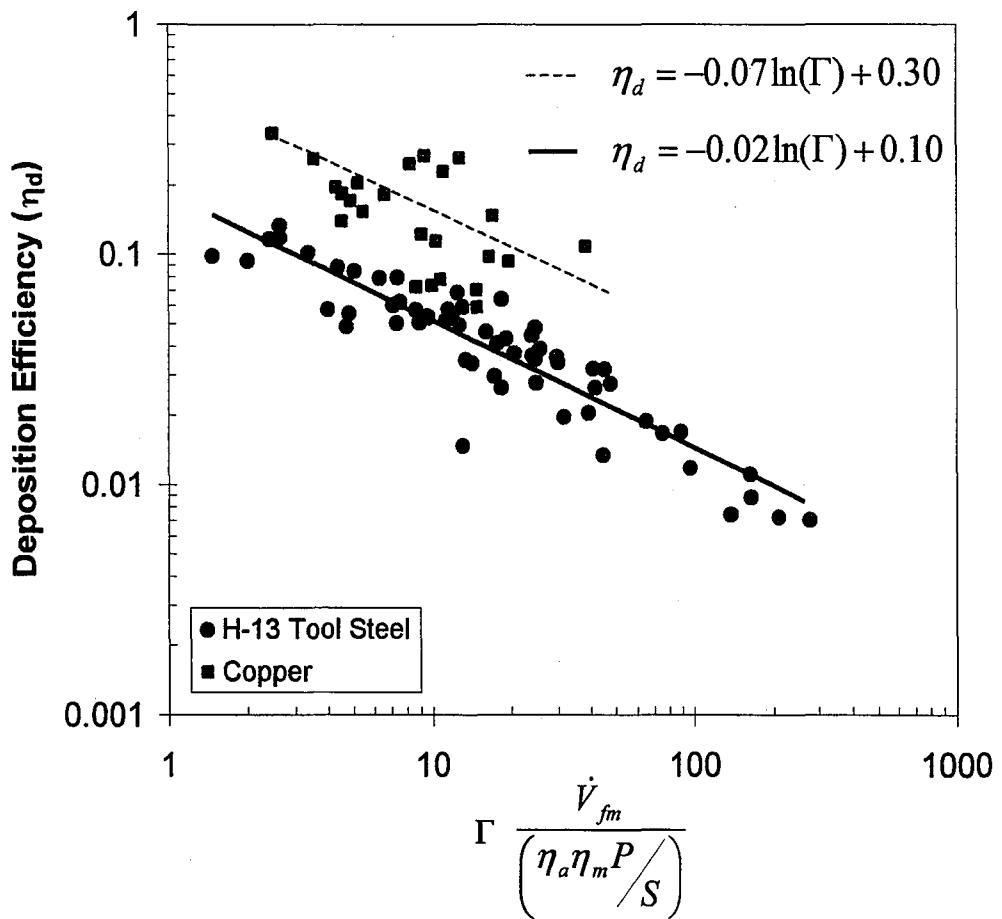
Figure 4- 25. Plot of deposition efficiency as a function of the ratio of volumetric powder feed rate to the actual heat input used for melting.

4.4 Dilution

The development of functionally graded materials for industry related applications has been one aspect of solid freeform fabrication research. Designers now have the ability to fabricate intricate shaped components with local compositional control, resulting in unique mechanical properties throughout the graded structure. The LENS™ process is one such solid freeform fabrication method that has the ability to produce functionally graded structures by selectively depositing different elemental powders or premixed blends into the molten pool at discrete locations. The adaptation of multiple powder feeders in the LENS™ system makes this feasible. Dissimilar powder materials are placed into separate powder hoppers. Computer software, which is integrated into the powder feed system, enables the user to precisely control the deposit composition as a function of position. During the build process, the powder feeders operate simultaneously at different motor speeds to deliver more or less of a specific powder to the melt pool.

The chemical composition in each layer of a LENS™ fabricated component is dependent upon the degree of mixing, or dilution, between the previously solidified layer and the newly formed deposit. Previous research has shown that the distribution of alloying elements is fairly uniform across the substrate and the deposit weld metal and that a concentration gradient exists over a distance of only ≈75μm, which is very small when compared to the overall deposit size.[19] Estimation of deposit composition from geometric measurements of dilution has been shown to be representative of the entire weld deposit composition.[19] For a functionally graded component, each layer will exhibit a discrete composition. This occurs because the composition of the incoming powder is

continuously changing between each pass. This is depicted in Figure 4- 26 where the initial composition in the first pass is of material A and as material B is functionally graded into successive layers the composition exhibits a "stepped" profile.
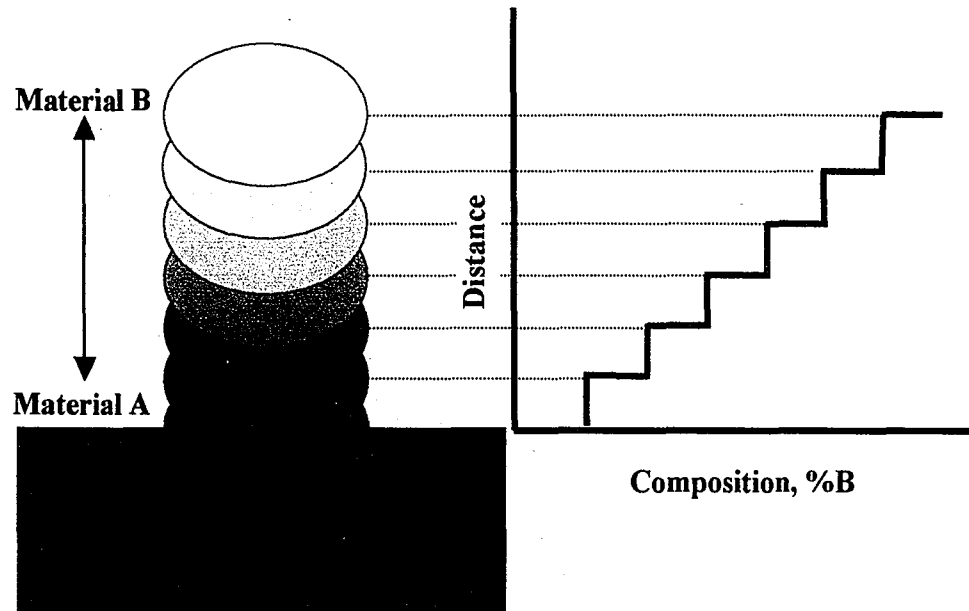
Figure 4- 26. Schematic illustration of a functionally graded line build with corresponding composition profile of material B into material A.

Composition control of each deposit is required to obtain the desired composition and microstructural profile. Composition in each layer can be estimated from a dilution standpoint using Equation [4-8] when the composition of the substrate and material to be deposited are known. The concentration of any alloying element, i, in the deposit is then related to the dilution by the following expression:

$$C^{i}{}_{dep} = C^{i}{}_{sub}D + (1-D)C^{i}{}_{pow} \qquad \text{[4-8]}$$

104

Where:

C^i_{dep} = Concentration of element i in the deposit
C^i_{sub} = Concentration of element i in the substrate
C^i_{pow} = Concentration of element i in the powder

Previous research has shown that excellent agreement exists between composition determined through geometric dilution and direct chemical analysis techniques.[19] The composition in multiple pass deposits is determined through an iterative approach. The composition in the first layer is determined by Equation [4-8], where C_{sub} is the composition of the substrate and C_{dep} is the composition of the incoming powder material. After mixing, the resultant composition of the deposit is given as C^1_{dep} (Refer to Figure 4- 27 a). The composition in the second pass is also determined from Equation [4-8]; however, C_{sub} now becomes C^1_{dep} and the resulting composition becomes C^2_{dep} (Refer to Figure 4- 27 b).

a   b
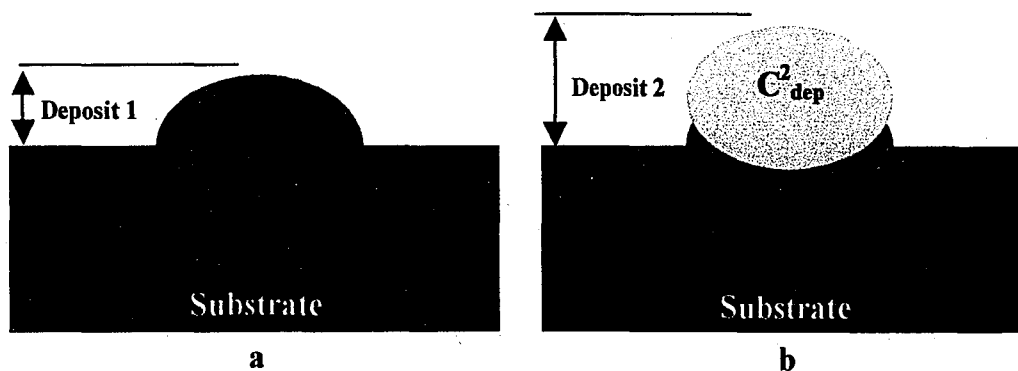
Figure 4- 27. Schematic illustration depicting composition in a) single pass and b) multiple pass LENS™ deposits.

C_{dep} remains the same if the composition of the incoming powder remains the same; otherwise, C_{dep} becomes the composition of new powder blend. This approach is used so

105

on and so forth depending on the number of discrete passes in the functional graded material structure.

4.4.1 Effect of Processing Parameters on Dilution

As with arc welding processes[37], dilution in the LENS™ process is controlled by the input power, travel speed, and filler metal mass flow rate. Dilution was measured for single pass H-13 tool steel and copper powder deposits on H-13 tool steel substrates as a function of laser power, travel speed, and powder mass flow rate. Single pass deposits were made in order to simplify the layer additive process so that the effects of process variables could be extensively explored in a simplistic manner.

The effect of processing parameters on dilution can be shown in a manner similar to the results presented in Section 4.3.2. Dilution was plotted as a function of laser input power under fixed travel speed and powder mass flow rate (Refer to Figure 4- 28). The plot displays a trend of increasing dilution with increasing laser input power. It has previously been shown in Section 4.2.1 that an increase in laser power will result in an increase in melting efficiency. A portion of the available energy for melting will effectively be used to melt the incoming powder material and the substrate material, while the rest is dissipated by thermal conduction to the rest of the substrate. As melting efficiency increases, more energy is available to melt a greater amount of the substrate. A portion of the energy available for melting will also be used to melt the incoming powder material. As evident in the corresponding micrographs in Figure 4- 28, the size of the deposit and melted substrate both increase with increasing laser input power. Since the powder mass flow rate is constant, there is a greater amount of energy available for localized melting of the substrate. The melted substrate area increases at a faster rate than

the deposit cross sectional area when laser input power is increased. Since the melted substrate cross sectional area increases much more than the deposit cross sectional area, it follows that dilution increases as well.

Dilution was observed to increase as travel speed increased for constant laser input power and powder mass flow rate (Refer to Figure 4- 29). The reason for this effect can be explained through examination of the following equation:

$$A_d = \frac{\eta_d \dot{V}_{fm}}{S}$$ [4- 9]

Where A_d is the cross sectional area of deposited filler material, η_d, is deposition efficiency, $\dot{V}_{fm}$ is the volumetric filler metal feed rate, and S travel speed. Recall that this equation is simply Equation [3-3] rewritten in terms of the deposit cross sectional area. If we assume a value of unity for η_d, it follows that the deposit cross sectional area is dependent upon the ratio of volumetric powder material feed rate to travel speed. As travel speed increases, there is less powder delivered to the melt pool, resulting in a decrease in the amount of material to be deposited. Also it has been shown that an increase in travel speed will result in an increase in melting efficiency, which will result in a greater amount of energy being utilized to melt the underlying substrate.[34] Therefore, the cross sectional area of the melted substrate increases, resulting in a subsequent increase in dilution. This is evident when examining the corresponding micrographs for

the data points in Figure 4- 29. The micrographs clearly depict a decrease in the deposit cross sectional area as travel speed increases.

Dilution was also observed to decrease with increasing powder mass flow rate when laser input power and travel speed are held constant (Refer to Figure 4- 30). This effect can also be explained from Equation [4-9]. From this equation it is apparent that when travel speed is constant, an increase in the volumetric powder material feed rate will result in an increase in the deposit cross sectional area since more material is made available for deposition. Examination of the micrographs in Figure 4- 30 shows this trend as well. As more powder is delivered to the melt pool a greater amount of energy is utilized to melt the incoming powder flux, leaving a lesser amount of energy to melt the underlying substrate. When this occurs, the melted substrate cross sectional area decreases. Thus, the fusion zone is comprised of a larger fraction of deposit material. Dilution therefore decreases as powder mass flow rate increases.
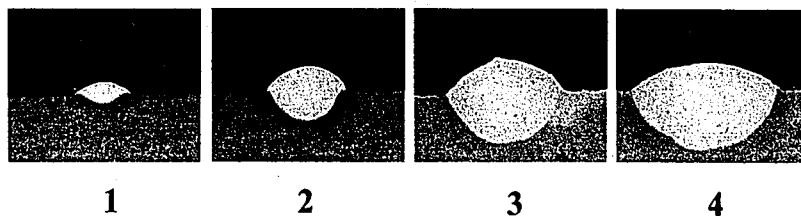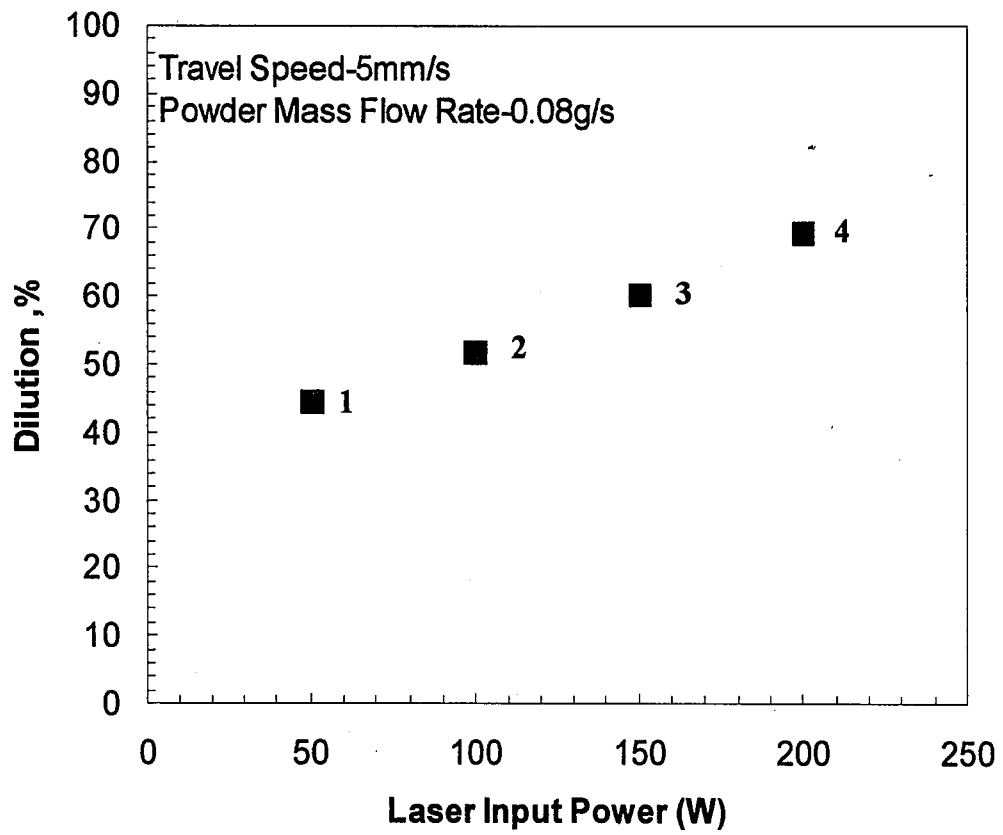
Figure 4- 28. Dilution as a function of laser input power for fixed travel speed and powder mass flow rate.
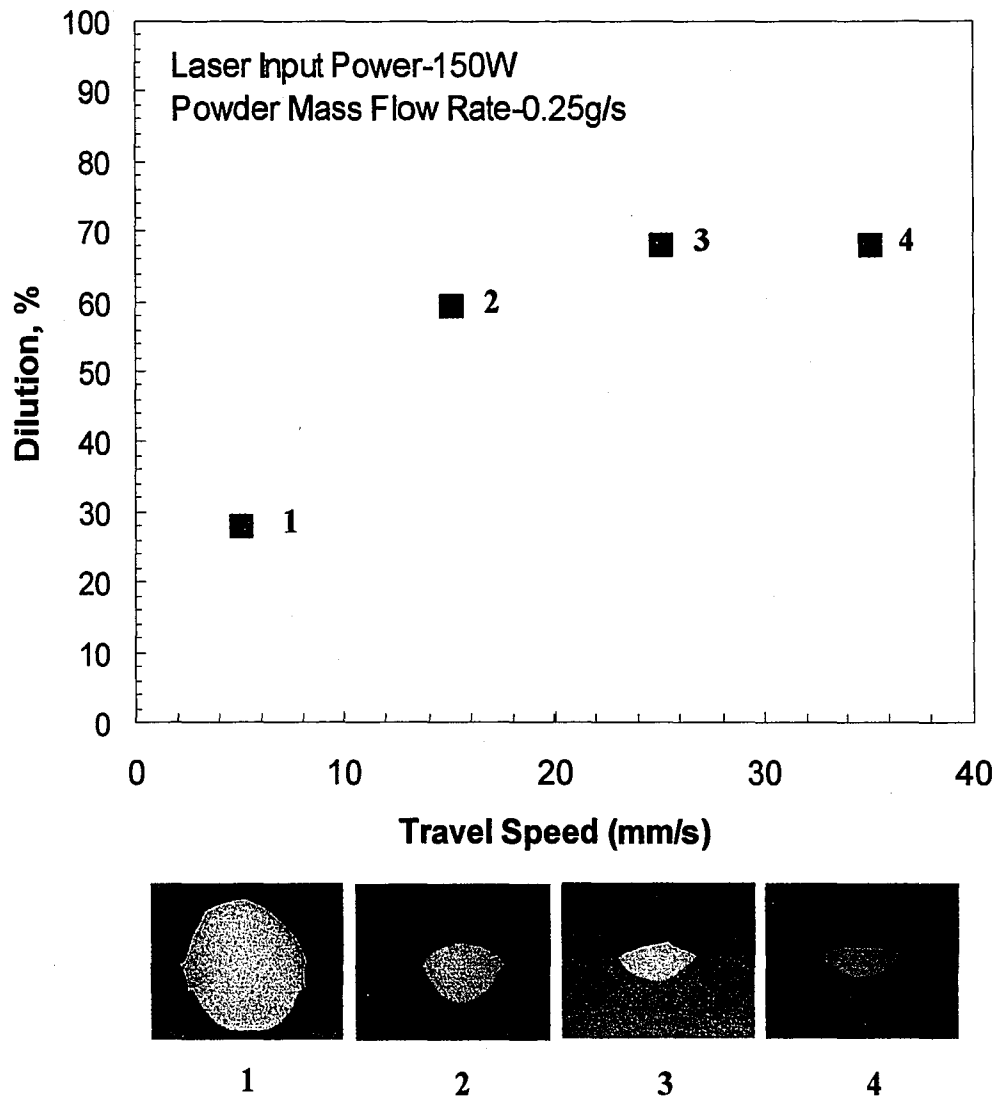
Figure 4- 29. Dilution as a function of travel speed for fixed laser input power and powder mass flow rate.
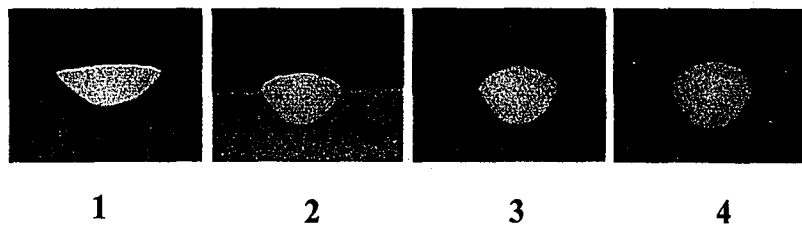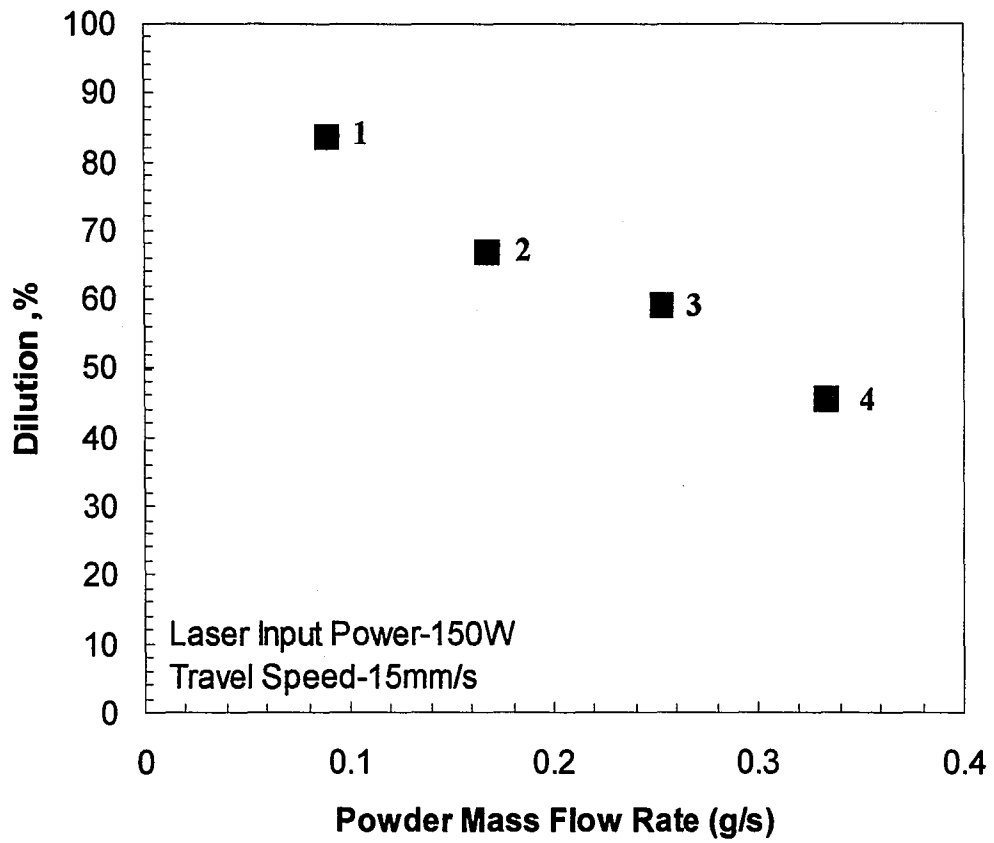
Figure 4- 30. Dilution as a function of powder mass flow rate for fixed laser input power and travel speed.

4.4.2 Methods of Predicting Dilution in LENS™ Deposits

A method of predicting dilution levels for arc welding processes, as a function of processing parameters, has been proposed by DuPont and Marder.[19] The model is based upon a power balance approach across the arc where the total energy available for melting is set equal to the energy required to melt the filler and substrate materials. The power balance can be seen in the following equation:

$$\eta_a \eta_m P = \eta_d \dot{V}_{fm} \Delta H_{m,f} + \dot{V}_s \Delta H_{m,s}$$

[4- 10]

Where the left side of the equation ($\eta_a \eta_m P$) represents the energy available for melting, i.e. melting power. The right side of the equation has two terms that represent the amount of energy required to melt a volumetric amount of material for the filler material and substrate material, respectively. Deposition efficiency (η_d) was incorporated into Equation [4-10] to account for powder losses that is delivered to, but not fused to substrate. Since the energy transfer and melting efficiencies can be estimated, rewriting Equation [4-10] in terms of the only unknown ($\dot{V}_s$) yields the following:

$$V_s = \frac{\eta_a \eta_m P - \eta_d \dot{V}_{fm} \Delta H_{m,f}}{\Delta H_{m,s}}$$

[4- 11]

As previously shown[19], Equation [3-4] can be rewritten in terms of volumetric melting rates of the filler metal and substrate. Rewriting this in another form results in the following:

$$\%D = \frac{\dot{V}_s}{\dot{V}_s + \eta_d \dot{V}_{fm}} = \left(1 + \frac{\eta_d \dot{V}_{fm}}{\dot{V}_s}\right)^{-1} \times 100\% \qquad \text{4-12]}$$

Substituting Equation [4-11] into Equation [4-12] yields an expression for dilution as a function of melting power, volumetric filler metal feed rate, and melting enthalpy of the substrate ($\Delta H_{m,s}$) and filler metal materials ($\Delta H_{m,f}$).

$$\%D = \left[1 + \frac{\eta_d \dot{V}_{fm} \Delta H_{m,s}}{\eta_a \eta_m P - \eta_d \dot{V}_{fm} \Delta H_{m,f}}\right]^{-1} \times 100\% \qquad \text{[4-13]}$$

Equation [4-13] is thus a predictive equation that can be used to estimate dilution since the energy transfer efficiency is known and melting efficiencies can be estimated from the dimensionless parameter model presented in Section 4.2.2. The results of Section 4.1.1 show that laser energy transfer efficiency was relatively insensitive to the range of processing parameters used in this study. Therefore an average η_a value of 0.4 was used in all calculations.

113

To determine if this model can be applied to predict dilution in the LENS™ process, the data from actual dilution measurements were compared to that of calculated dilution values using Equation [4-13]. The melting efficiency term in Equation [4-13], was calculated using Equation [4-5] as described in Section 4.2.2 in order to yield an expression that is based fully on values that are predicted from processing parameters. A plot of measured dilution versus calculated dilution from Equation [4-13] is displayed in Figure 4-31. The results indicate that there is reasonable correlation between dilution that was found using actual experimental measurements to those calculated using the predictive model that was based solely as a function of processing parameters and material thermophysical properties. The correlation begins to break down at low levels of dilution. The deviation from the 1:1 correlation line in the plot is the result of the difficulty in predicting melting efficiency as previously described in Section 4.2.2 and by DuPont and Marder.[19] Overall, Equation [4-13] can be used to estimate dilution for single pass LENS™ deposits with good agreement between experimentally measured and calculated dilution values. However future work is still needed to determine if this model is applicable for multipass LENS™ deposits.
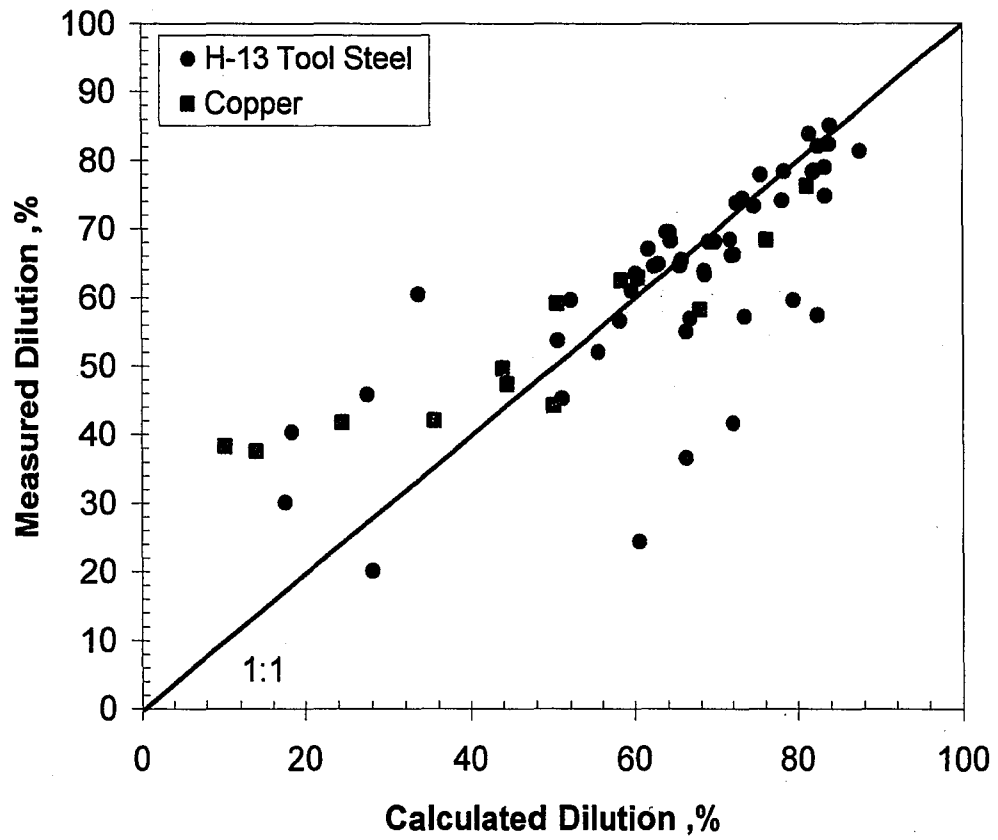
Figure 4- 31. Comparison between measured dilution and dilution calculated from Equation [4-13] for H-13 tool steel and copper powder deposits on H-13 tool steel substrates.

Another method of predicting dilution from a process parameter standpoint is by using Rosenthal's analytical heat flow solution[7] to solve for the cross sectional area of the melted substrate as a function of processing parameters. One of the limitations of Rosenthal's moving heat flow solutions is that powder mass additions into the melt pool are not incorporated into the solutions for heat flow during welding. Melted substrate cross sectional areas were determined through the Rosenthal solutions using a commercially available MATLAB based software program called SOAR (Smartweld Optimization and Analysis Routines).[38] The ISO 3-D routine in the SOAR program enables users to easily compute constant temperature isotherms for a given set of weld variables by rapidly solving for Rosenthal's heat flow solution.

To compute melt pool isotherms, laser input power ($\eta_a P$) and travel speed were used as input parameters to solve for the melted substrate cross sectional areas using the available 1018 steel thermal property database. The 1018 steel thermal property database includes thermophysical properties such as thermal diffusivity and thermal conductivity values of which are used to as inputs into the Rosenthal solution. Example output results can be seen in Figure 4- 32. Actual melt pool cross sectional areas, taken from experimental measurements, were compared to melt pool cross sectional areas estimated by Rosenthal's 3-D heat flow solution using SOAR (Refer to Figure 4- 33). Results indicate a good correlation between the two even though Rosenthal's solution does not take into account powder additions into the weld pool. The good correlation arises from experimentally fitted thermal property values. To determine effective thermal conductivity and effective thermal diffusivity values, a least squares fitting method was employed to fit measured cross sectional area data to the conduction model.[39] The

resultant effective thermal diffusivity and effective thermal conductivity were 6.2mm^2/s

and 44W/m-K, respectively.
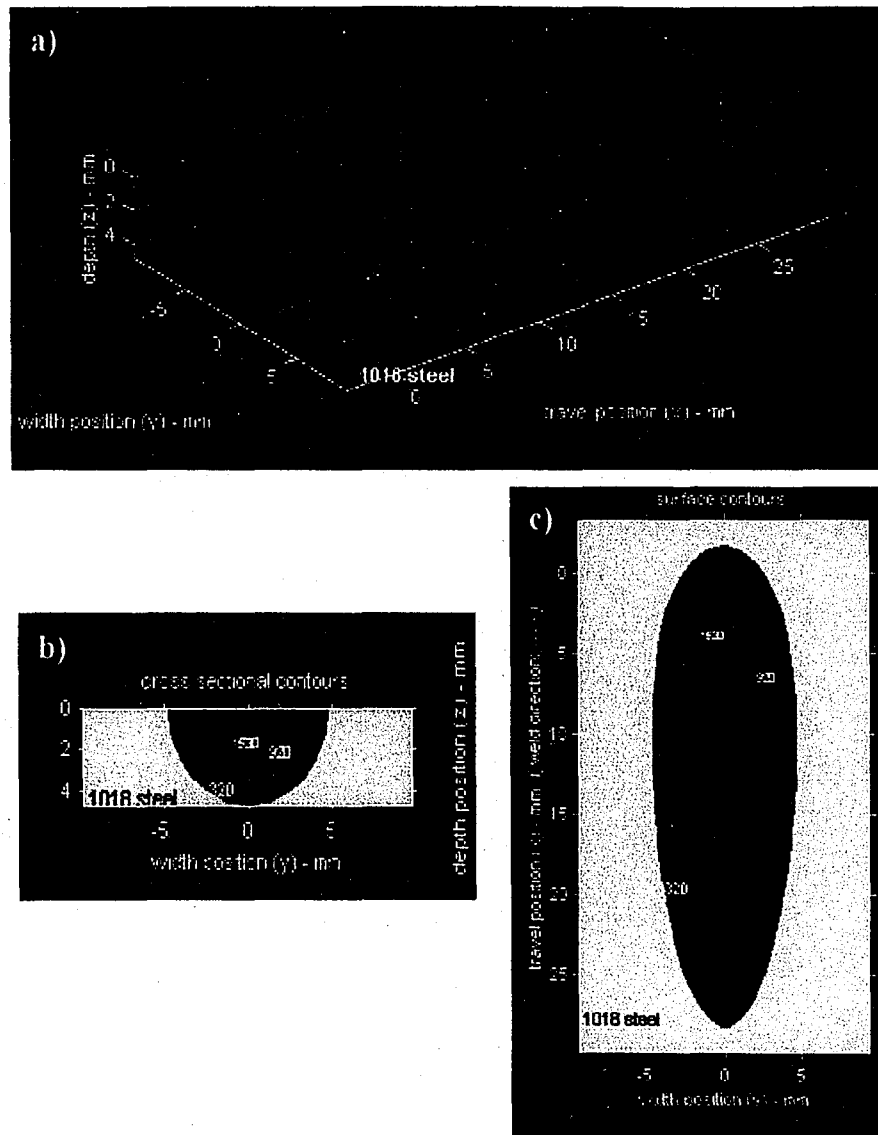
Figure 4- 32. Example visual output results from SOAR program ISO 3-D function. a) 3-D isotherm contours, b) cross section view, and c) top view.

resultant effective thermal diffusivity and effective thermal conductivity were 6.2mm^2/s
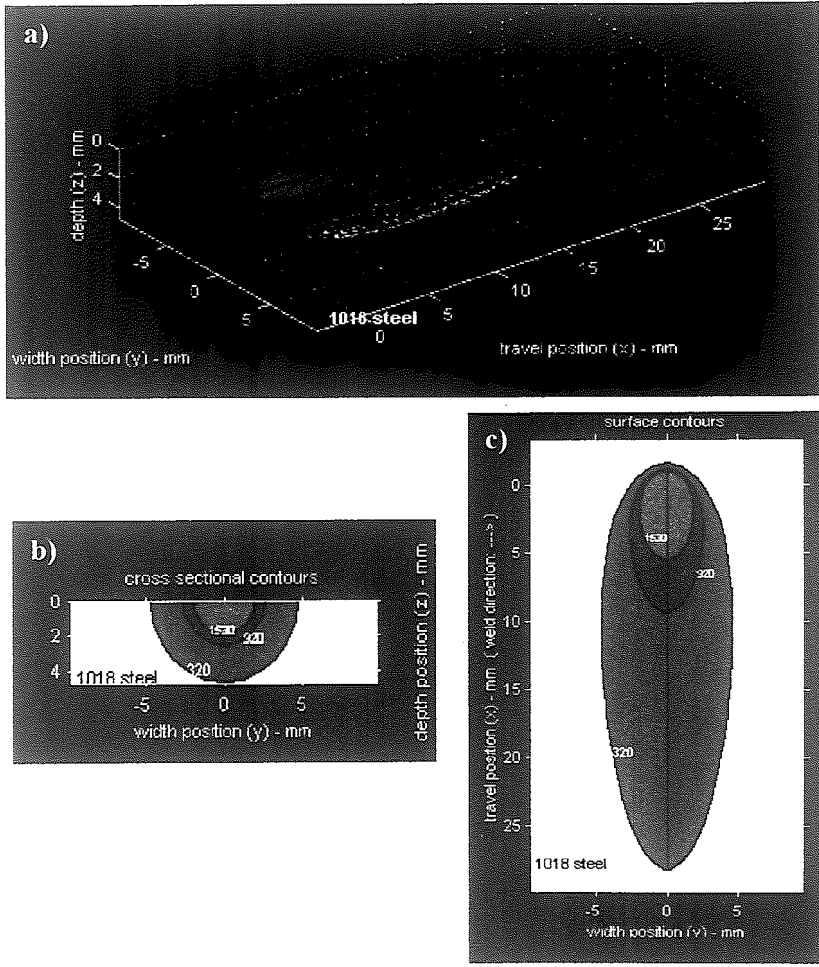
and 44W/m-K, respectively.

Figure 4- 32. Example visual output results from SOAR program ISO 3-D function. a) 3-D
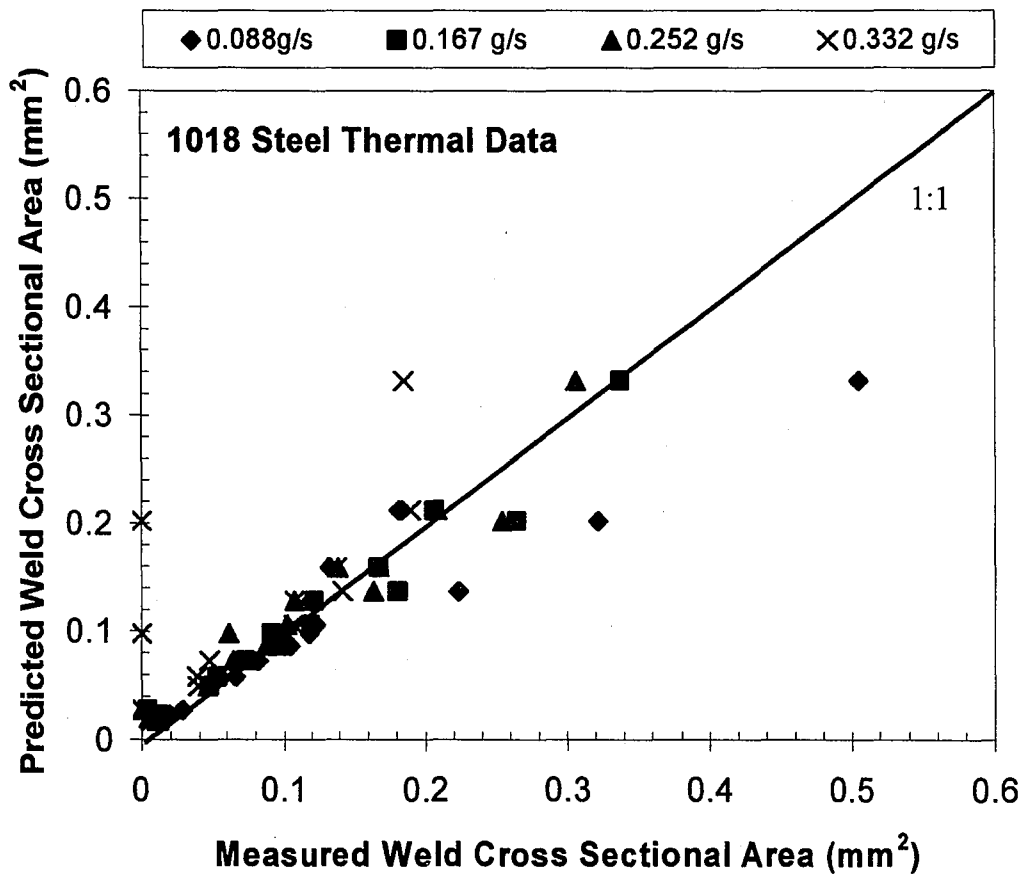isotherm contours, b) cross section view, and c) top view.

117

Figure 4- 33. Comparison between experimentally measured weld cross sectional areas and weld cross sectional areas estimated using Rosenthal's 3-D heat flow solution at varying powder mass flow rates.

To use the results presented above to estimate dilution, the SOAR program was used to predict melted substrate cross sectional areas as a function of laser input power and travel speed. Recall that calculation of dilution requires geometric measurements of melted substrate and deposit cross sectional area. To estimate the deposit cross sectional area for the H-13 tool steel and copper deposits, Equations [4-6] and [4-7] were first used to predict deposition efficiency for the same processing parameters used in the Rosenthal solution. Once the deposition efficiency was known for the given set of parameters, the deposit cross sectional areas were then back calculated using Equation [4-9]. Good agreement was found between experimentally measured deposit cross sectional areas and calculated deposit cross sectional areas using Equation [4-9] as evident in Figure 4- 34 for the H-13 tool steel data. The poor correlation for the copper data is attributed to the initial scatter in data in Figure 4- 25.

In order to calculate dilution, estimated substrate melted cross sectional areas from the Rosenthal solution and deposit cross sectional areas from Equation [4-9] were incorporated into Equation [3-4]. A comparison between experimentally measured and calculated dilution can be seen in Figure 4- 35. The plot shows good correlation between measured and calculated dilution levels for the H-13 tool steel deposits; however, there are deviations from the 1:1 correlation line for the copper deposits. Deviations from the 1:1 correlation line in Figure 4- 35 appears to be from the deviations in estimated deposit cross sectional areas in Figure 4- 34.
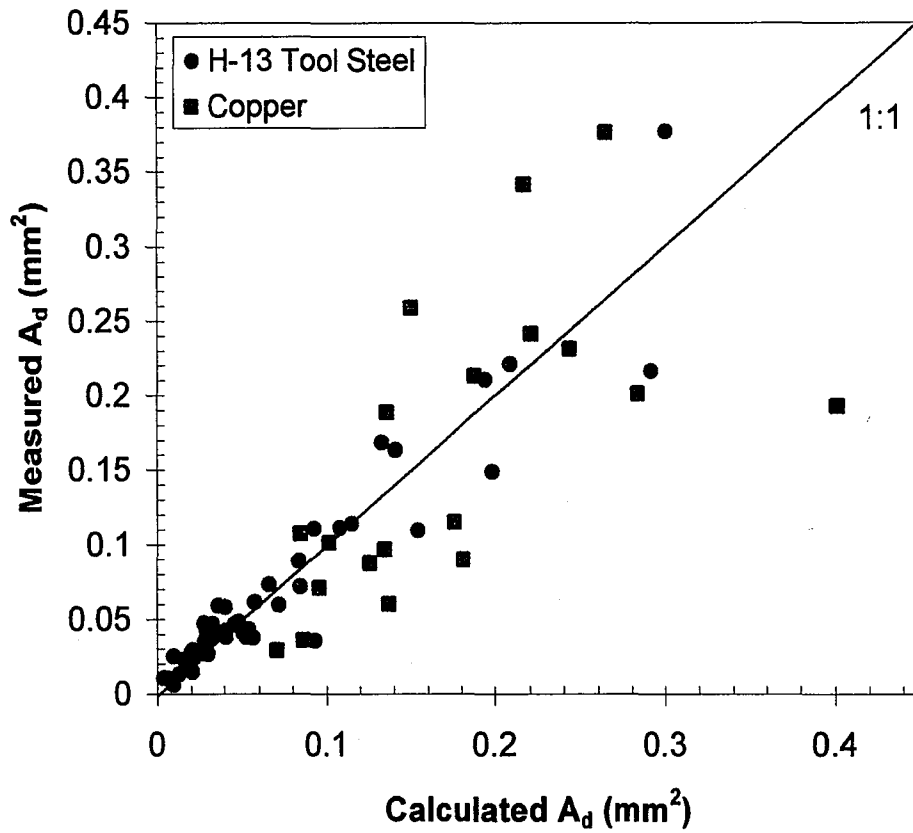
Figure 4- 34. Comparison between experimentally measured deposit cross sectional areas and predicted deposit cross sectional areas using Equation [4-9] for H-13 tool steel and copper deposits on H-13 tool steel substrates.
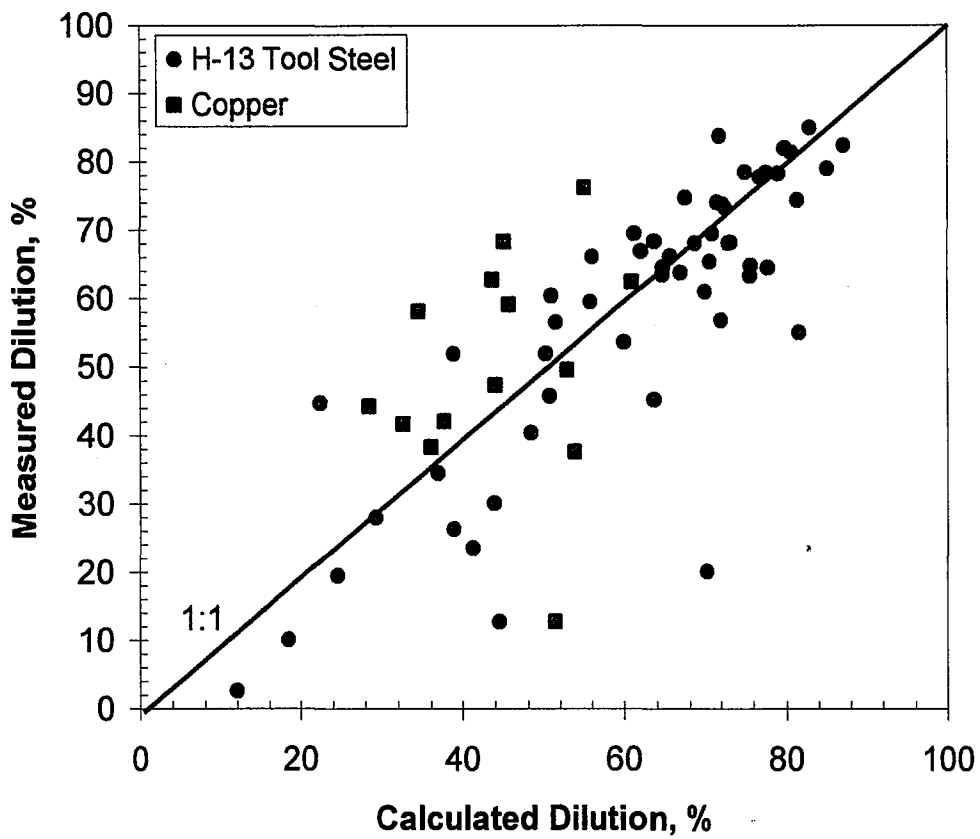
Figure 4- 35. Comparison between experimentally measured dilution and dilution calculated from predictive melted substrate and deposit cross sectional areas.

5.0 RESEARCH SUMMARY AND CONCLUSIONS

Laser energy transfer, melting, and deposition efficiencies were measured for the LENS™ process for H-13 tool steel and copper powder deposits on H-13 tool steel substrates. The influence of laser power, travel speed, and powder mass flow rate on these process efficiencies were investigated and the following results were revealed:

1) Laser energy transfer efficiency varied from 30-50% under the range of processing parameters tested. Laser beam absorption was relatively insensitive to changes in laser output power and travel speed. Powder feed rate and the type of powder delivered to the molten pool showed no effect on laser beam absorption.

2) Melting efficiency was shown to increase with increasing laser input power, travel speed, and powder mass flow rate.

3) A dimensionless parameter model that has been used to predict melting efficiency for laser beam welding processes was applied to the LENS™ process. Calculated melting efficiency values predicted from the model correlated reasonably well with experimentally measured melting efficiencies for H-13 tool steel deposits at high melting efficiency values.

4) The influence of processing parameters on deposition efficiency was described by the Γ parameter $[V_{fm}/(\eta_a \eta_m P/S)]$. Deposition efficiency was observed to increase when the Γ parameter is small and decreases when the Γ parameter is large. A semi-empirical model utilizing the Γ parameter was developed to predict deposition efficiency as a function of processing parameters.

5) A semi-empirical model relating utilizing the Γ parameter was developed to predict deposition efficiency as a function of processing parameters.

122

6) Processing parameters were shown to influence dilution. Varying laser power, travel speed, or powder mass flow rate independently or simultaneously will alter dilution.

7) Dilution in multiple pass deposits can be determined by Equation [4-8] when dilution and the compositions of the substrate and incoming powder are known.

8) A previous model that was developed to predict dilution for arc welding processes as a function of process variables and process efficiencies was shown to be applicable for the LENS™ process with good correlation between calculated and experimentally measured dilution values.

9) A method of predicting dilution was introduced which incorporates Rosenthal's heat flow solution and the semi-empirical model developed to predict deposit cross sectional areas. Good correlation was demonstrated when dilution found from this approach was compared to experimentally measured values.

6.0 REFERENCES

1. Beaman, J.J., et al, <u>Solid Freeform Fabrication: A New Direction in Manufacturing</u>. Dordrecht; Boston, Kluwer Academic Publisher. (1997)

2. Mazumder, J., Koch, J., Nagarthnam, K., Choi, J., Rapid Manufacturing by Laser Aided Directed Deposition of Metals. Advances in Powder Metallurgy & Particulate Materials, Vol. 4. (1996)

3. Keicher, D.M., Romero, J.A., Atwood, C.L., Smugeresky, J.E., Griffith, M.L., Jeantette, F.P., Harwell, L.D., Greene, D.L., Freeform Fabrication Using the Laser Engineered Net Shaping (LENS™) Process, Advances in Powder Metallurgy & Particulate Materials, Vol. 4. (1996)

4. Keicher, D.M., Smugeresky, J.E., The Laser Forming of Metallic Components Using Particulate Materials. JOM, 49(5), 1997, pp. 51-54.

5. Griffith, M.L., et al, Freeform Fabrication of Metallic Components using Laser Engineered Net Shaping (LENS™), SFF Symposium Proceedings, 1996, pp. 125-131.

6. Smugeresky, J.E., et al. Laser Engineered Net Shaping (LENS™) Process: Optimization of Surface Finish and Microstructural Properties Advances in Powder Metallurgy and Particulate Materials, 1997, pp. 21-33.

7. Rosenthal, D., Theory of Moving Sources of Heat and its Application to Metal Treatments, Trans ASME, vol. 68, 1946, pp. 849-866.

8. Kou, S., Welding Metallurgy, John Wiley & Sons, 1987, pg. 46.

9. Hofmeister, W. et al, Investigating Solidification with the Laser Engineered Net Shaping (LENS™) Process. JOM, vol. 51, no. 7, July 1999.

10. McLean, M.A., Shannon, G.J., Steen, W.M., Laser Direct Casting High Nickel Alloy Components, Advances in Powder Metallurgy and Particulate Materials, 1997, pp 21-33.

11. Fuerschbach, P.W., Measurement and Prediction of Energy Transfer Efficiency in Laser Beam Welding, Supplement to the Welding Journal, 1996, pp 24-34.

12. Steen, W.M., Laser Materials Processing, Springer-Verlag, 1998, pg. 47.

13. Ready, J., LIA Handbook of Laser Materials Processing, Magnolia Publishing, 2001, pg 48.

14. Ready, J., <u>LIA Handbook of Laser Materials Processing</u>, Magnolia Publishing, 2001, pg 180.

15. Giedt, W.H., Tallerico, L.N., Fuerschbach, P.W., GTA Welding Efficiency: Calorimetric and Temperature Field Measurements, Supplement to the Welding Journal, 1989, pp. 28-32.

16. DuPont, J.N., Marder, A.R., Thermal Efficiency of Arc Welding Processes, Supplement to the Welding Journal, 1995, pp. 406-416.

17. Wells, A.A., Heat Flow in Welding, Welding Journal, 31, (5), 1952, pp. 263s-267s.

18. Okada, A., Applications if Melting Efficiencies and it Problems, Journal of the Japan Welding Society, 46 (2), 1977, pp. 53-61.

19. DuPont, J.N., Marder, A.R., Dilution in Single Pass Arc Welds, Metallurgical and Materials Transactions B, Volume 27B, 1996, pp. 481-489.

20. Fuerschbach, P.W, and Knorovsky, A Study of Melting Efficiency in Plasma Arc and Gas Tungsten Arc Welding, Welding Journal 70 (11), 1991, pp. 287s to 297-s.

21. Fuerschbach, P.W., A Dimensionless Parameter Model for Arc Welding, Trends Weld. Res. Proc. Int. Conf., 4th, 1996, pp. 493-497.

22. Fuerschbach, P.W., Melting Efficiency in Fusion Welding, The Metal Science of Joining Proceedings, The Minerals, Metals and Materials Society, 1992, pp. 21-29.

23. Irving, R., Taking a Powder: Laser Processing, International Journal of Powder Metallurgy, Vol. 36, No. 4, 2000, pp. 69-74.

24. Brice, C.A., Process Variable effects on laser deposited Ti-6Al-4V. SFF Symposium Proceedings, 1999, pp. 369-374.

25. Fessler, J., Nickel, A., Link, G., Prinz, F., Functional Gradient Metallic Prototypes through Shape Deposition Manufacturing, SFF Symposium Proceedings, 1997, pp. 521-528.

26. Jepson, L. et al, SLS Processing of Functionally Gradient Materials, SFF Symposium Proceedings, 1997, pp. 67-79.

27. Pei, Y.T., De Hosson, J.Th.M., Functionally Graded Materials Produced by Laser Cladding, Acta Materialia, (48), 2000, pp. 2617-2624.

28. Seefeld, T., Laser Generation of Graded Metal-Carbide Components, Materials Science Forum, Vols. 308-311, 1999, pp. 459-466.

29. Zhang, Y. H., Rapid Prototyping and Combustion Synthesis of TiC/Ni Functionally Graded Materials, Materials Science & Engineering A: Structural Materials: Properties, Microstructure & Processing. Vol. 299, n 1-2, 2001, pp. 218-224.

30. Griffith, M.L. et al, Multi-Materials Processing by LENS™, SFF Symposium Proceedings, 1997, pp. 387-393.

31. Mazumder, J. Choi, J., Nagathnam, K., Koch, J., Hetzner, D., The Direct Metal Deposition of H-13 Tool Steel for 3-D Components, JOM, Vol. 49, No.5, 1997, pp. 55-60.

32. Maziasz, P.J., Payzant, E.A., Schlienger, M.E., McHugh, K.M., Residual Stresses and Microstructure of H-13 Steel Formed by Combining Two Different Direct Fabrication Methods, Scripta Materialia, Vol. 39, No. 10, 1998, pp. 1471-1476.

33. Fine, H.A., Geiger, G.H., Handbook on Materials and Energy Balance Calculations in Metallurgical Processes, AIME, Warrendale, PA, (1979)

34. Fuerschbach, P.W., and Eisler, G.R., The Effect of Very High Travel Speeds on Melting Efficiency in Laser beam Welding, SAE, 1999, pp. 824-829.

35. DuPont, J.N., A Quantitative Method of Optimizing Weld Overlay Processing Parameters and Comparing Process Performance, M.S. Thesis, Lehigh University, 1994, pg 115.

36. Touloukian, Y. S.; Powell, R. W.; Ho, C. Y.; Nicolaou, M. C. Thermal Diffusivity Thermophysical Properties of Matter, IFI/Plenum, New York, N. Y., Vol. 10, (1973)

37. Banovic, S. W.; DuPont, J. N.; Marder, A. R. Dilution Control in Gas-Tungsten-Arc Welds Involving Superaustenitic Stainless Steels and Nickel-Based Alloys. Metallurgical and Materials Transactions B: Process Metallurgy and Materials Processing Science, Vol. 32B, 2001, pp 1171-1176.

38. Fuerschbach, P.W., Eisler, G.R., Steele, R.J. Weld Procedure Development with OSLW, Trends in Welding Research, Proceedings of the International Conference, 5th, Pine Mountain, Ga., June 1-5, 1998 (1999)

39. Fuerschbach, P.W., Eisler, G.R., Determination of Material Properties for Welding Models by Means of Arc Weld Experiments, Trends in Welding Research, Proceedings of the International Conference, 6th, Pine Mountain, Ga., April 15-19, (2002)

7.0 VITA

Raymond Robert Unocic was born in Taipei Taiwan R.O.C. on June 15, 1978 to

the parents of Robert and Fu-Hsia Unocic. He is the younger brother to Frank Unocic and

Jennifer Unocic. He graduated from Mojave Sr. High School in Mojave, California in

June of 1996. After graduating high school, he attended The Ohio State University and

graduated with a B.S. in Metallurgical Engineering in June of 2000. During his senior

year at Ohio State, his undergraduate research on ceramic composite processing won the

2000 National Collegiate Inventor's Competition. A U.S. Patent was filed and the

processing method was profiled in the developments to watch section in the September

25, 2000 issue of Business Week magazine. After Ohio State, he then went on to pursue a

M.S. in Materials Science and Engineering at Lehigh University. During the second year

of graduate studies he received the New Jersey Zinc Fellowship and won 3rd place in the

2002 American Welding Society poster competition. After graduation, he will return to

The Ohio State University to pursue a Ph.D. in Materials Science and Engineering,

conducting research on novel processing methods for fabricating ceramics and ceramic

composites.

END OF
TITLE